Master Programme
in *Flood Risk Management*

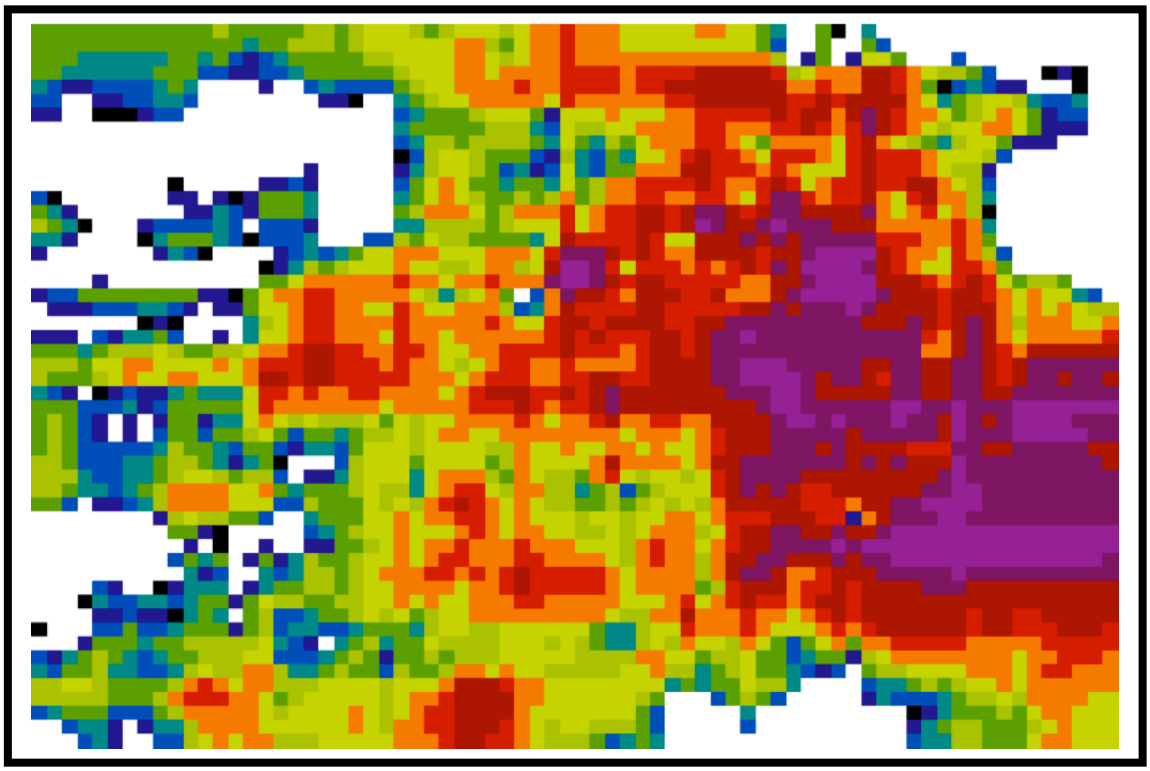

Evaluation of TRMM rainfall products for hydrological uses at different scales

Md. Atiqul Islam

MSc Thesis (36026)
August 2013

UNESCO-IHE Institute for Water Education
TECHNISCHE UNIVERSITÄT DRESDEN
UNIVERSITAT POLITÈCNICA DE CATALUNYA BARCELONATECH
Univerza v Ljubljani
Centre de Recerca Aplicada en Hidrometeorologia
UNIVERSITAT POLITÈCNICA DE CATALUNYA

Univerza v Ljubljani

Evaluation of TRMM rainfall products for hydrological uses at different scales

Master of Science Thesis
by
Md. Atiqul Islam

Supervisors
Prof. Dr. Daniel Sempere Torres (CRAHI-UPC)
Dr. Marc Berenguer i Ferrer (CRAHI-UPC)

Examination committee
Prof. Dr. Allen Bateman (GITS-UPC), Chairman
Prof. Dr. Daniel Sempere Torres (CRAHI-UPC)
Dr. Marc Berenguer i Ferrer (CRAHI-UPC)
Dr. Biswa Bhattacharya (UNESCO-IHE)

This research is done for the partial fulfillment of requirements for the Master of Science degree at the UNESCO-IHE Institute for Water Education, Delft, the Netherlands

Barcelona
August 2013

Acknowledgement

It would not have been possible to write this M.Sc. thesis without the help and support of the kind people around me, to only some of whom it is possible to give particular mention here.

Above all, I would like to thank my supervisor Prof. Dr. Daniel Sempere Torres for his help and support. The good advice and support of my co-supervisor, Dr. Marc Berenguer, has been invaluable on both an academic and a personal level, for which I am extremely grateful. This thesis would not have been possible without his help and patience, not to mention his advice and unsurpassed knowledge of the field of study. I am also grateful to CRAHI-UPC (Centre of Applied Research in Hydrometeorology, Univesitat Politecnica de Catalunya) for providing me the computers, software facilities, and rain gauge data of Catalunya.

I would like to acknowledge European Commission for the financial support and the four institutes UNESCO-IHE, Institute for Water Education, Delft, The Netherlands; Technical University of Dresden, Germany; Universitat Politecnica de Catalunya, Barcelona, Spain; and University of Ljubljana, Slovenia for their outstanding academic and technical support. I offer my sincerest gratitude to Dr. Biswa Bhattacharya, Prof. Dr. Allen Bateman, Prof. Dr. Dimitri Solomatine, Prof. Dr. Christian Bernhofer, and Prof. Dr. Mitja Brilly for their help and support throughout the study period.

I would like to convey my deepest gratitude to my late parents, without their inspiration and sacrifice it was not possible for me to reach at this level of study and research. My wife, brother, and sisters have given me their unequivocal support throughout, as always, for which my mere expression of thanks likewise does not suffice.

The satellite rainfall data (TRMM) used in this effort were acquired as part of the activities of NASA's Science Mission Directorate, and are archived and distributed by the Goddard Earth Sciences (GES) Data and Information Services Center (DISC). I gratefully acknowledge the Catalan Weather Service and the Catalan Water Agency for providing rain gauge data in Catalunya, Bangladesh Meteorological Department (BMD) for providing rain gauge data in Bangladesh, and Climate Systems Analysis Group, Computing Center for Water Research (CCWR), and South African Weather Service (SAWS) for rain gauge data in South Africa.

Abstract

The principal objectives of the thesis are two: firstly to study the accuracy of the satellite rainfall products in climatologically distinctive places at different scales and secondly to find the possibility of using satellite-rain gauge blended rainfall products for hydrological purposes.

Three case study areas Catalunya, Bangladesh, and South Africa have been chosen for the analysis using the satellite rainfall products (TMPA) and rain gauge records for the period from January 2005 to December 2009. The areal pattern of rainfall has been presented using satellite rainfall products over the case study areas. Both daily and monthly products are showing good agreement with rain gauge records although it is highly variable with space and seasonality. From the results, it can be shown that TRMM satellite identified the seasonal variability of rainfall. Moreover, the mean TRMM rainfall products show same pattern as like mean rain gauge observations in daily and monthly scale in all case study areas.

Finally, a blending technique is applied (originally used for radar-rain gauge blending) to conform satellite rainfall products to rain gauge observations. This blended product is also tested against the rain gauge records to verify the improvement of the blended rainfall products over the original satellite products. Results of blended rainfall products enlightens few aspects or issues that should consider before applying blending technique including density of rain gauge network and resolution of TRMM pixel.

Contents

CHAPTER 1. INTRODUCTION

1.1. Background

Precipitation is the natural starting point for the hydrologic cycle and main input to the hydrologic systems and plays a significant role in weather research, monitoring, and predictions. Improving our understanding of weather and climate, along with the development of reliable and uninterrupted measurements, are essential for proper assessment of weather conditions. Currently, in-situ and radar-based precipitation observations are the major input for stream flow forecasts, flash flood warnings, and weather observations around the world. However, in many parts of the globe (except in a few developed countries), radar installations for precipitation measurements are not available and poor spatial sampling of rain gauge networks makes them inadequate to monitoring, detection, and forecast studies. Clearly, the lack of ground-based precipitation measuring networks hampers the development and use of flood and drought warning models, hydrological models, and extreme weather monitoring and decision-making systems. Therefore, there exists the need to achieve alternative estimates of precipitation with sufficient sampling density, reliability, and accuracy to enable utilization of data for operational applications.

Satellite-derived precipitation estimates have the potential to improve precipitation observation at a global scale. In recent years, the National Aeronautics and Space Administration (NASA) and the National Oceanic and Atmospheric Administration (NOAA), and many other international satellite missions have led to an increase in available precipitation data. These remotely sensed data have several advantages over in situ measurements, including higher spatial resolution and uninterrupted coverage. However, these data have not yet been fully integrated into hydrologic and water resources management and decision-making system, mainly because of undetermined uncertainties associated with satellite rainfall / precipitation estimates.

Currently, many efforts are being made by many scientists around the world to utilize space-borne precipitation data as a supplementary and / or key decisive (for ungauged basins) source of information for weather monitoring and detection, forecasting, and water resources management. The emergence of various satellite-based precipitation products with high special resolution and global coverage could be considered good alternatives or complement

to in situ measurements. For example, Li and Shao (2010) studied to merge satellite rainfall estimates and rain gauge data to estimate the areal precipitation where the rain gauge network is sparse in Australia, especially for local convective events, AghaKouchak et al. (2011) evaluated the performance of different satellite-retrieved precipitation products to detect extreme precipitation rates across the central United States, Bitew and Gebremichael (2011) assessed the suitability of satellite rainfall products for stream flow simulation in medium watersheds of Ethiopian highlands and also studied the accuracy through hydrologic simulation in a fully distributed hydrologic model [Bitew and Gebremichael (2011)], Duncan and Biggs (2012) assessed the accuracy and applied use of satellite-derived precipitation estimates over Nepal, Haile et al. (2013) inter-compared different satellite rainfall products for representing rainfall diurnal cycle over the Nile basin.

1.2. Satellite measurement of precipitation in ungauged basins

Many hydrologic simulation studies, whether related to climate change scenarios, flood forecasting, or water management, depend heavily on the availability of good-quality precipitation estimates. Difficulties in estimating precipitation arise in many remote parts of the world and particularly in developing countries where ground-based measurement networks (rain gauges or weather radar) are either sparse or nonexistent, mainly due to the high costs of establishing and maintaining infrastructure. For rivers that cross international boundaries, inconsistencies in instrumentation, and administrative limitations to data access further hamper the effective use of hydrological models in support of reliable flood and drought diagnosis and prediction [Su et al. (2008)]. These situations impose an important limitation on the possibility and reliability of hydrologic forecasting and early warning systems in these regions. For example, monsoon flooding (June–July 2004) in Bangladesh caused massive damage to the land, infrastructure, and economy and affected more than 23 million people [Yilmaz et al. (2005)].

The International Association of Hydrological Sciences (IAHS) launched an initiative called the Decade on Predictions in Ungauged Basins (PUB), aimed at achieving major advances in the capacity to make reliable predictions in “ungauged” basins [Sivapalan et al. (2003)]. Ungauged is used to indicate locations where measurements of the variables of interest are either too few or too poor in quality, or not available at all. In particular, where measurements

of the system response (e.g., streamflow) are lacking, prior estimates of the model parameters cannot be improved via calibration [Gupta et al. (2005)]. However, where measurements of the system input (e.g., precipitation) are missing, the model cannot even be driven to provide forecasts.

Whether measured directly by rain gauges or indirectly by remote sensing techniques, all precipitation estimates contain uncertainty. While rain gauges provide a direct measurement of precipitation reaching the ground, they may contain significant bias arising from coarse spatial resolution (yielding underestimation especially during events with low spatial coherency, i.e., convective showers), location, wind, and mechanical errors among others [Groisman and Legates (1994)]. According to Legates and DeLiberty (1993) rain gauges may underestimate the true precipitation by about 5%. Radar estimates hold promise for hydrologic studies by providing data at high spatial and temporal resolution over extended areas but suffer from bias due to several factors including hardware calibration, uncertain Z–R relationships [Winchell et al. (1998); Morin et al. (2003)], ground clutter, brightband contamination, mountain blockage, anomalous propagation, and range-dependent bias [Smith et al. (1996)]. Recent advances in satellite-based remote sensing have enabled scientists to develop precipitation estimates having near-global coverage, thereby providing data for regions where ground-based networks are sparse or unavailable [Sorooshian et al. (2000)]. However, this advantage is offset by the indirect nature of the satellite observables (e.g., cloud-top reflectance or thermal radiance) as measures of surface precipitation intensity [Petty and Krajewski (1996)].

In general, satellite-based precipitation estimation algorithms use information from two primary sources. The infrared (IR) channels from geosynchronous satellites are used to establish a relationship between cloud top conditions and rainfall rate at the base of the cloud. This relationship can be developed at relatively high spatial (~ 4 km X 4 km) and temporal (30 min) resolution. The microwave (MW) channels from low-orbiting satellites are used to more directly infer precipitation rates by penetrating the cloud, but a low-orbiting satellite can retrieve only one or two samples per day. The relative strengths and weaknesses of various sources have been exploited in the development of algorithms that combine and make the best use of each source [Yilmaz et al. (2005)].

Numerous satellite precipitation validation studies (e.g., "ground truthing") have been implemented with a view to providing both users and providers information about the quality of satellite precipitation estimates [Krajewski et al. (2000); Adler et al. (2001); McCollum et al. (2002); Gottschalck et al. (2005); Brown (2006); Ebert et al. (2007)]. Comparatively little work has been done to evaluate the suitability of existing satellite precipitation products as input for hydrologic models. Yilmaz et al. (2005) investigated the use of the Precipitation Estimation from Remotely Sensed Information using Artificial Neural Networks (PERSIANN) satellite precipitation algorithm [Sorooshian et al. (2000)] in streamflow forecasting with a lumped hydrologic model over several medium-size basins in the southeastern United States. Artan et al. (2007) evaluated a satellite rainfall product for streamflow modeling with a spatially distributed hydrologic model over four sub-basins of the Nile and Mekong Rivers. Both studies demonstrated improved performance of remotely sensed precipitation data in hydrologic modeling when the hydrologic model was calibrated with satellite data. Other studies have been conducted either over very small basins [Hossain and Anagnostou (2004)] or with satellite products that are not widely available [Tsintikidis et al. (1999); Grimes and Diop (2003); Wilk et al. (2006)].

1.3. The TRMM mission

With the advent of meteorological satellites in the 1970s, great efforts have been directed to estimating precipitation from satellite images, which cover most of the Globe. The Tropical Rainfall Measuring Mission (TRMM), a joint project by the National Aeronautics and Space Administration (NASA) of the United States of America (USA) and the Japan Aerospace Exploration Agency (JAXA, formerly, NASDA) launched on November 27th, 1997, provides a wealth of information on global tropical rainfall [Kummerow et al. (2000)]. As the first satellite with a precipitation radar (built by the Communication Research Laboratory in Japan) dedicated to rainfall measurement, TRMM indirectly estimates precipitation with the deployment of several passive microwave sensors. Due to the limitations in weight, power and size, and the need for narrow beams in order to get an acceptable resolution at ground level, TRMM-PR operates at K_u band. This makes its measurement seriously affected by attenuation due to the scatter of the hydrometeors. The basic principle of TRMM precipitation estimates is based on the relationship between microwave radiation and the amount of water in the cloud through Planck's law [Li and Shao (2010)].

TRMM is set in an inclination angle of 35° and period 90 minutes and covers between 40°N and 40°S. The average revisit time is around 9 hours, however, since it is a Low Earth Orbiting (LEO) satellite flying at 350 km / 402.5 km, the revisit time is highly irregular and highly dependent on the latitude of study [Bell et al. (1990)].

TRMM satellite was initially set at 350 km altitude, but to increase the life of the mission it was moved to 402.5 km in August 2001 (the loss of fuel due to the boost will be compensated by the less consumption at the new orbit). The change of the altitude of the satellite had an impact on the TRMM-PR resolution [see Table 1.1 for characteristics of TRMM-PR before and after the boost; Llort (2010)]. Several authors such as Shimizu et al. (2008), Shimizu et al. (2009), and Liu et al. (2012) studied the impact of the boost in the rainfall estimation by TRMM-PR.

Table 1:1 Specification of the TRMM-PR before and after the boosting

Property	**Unit**	**Before Boost**	**After Boost**
Height	km	350	402.5
Velocity of Nadir at Ground	km/s	7	-
Power Transmitted	W	500	-
PRF	Hz	2776	-
Frequency (K_u: 2.2 cm)	GHz	13.8	-
Beam Width	Degree	0.71	-
Pulse Duration	μs	1.6	-
Number of Beams	-	49	-
Cross Track Scan Angle	Degree	±17	-
Number of Gates	-	Between 122 and 139	-
Horizontal Resolution	km	4.3	5
Vertical Resolution	m	250	-
Swath	km	220	245 – 250
Detectable Z Factor	dBZ	19.5	20.7

1.4. Motivation and thesis outline

As mentioned above, there is a need for good-quality, high spatial and temporal resolution, and uninterrupted coverage of precipitation record for developing hydrological models, flood and drought warning models, water resource management, and decision-making systems in many parts of the world especially the places where ground-based measurement is not available or sparse. Satellite-derived precipitation estimates have the possibility to be used in model development, water management, and decision-making systems though these products have undetermined uncertainty associated with the estimation algorithms. Thus, the motivations of this thesis is to address the following two objectives:

The first objective is to determine the accuracy of satellite products in climatologically distinctive places at different scales. This will help us to interpret the measurements of a given instruments (working with a specific scale) and to merge estimates from various instruments operating at different scales.

The second objective is to study the possibility of using TRMM precipitation – rain gauge blended products for hydrological purposes.

After the present chapter, the work that has been done in this thesis will be presented according to the following order:

Chapter 2 describes the three case study areas with different climatology and presents data sets along with their corresponding spatial and temporal resolution and brief estimation procedure.

Chapter 3 presents the comparison between satellite estimation and ground-based rain gauge measurements in daily and monthly temporal scales measuring three statistical parameters at the three case study areas.

Chapter 4 explains the blending technique that has been adopted in this thesis at the three case study areas and also assessed the suitability of the technique.

Chapter 5 presents the conclusions of the thesis.

CHAPTER 2. STUDY AREA AND DATA SET DESCRIPTION

2.1. Introduction

With the aim of investigating the performance of space borne radar at local scale (i.e. a part of a country or a country) three case study areas have been selected. The inter-comparison between satellite rainfall estimation and ground-based estimation has done to better evaluate the reasons of the discrepancies and formulate an approach for using these products at local scale.

There are several TRMM precipitation products available by combining measurements from different sensors in the estimation algorithm. 3B42 and 3B43 are based on multi-satellite data involving other instruments rather than only the TRMM-PR. From each TRMM product there are several versions. Between versions there are some changes in the algorithms used to obtain the products. The 3B42 processing is designed to maximize the data quality, so 3B42 is strongly recommended for any research work not especially focused on real-time applications.

All data can be obtained through GES DISC (Goddard Earth Sciences Data and Information Services Center) website. For older versions, GES DISC should be contacted directly.

2.2. Study areas

2.2.1. Catalunya, Spain

Catalunya with a land area of over 32,000 km^2, is situated within 40°N - 44°N and 0° - 4°E at the north-eastern corner of the Iberian Peninsula with nearly 400 km Mediterranean coast [Lana et al. (2009)]. The climate of Catalunya is associated with cold and arid periods, with average annual rainfall ranging from less than 400 mm in the dry lowlands in Lleida to more than 1250 mm in certain parts of the Pyrenees [Llebot (2012)]. Figure 2.1 shows monthly distribution of casualties due to floods in Catalunya for the period from 1982 to 2007 [Llasat et al. (2010)]. In this study, we have used 284 remotely operated rain gauge stations with temporal resolution 5 minutes.

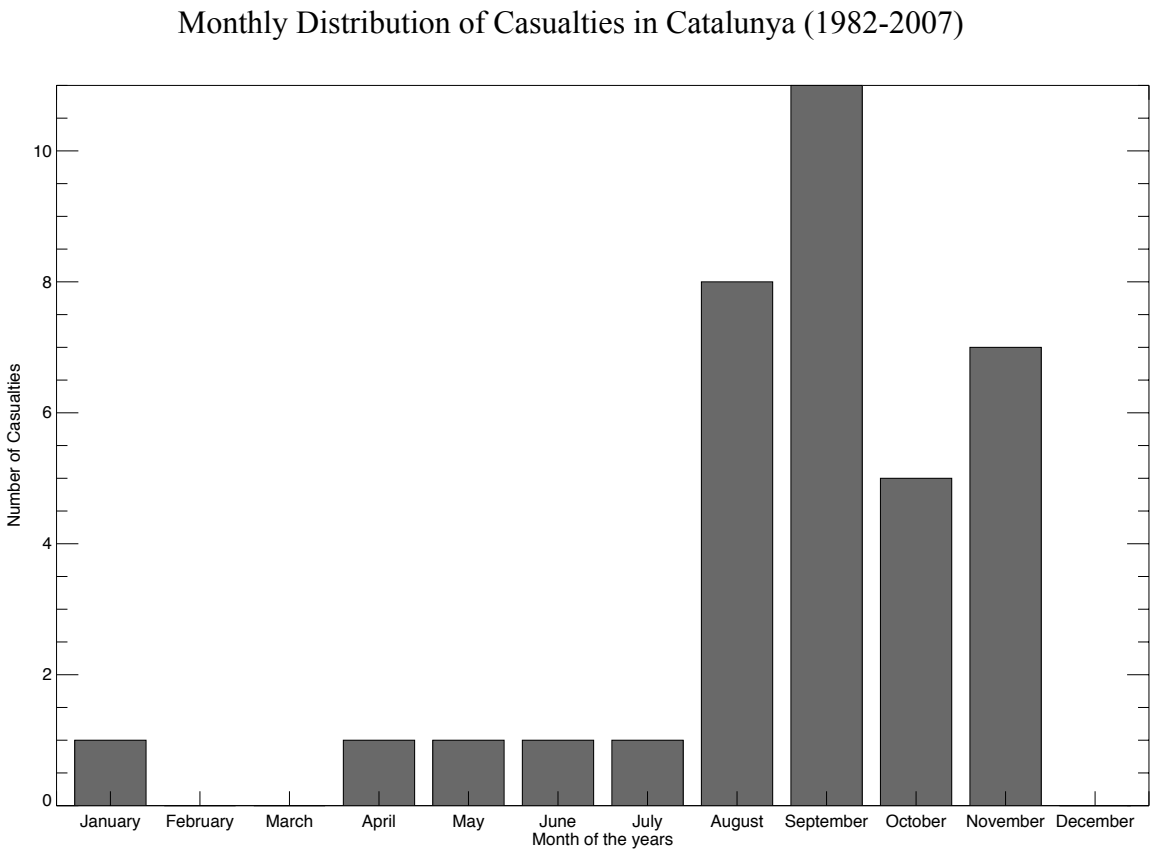

Figure 2.1: Monthly distribution of casualties produced by floods in Catalunya (1982-2007)

2.2.2. Bangladesh

Bangladesh with a gross land area of 147,570 km^2, is located within 20°N - 27°N and 88°E - 93°E at the north-eastern part of South Asia. It has approximately 710 kilometers of exposed coastline along the Bay of Bengal on its south. Bangladesh receives a sub-tropical monsoon climate, with the monsoon starts in June and continues up to October. This period accounts 80% of the total annual rainfall. The average annual rainfall varies from 1,429 mm in the western and northern parts to 4338 mm in the coastal and north-eastern parts of the country [Framji et al. (1982)]. Extreme precipitation, floods, droughts, and cyclones, among other events, are common in the study area. There are 35 rain gauge stations all over Bangladesh with 3 hours temporal resolution.

2.2.3. South Africa

South Africa occupies the southernmost part of the African continent, stretching from 22°S to 35°S and from 17°E to 33°E. It is bordered to the north by Namibia, Botswana, Zimbabwe, and Mozambique, in the west by the Atlantic Ocean and in the south and east by the Indian Ocean. The total land area is 1,219,090 km^2. It has a coastline of about 3,000 km [GCIS (2013)]. With a mean annual rainfall of approximately 450 mm, the climate of South Africa is regarded as semi-arid. There is, however, wide regional variation in annual rainfall, from less than 50 mm in the Richtersveld on the border with Namibia, to more than 3,000 mm in the mountains of the south-western Cape, however only 28% of the country receives more than 600 [©FAO (2005)]. There are 4,012 rain gauge stations all over South Africa with daily temporal resolution and different period of records. In this work, we have used 2,185 rain gauge stations for the period from January 2001 to December 2010.

2.3. Data set description

2.3.1. TRMM products 3B42 and 3B43

In this study, we have used TRMM Multi-Satellite Precipitation Analysis (TMPA) products. More specifically, 3B42 and 3B43 data, version 7 [Huffman and Bolvin (2013)]. TMPA is a calibration-based sequential scheme for combining precipitation estimates from multiple satellites, as well as gauge analyses where feasible, at fine scales [Huffman et al. (2007)]. The goal of TMPA is to provide the "best" estimate of precipitation in each grid box at each observation time. TMPA has been computed for the entire TRMM period and is available both in real time (January 2002 – present) and as a post processed product (January 1998 – present), based on calibration by the TRMM Combined Instrument (TCI) and TRMM Microwave Imager (TMI) precipitation products, respectively. The real-time and retrospective data are referred to as the RT and research products, respectively.

In reality, 3B42 and 3B43 are the post-real time precipitation estimation with respect to 3B40RT, 3B41RT, and 3B42RT data products. Because, 3B40RT, 3B41RT, and 3B42RT are the experimental best-effort real-time monitoring product about 9 hour after real time while 3B42 and 3B43 are produced about 2 months after the end of each month. Huffman et al.

(2007) presented two important differences between the real-time and research products. First, the RT product uses TMI precipitation as the calibrator and the research product uses the TCI, which is considered to be better but is not available in real time. Second, the research product rescales the monthly sums of the 3-hourly fields to a monthly gauge analysis, but such a rescaling is not available in real time. The Climate Assessment and Monitoring System (CAMS) 0.25° X 0.25° monthly gauge analysis is used to adjust the initially processed (IP) TMPA estimates; the Global Precipitation Climatology Center (GPCC) 1.0° X 1.0° monthly monitoring product is used to adjust the reprocessed (RP) TMPA [Su et al. (2008)]. Currently, the RP TMPA begins 1 January 1998 and ends March 2005. The IP TMPA starts in April 2005 and continues to the present. The gauge adjustment only applies to the research product; the real-time TMPA is currently not corrected.

3B42 and 3B43 data sets have same temporal coverage (from 1998-01-01 to present), geographic coverage (latitude: 50°S - 50°N and longitude: 180°W - 180°E), and horizontal resolution (0.25° X 0.25°; nlat = 400 and nlon = 1440) with 1440 columns and 400 rows to cover the globe [Huffman and Bolvin (2013)].

3B42 3-Hourly product is the combined microwave-infrared estimated rainfall with gauge adjustment centered at the middle of each 3-hour period [Huffman and Bolvin (2013); Figure 2.2]. Figure 2.3 shows the daily accumulation of 7 August 2012.

3B43 monthly data is the monthly precipitation accumulation and is produced about two months after the end of each month using TRMM and other satellites product 3B42 and the CAMS (Climate Anomaly Monitoring System) global gridded rain gauge data, produced by NOAA's Climate Prediction Center and the global rain gauge product produced by the Global Precipitation Climatology Center [GPCC; Huffman and Bolvin (2013); Figure 2.4].

We have compared the 3B42 monthly accumulation with daily and/or 3-hourly accumulations. Since, daily product is the sum of the individual 3-Hourly products for the specified day, it is rational to compare monthly accumulation with anyone of the daily or hourly accumulation. Figures 2.5 (a) and 2.5 (b) represent the monthly accumulation for the month of July 2012 by using 3B42 3-hourly and 3B43 monthly products respectively.

Figures 2.5 (a) and 2.5 (b) shows the comparison of monthly accumulation between 3B42 and 3B43 products; since 3B43 is produced about two months after at the end of each month by using 3B42 and/or gridded rain gauge data, sometimes this product could be more quality controlled than 3B42. Figure 2.6 shows the absolute difference between 3B43 and 3B42 for the month of July 2012. From the Figure 2.6 it is shown that the maximum difference between 3B43 and 3B42 could be more than 10 mm. Actually, the maximum difference is 208 mm. The number of pixel that has precipitation value greater than 10 mm is 5780. 795 pixels have rainfall value between 50 mm and 100 mm. 93 pixels show between 100 mm and 150 mm. There are 25 pixels that have precipitation value within the range from 150 mm to 200 mm. One pixel has precipitation value greater than 200 mm.

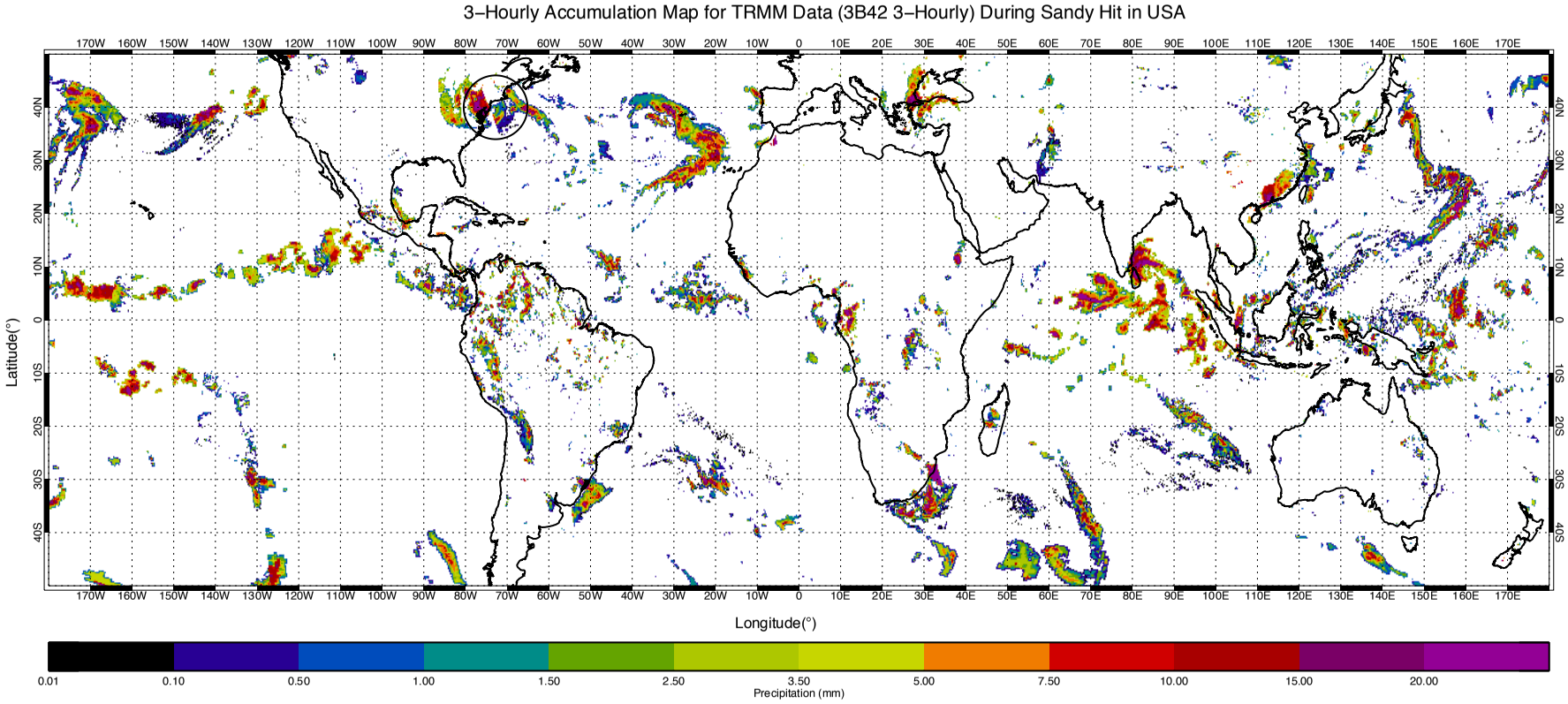

Figure 2.2: Image of the 3B42 3-Hourly product on 29 October 2012 during devastating Hurricane Sandy hit North-Eastern part of United States (showing by circle on the image).

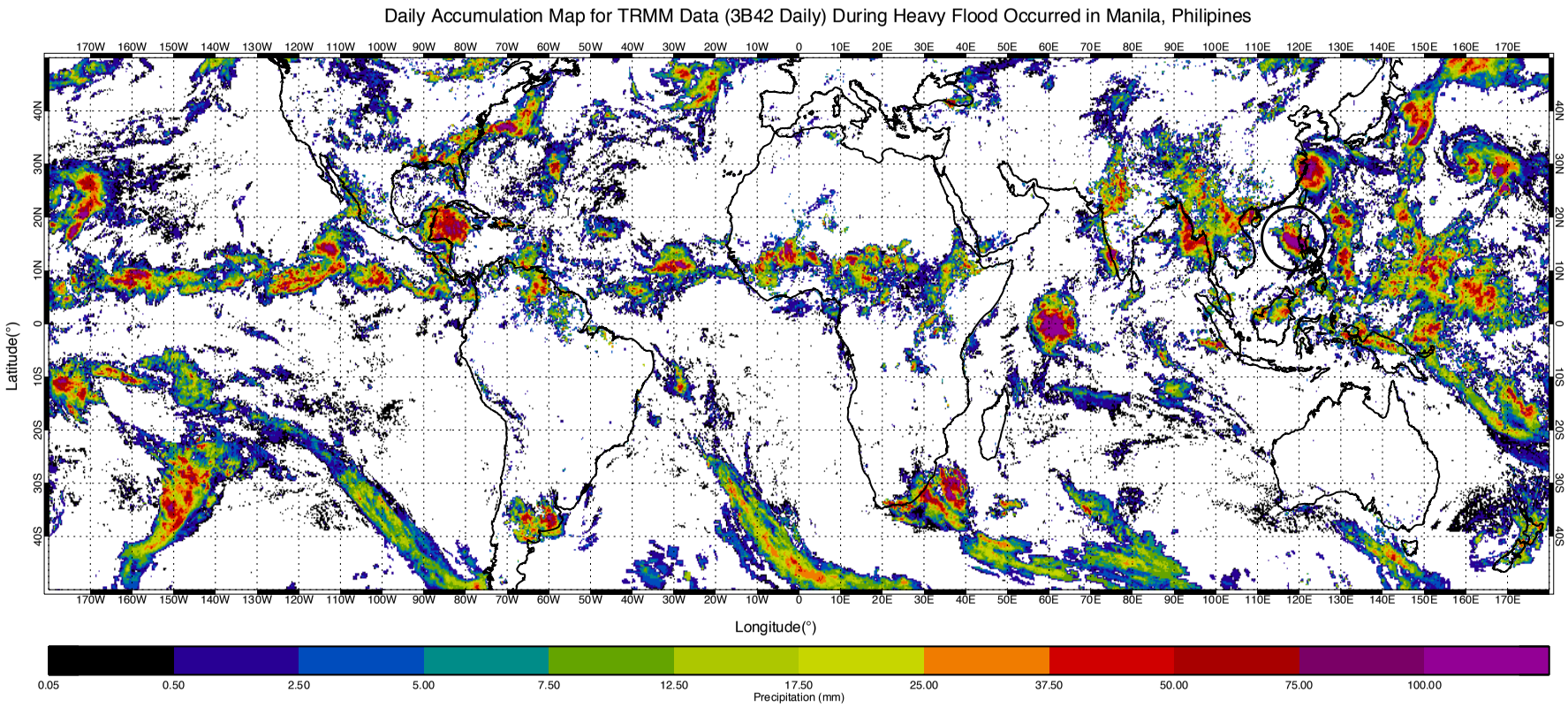

Figure 2.3: Image of the 3B42 Daily product on 7 August 2012 during heavy flood occurred in Manila, Philippines (showing by circle on the image).

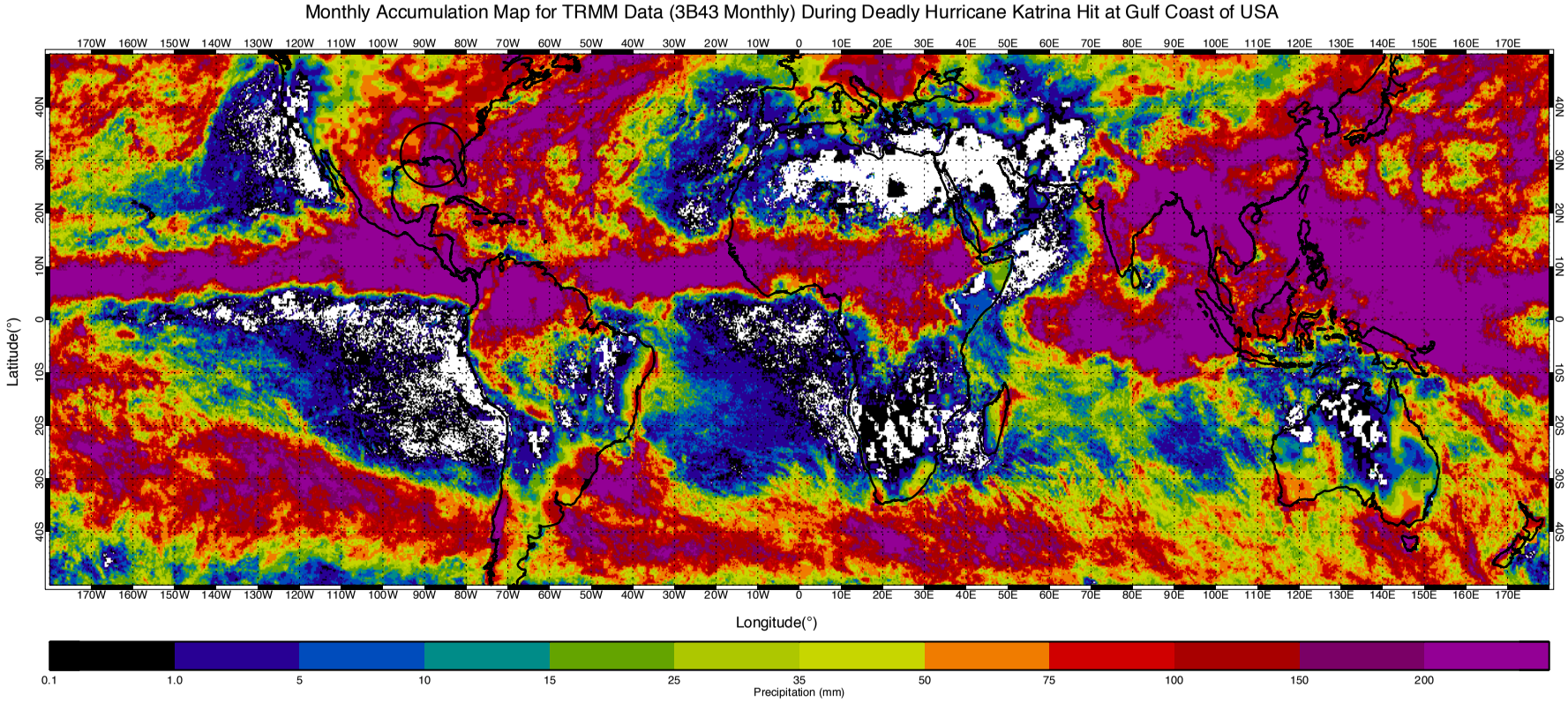

Figure 2.4: Image of the 3B43 Monthly product for the month of August 2005 during devastating Hurricane Katrina hit at Gulf coast of United States of America (showing by circle on the image).

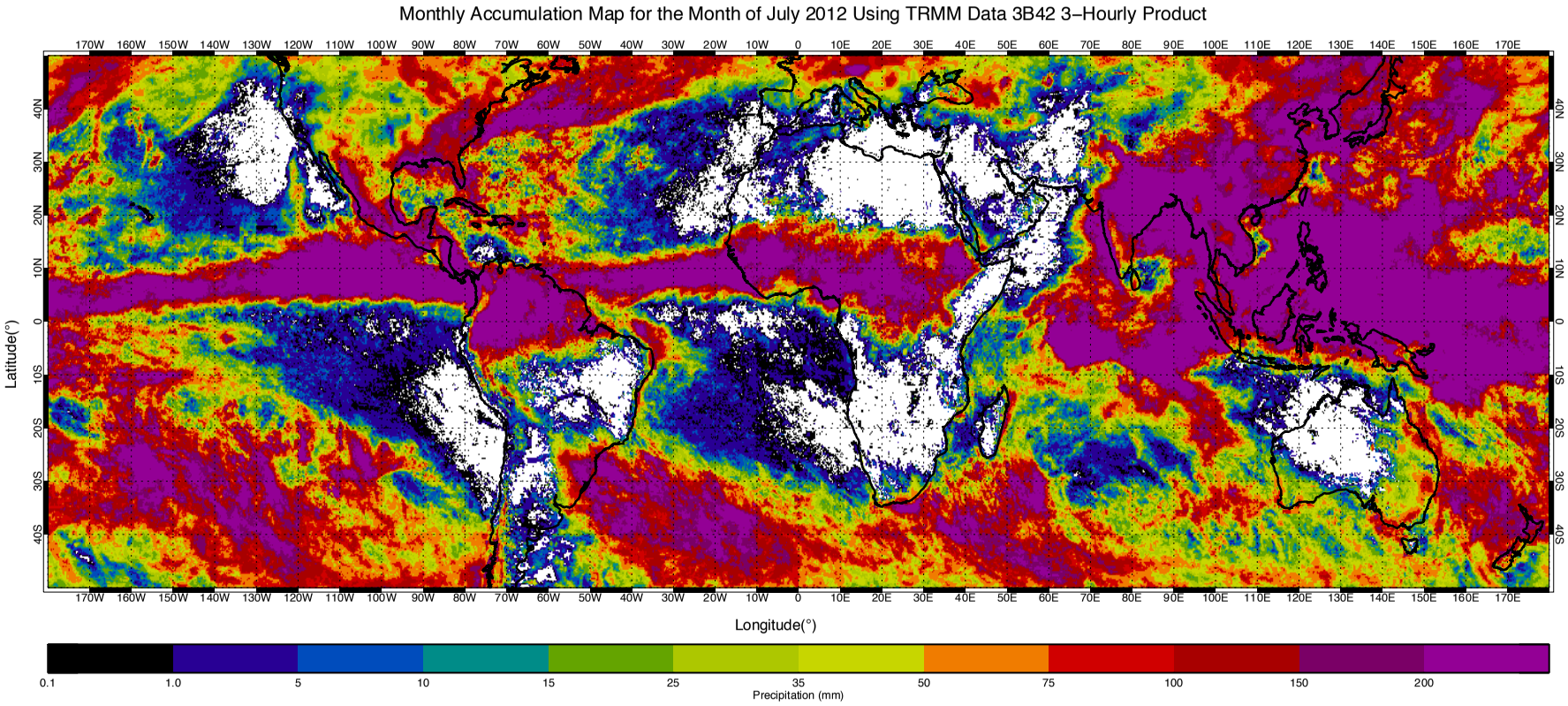

Figure 2.5: (a) Image of the monthly accumulation map for the month of July 2012 using 3B42 3-hourly product.

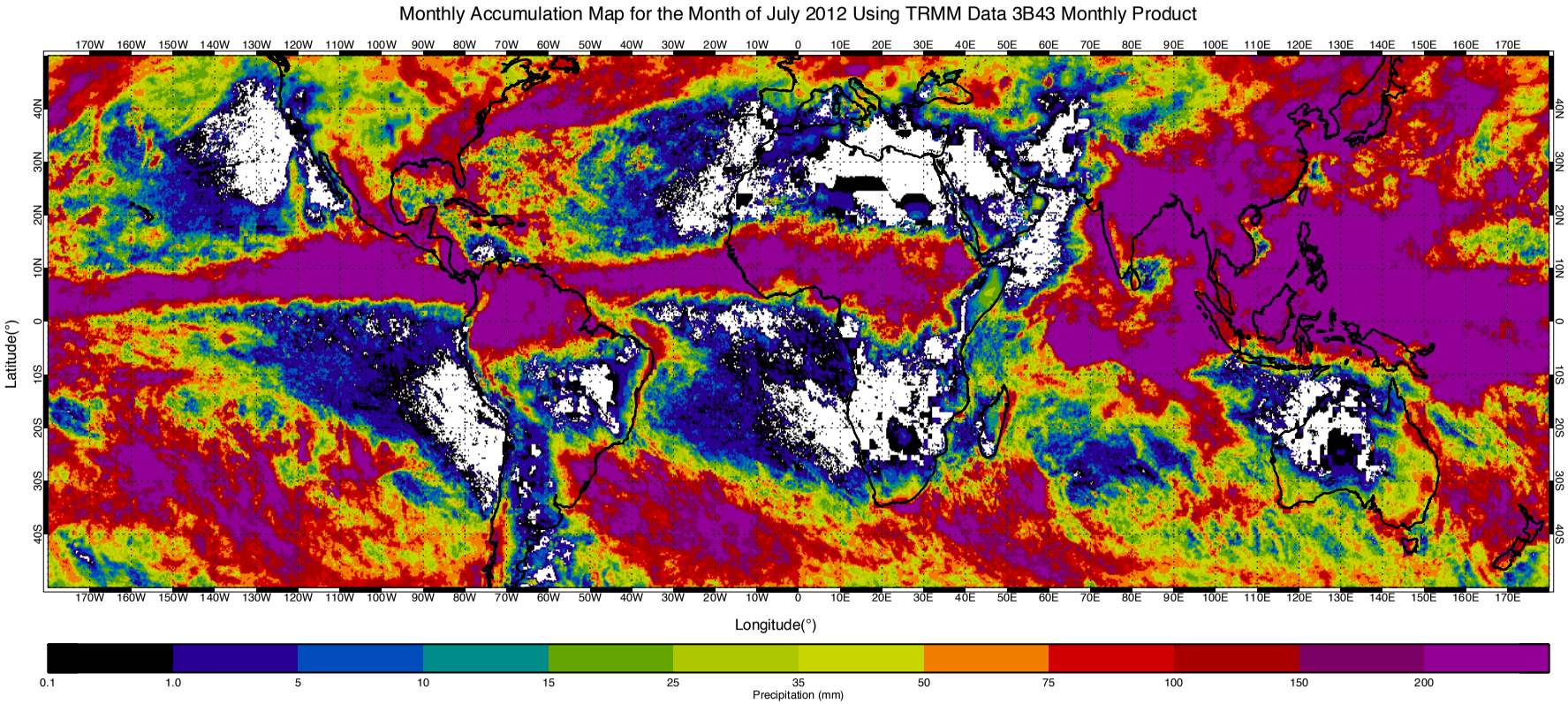

Figure 2.5: (b) Image of the monthly accumulation map for the month of July 2012 using 3B43 monthly product.

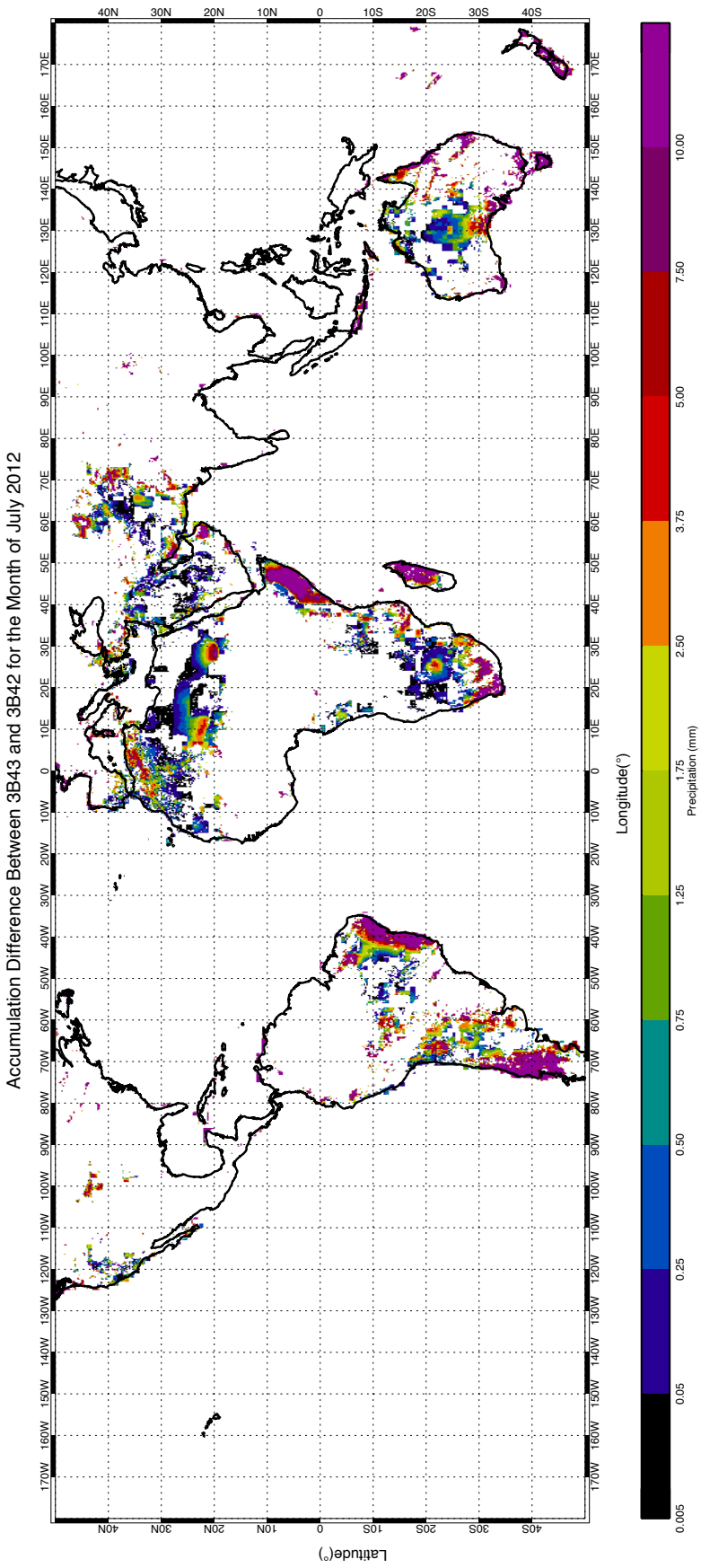

Figure 2.6: Image of the accumulation defference between 3B43 and 3B42 for the month of July 2012.

CHAPTER 3. COMPARISON BETWEEN TRMM AND RAIN GAUGE

3.1. Introduction

As mentioned earlier, our main intention is to verify the performance of space borne satellite product (i.e. 3B42 daily and 3B43) at local scale and also to implement an approach to apply these products at local scale. For the first reason, three statistical parameters coefficient of correlation, bias, and root mean square error are calculated for daily and monthly temporal resolutions at the above-mentioned three case study areas to get an insight of the satellites products performance. In this chapter, measured statistical parameters are discussed at each case study area.

3.2. Statistical parameters

3.2.1. Coefficient of correlation (R)

Here, we have calculated the linear Pearson correlation coefficient. Simply, it is a measure of the linear interdependence of two variables that ranges in value from -1 to +1, indicating perfect negative correlation at -1, absence of correlation at zero, and perfect positive correlation at +1. The correlation between satellite rain estimates and rain gauge measurements has been estimated as:

$$R = \frac{n\sum_{i=1}^{n}\left(P_{rag}P_{sat}\right) - \left(\sum_{i=1}^{n}P_{rag}\right)\left(\sum_{i=1}^{n}P_{sat}\right)}{\sqrt{\left[n\sum_{i=1}^{n}P_{rag}^{2} - \left(\sum_{i=1}^{n}P_{rag}\right)^{2}\right]\left[n\sum_{i=1}^{n}P_{sat}^{2} - \left(\sum_{i=1}^{n}P_{sat}\right)^{2}\right]}} \quad (1)$$

where P_{sat} are satellite estimates in millimeters (mm), P_{rag} are rain gauge estimates in millimeters (mm), and n is the number of concurrent observations. Here, the index i is not used to simplify the equations $P_{sat_i} = P_{sat}$.

3.2.2. Bias

Bias is defined as the mean difference between satellite-based precipitation accumulations and rain gauge accumulations. It is expressed in millimeters (mm).

$$Bias = \frac{\sum_{i=1}^{n} P_{sat} - P_{rag}}{n} \ (mm) \tag{2}$$

where P_{sat}, P_{rag}, and n are as defined in equation (1).

3.2.3. Root mean square error

The difference between satellite-based observations and rain gauge observations are each squared and are then averaged over the sample. Finally, the square root of the average value is taken. Here, it is expressed in millimeter (mm). RMSE can be expressed as follows:

$$RMSE = \sqrt{\frac{\sum_{i=1}^{n}\left(P_{sat} - P_{rag}\right)^2}{n}} \ (mm) \tag{3}$$

where P_{sat}, P_{rag}, and n are as defined in equation (1).

3.3. Study areas

In these sections, one daily and one monthly product with large amount of precipitation are discussed for each case study area individually. Later, for each case study area we have computed the three statistical parameters for the time period from January 2005 to December 2009, are also discussed.

3.3.1. Precipitation over case study areas (2005-2009)

Precipitation over the three case study areas shows very distinct pattern with different areal distribution. All case study areas have coast with different geography and orography. Orography plays a very important role in rainfall distribution. Here, we have determined the

mean yearly precipitation at each case study area and compared with the average precipitation for the five years from 2005 to 2009.

To determine the average (2005-2009) and mean yearly precipitation, we have measured the pixel value over each rain gauge station and divided the total of all pixels value by the number of rain gauge. In case of Catalunya and South Africa, we have reduced the number of rain gauge station to calculate both the average and yearly mean simply because if the number of rain gauge below a TRMM pixel is more than one the impact of this pixel will be more than the pixel which has only one rain gauge. To do so, more than 0.125° is used as the minimum distance between the gauges. Table 3.1 shows the departure of mean yearly precipitation from the average (2005-2009) value. Positive departure denotes surplus rainfall with reference to average precipitation and negative departure denotes vice versa.

Table 3:1 Comparison of mean yearly precipitation with average rainfall (2005-2009)

	Average (2005-2009), mm	Departure from average, mm				
		2005	2006	2007	2008	2009
Catalunya	652	23	-76	-59	101	12
Bangladesh	2386	73	-251	459	-103	-181
South Africa	635	-85	-102	29	-4	162

Figures 3.1, 3.2, and 3.3 represent the average (2005-2009) and mean annual precipitation over Catalunya, Bangladesh, and South Africa respectively. The average rainfall over Catalunya was 652 mm for the time period 2005-2009 and maximum 101 mm excess rainfall was observed in 2008 while maximum less precipitation was found 76 mm in 2006 (Table 3.1 and Figure 3.1). Out of these three case study areas, maximum 2386 mm average precipitation was observed in Bangladesh, which is certainly very high with respect to Catalunya and South Africa. Maximum 459 mm excess rainfall was found over Bangladesh in 2007 whereas maximum 251 mm less precipitation was estimated in 2006 with respect to the average value (Table 3.1 and Figure 3.2). In South Africa maximum 162 mm extra precipitation with respect to the average value was estimated in 2009 and highest 102 mm negative departure was observed in 2006 (Table 3.1 and Figure 3.3). From Table 3.1 it is shown that for all three case

study areas maximum negative departure i.e. less rainfall with reference to the average estimation was observed in 2006.

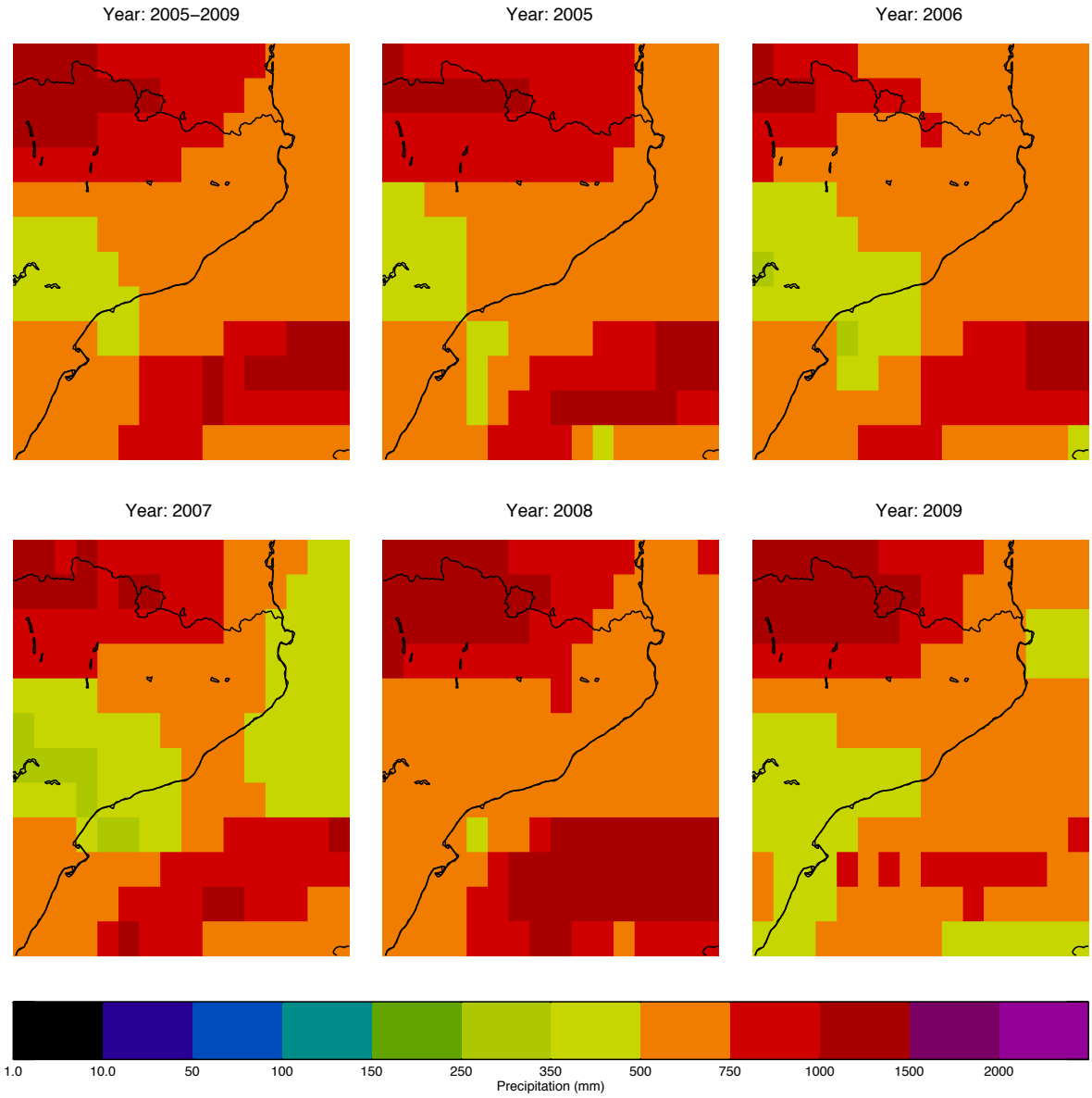

Figure 3.1: Average (2005-2009) and mean annual precipitation over Catalunya using TRMM (3B43) product.

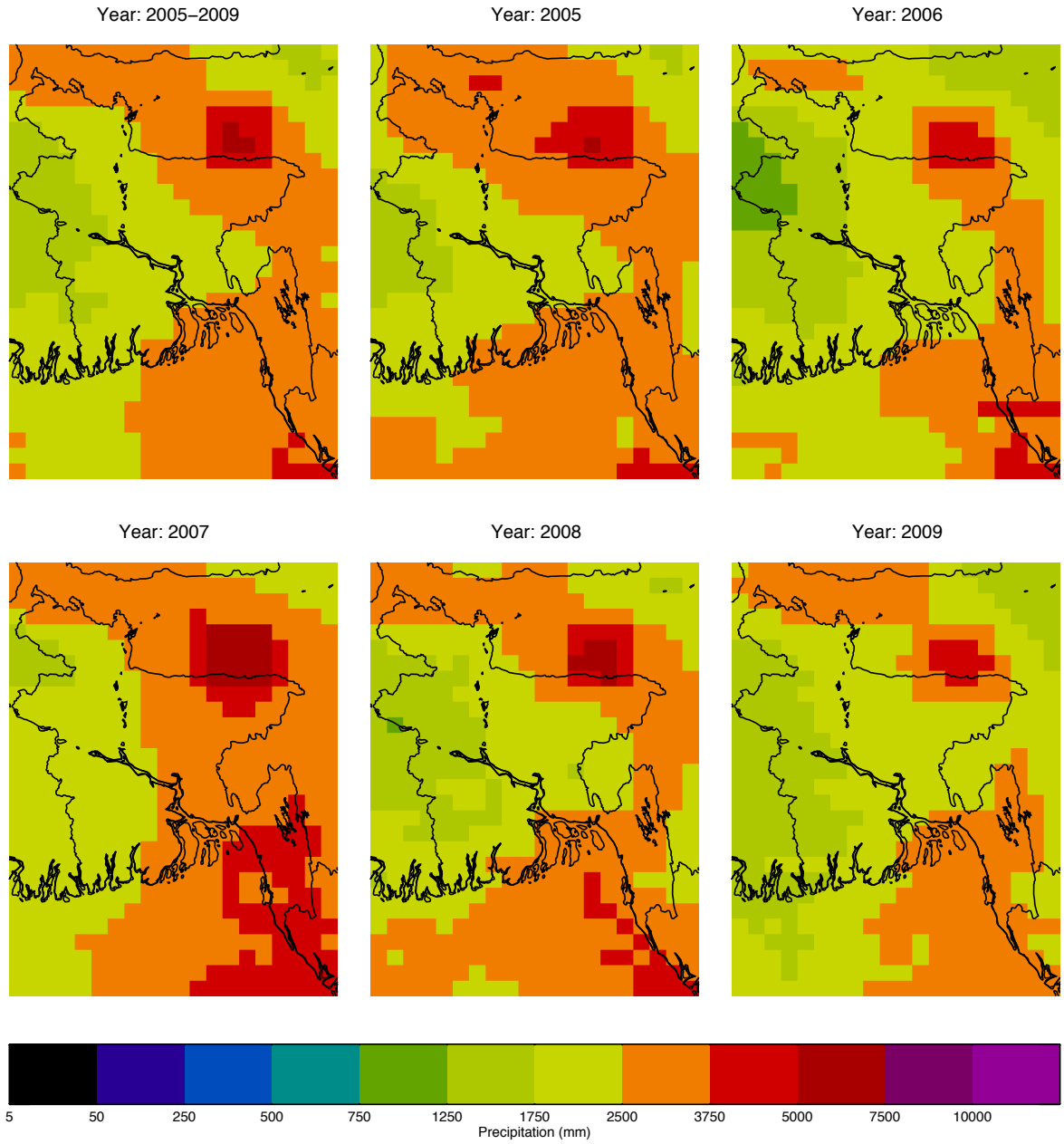

Figure 3.2: Average (2005-2009) and mean annual precipitation in Bangladesh using TRMM (3B43) product.

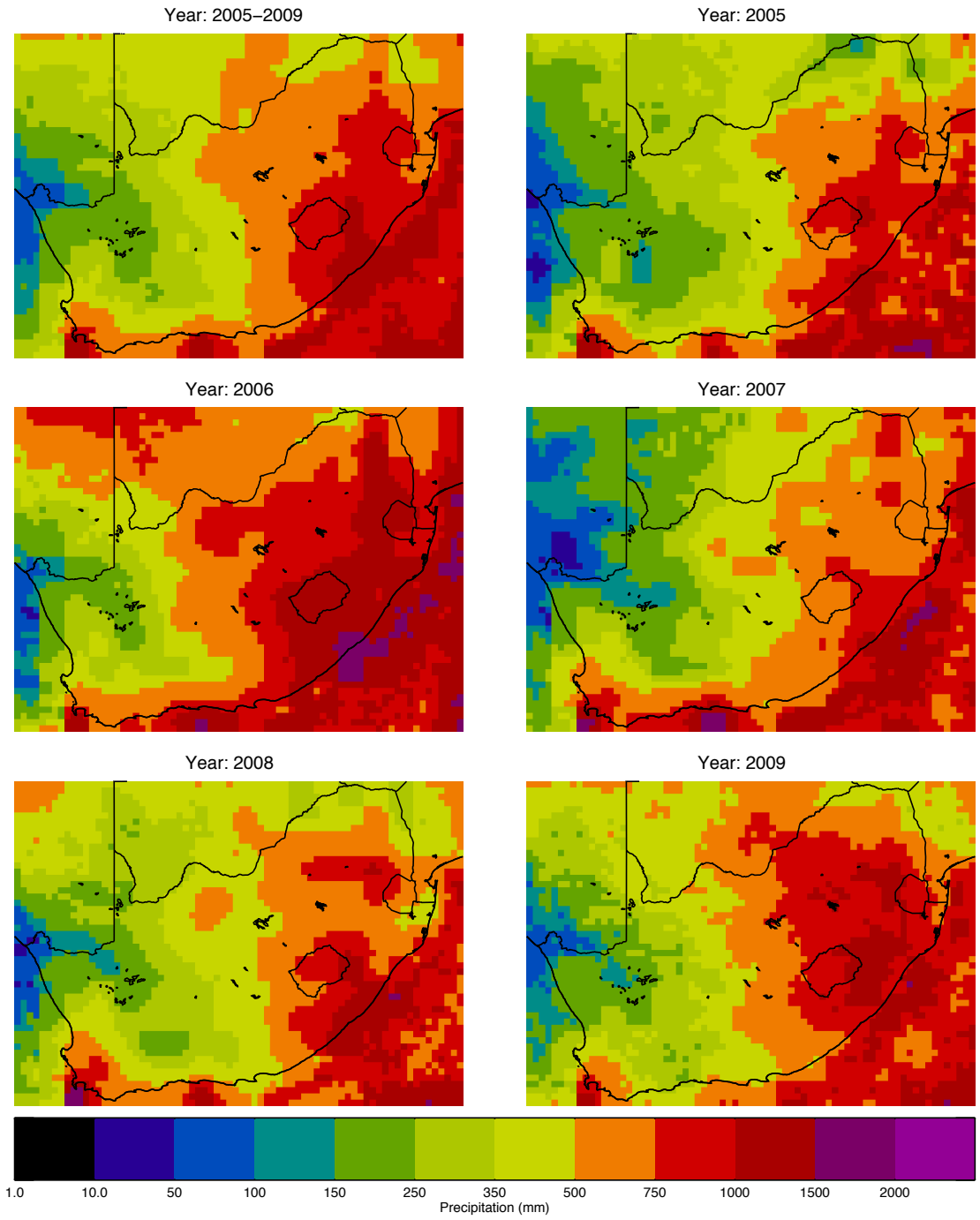

Figure 3.3: Average (2005-2009) and mean annual precipitation over South Africa using TRMM (3B43) products.

3.3.2. Catalunya, Spain

We have studied several days and months with large rainfall amounts over Catalunya. Each event is showing different results from others.

3.3.2.1 Daily event on 9 October 2002

Between 8 and 10 October 2002 there were several heavy rainfall events over Catalunya. The maximum rainfall was recorded in the coast near Barcelona, resulting in the closure of Barcelona Airport. 196.5 mm rainfall over a period of 48 hours was recorded at Baix Llobregat area and out of which 174.1 mm rainfall was collected over a period of 24 hours at the station of Sant Joan Despi [Llasat et al. (2004)]. Other stations at the same area collected rainfall with different temporal scale such as 162.4 mm in 12 hours at Olivella, 127.7 mm in 6 hours and 50.2 mm in 1 hour at the stations in Sant Joan Despi. Figure 3.4 shows the daily accumulation map for TRMM data 3B42 daily over Catalunya on 9 October 2002.

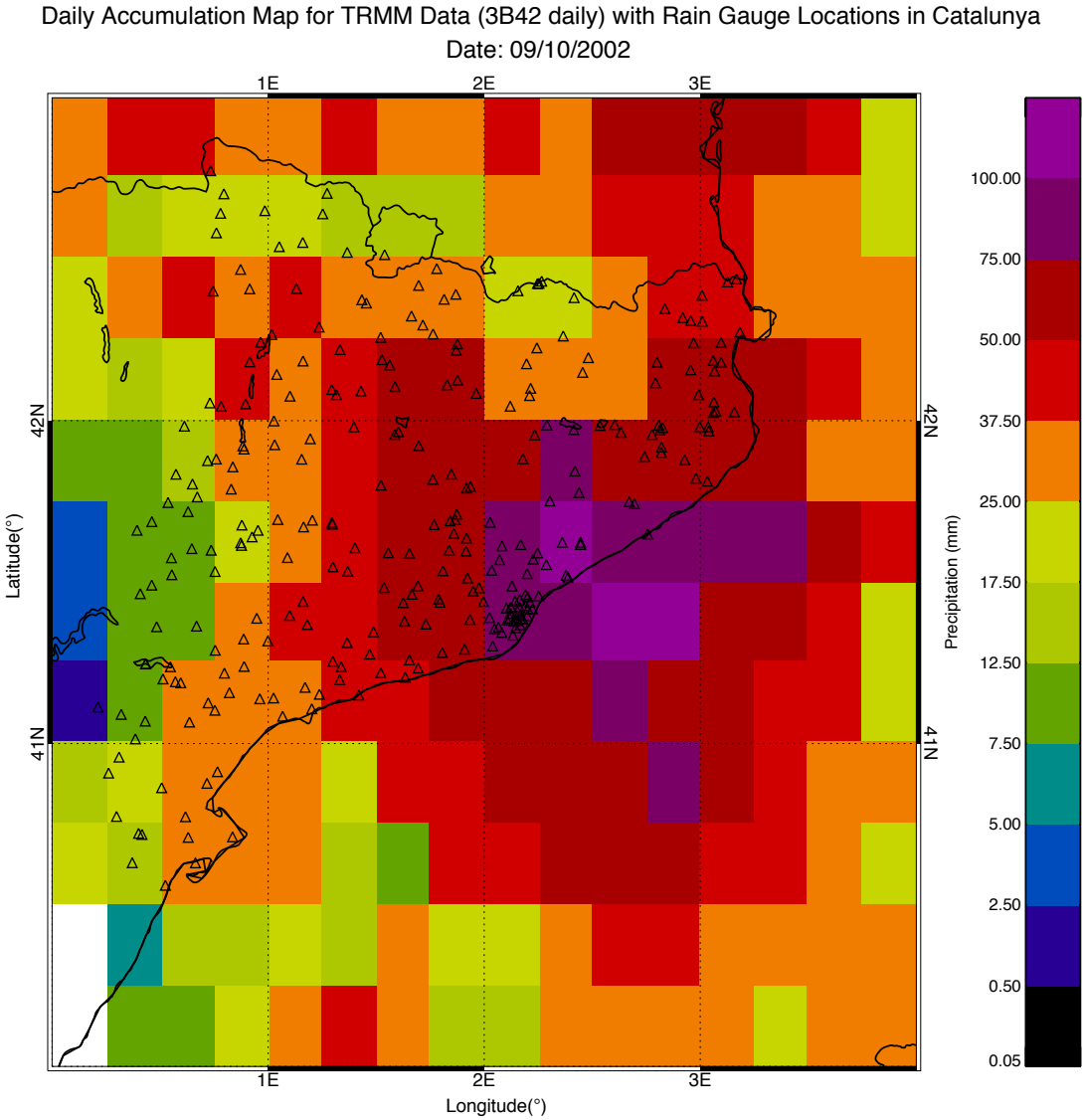

Figure 3.4: Daily accumulation map for TRMM data 3B42 daily over Catalunya on 9 October 2002 with rain gauge locations.

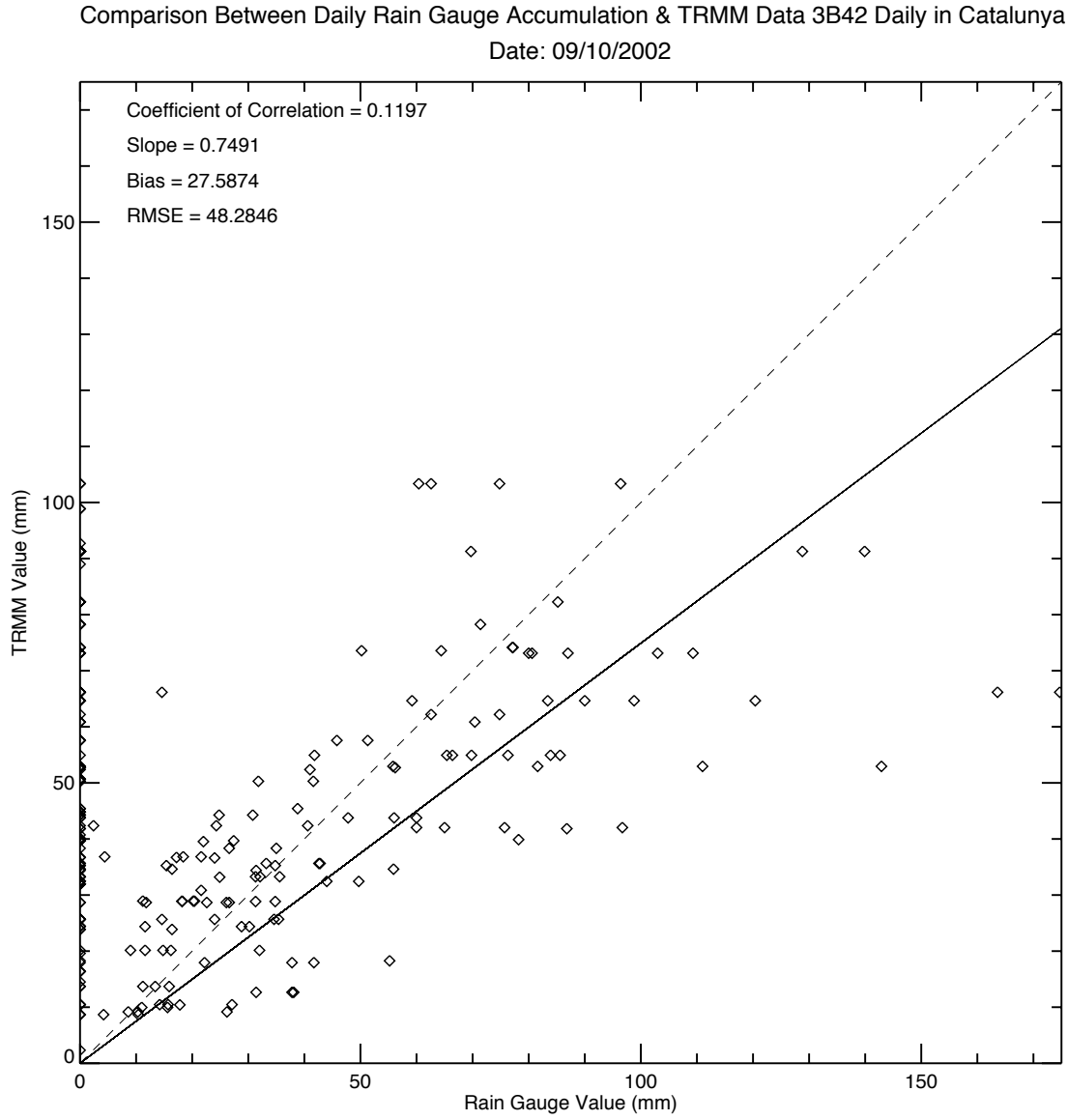

Figure 3.5: Comparison between rain gauge observations and TRMM estimates before discarding zero rain gauge values.

Figures 3.5 and 3.6 show the comparison between rain gauge and satellite estimates over Catalunya on 9 October 2002 before and after removing zero rain gauge values respectively. If we remove the zero rain gauge values from the data set, the coefficient of correlation value increases from 0.12 to 0.71 while the slope remains same. Bias changes from 28 mm to -5 mm, the latter indicating underestimation by the satellites. The higher rain gauge values keeps the slope lower than 1. TRMM pixel shows the average value over a region while several

gauge stations could estimate different values under the same pixel because precipitation is highly variable with respect to space and time.

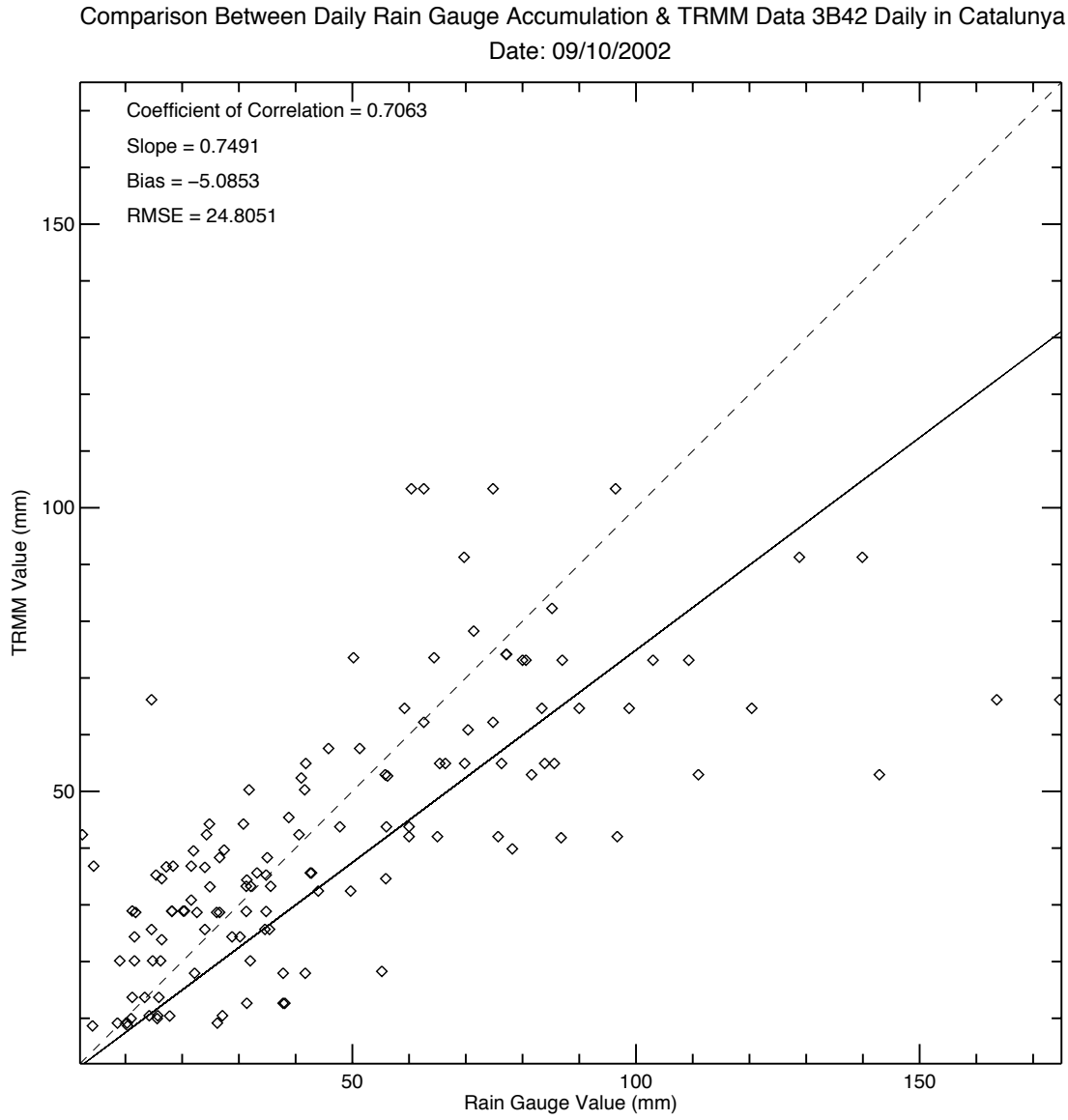

Figure 3.6: Comparison between rain gauge and TRMM estimation after discarding zero rain gauge values.

3.3.2.2 Monthly rainfall on October 2000

A torrential precipitation event affected eastern Spain during 21 to 24 October 2000. Total accumulated rainfall higher than 500 mm was registered at some locations, with values up to

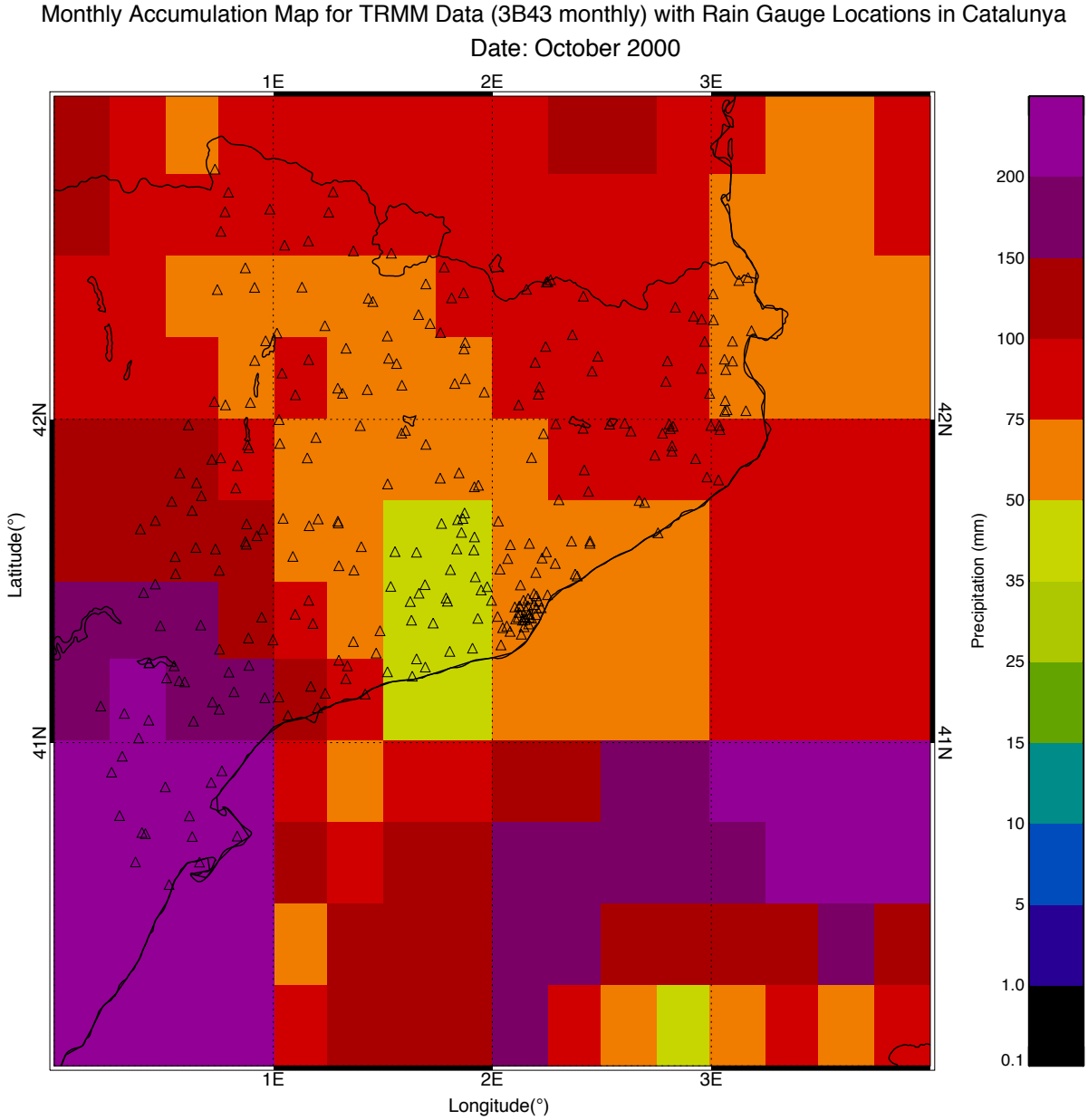

Figure 3.7: Monthly accumulation map for TRMM data 3B43 over Catalunya on October 2000 with rain gauge locations.

300 mm in a 24-h period. Total rainfall amounts in excess of 500 mm were registered in the locations of Valencia and Catalunya during 21 to 24 October. Serious floodings produced 8 casualities, as well as critical damages to fruit crops and populated areas. Roads and railways of the area were damaged and the total economical loss estimated by insurance companies was 100 million euro [Homar et al. (2002)]. The synoptic-scale meteorological setting of the event is characterized mainly by the presence of a cold cutoff low aloft, south of the Iberian Peninsula, and an easterly maritime flow toward the Spanish coast at low levels. The situation

was very stationary (4 – 5 days) and therefore ensured a continuous moisture supply and convective instability replenishment [Homar et al. (2002)]. Figure 3.7 shows the monthly accumulation map of TRMM data 3B43 over Catalunya with the rain gauge locations.

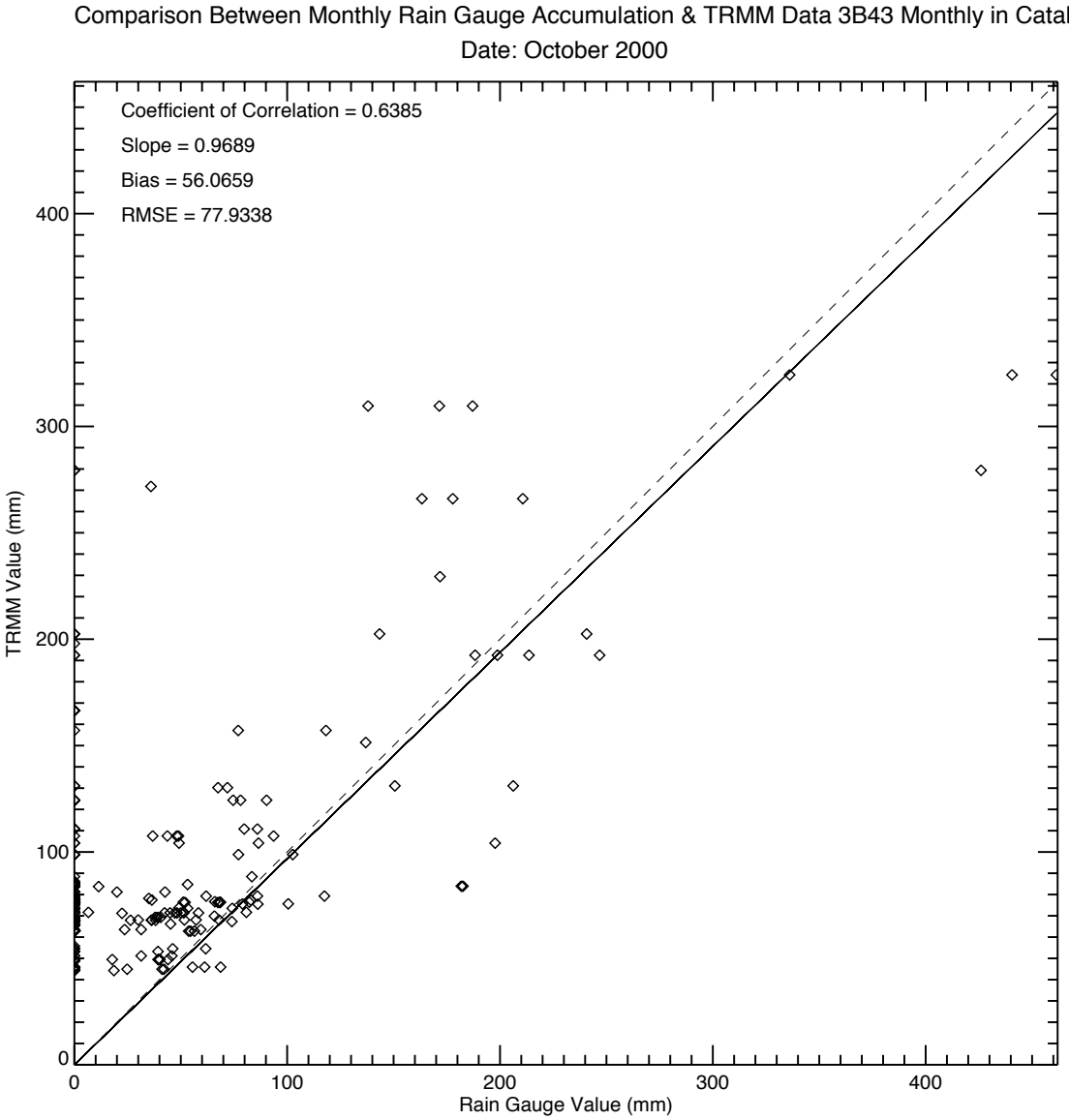

Figure 3.8: Comparison between rain gauge and TRMM estimation before discarding zero rain gauge values.

Figures 3.8 and 3.9 show the comparison between rain gauge and satellite estimates over Catalunya for the month of October 2002 before and after discarding zero rain gauge values respectively. If we remove the zero rain gauge values from the data set, the coefficient of correlation value increases from 0.64 to 0.79 while the slope remains same, 0.97 (Figures 3.8

and 3.9). Bias changes from 56 mm to 18 mm, which still indicates overestimation by the satellite. RMSE value also improves from 78 mm to 54 mm. The results could also be improved if we take the mean value of the rain gauge stations under the same TRMM pixel.

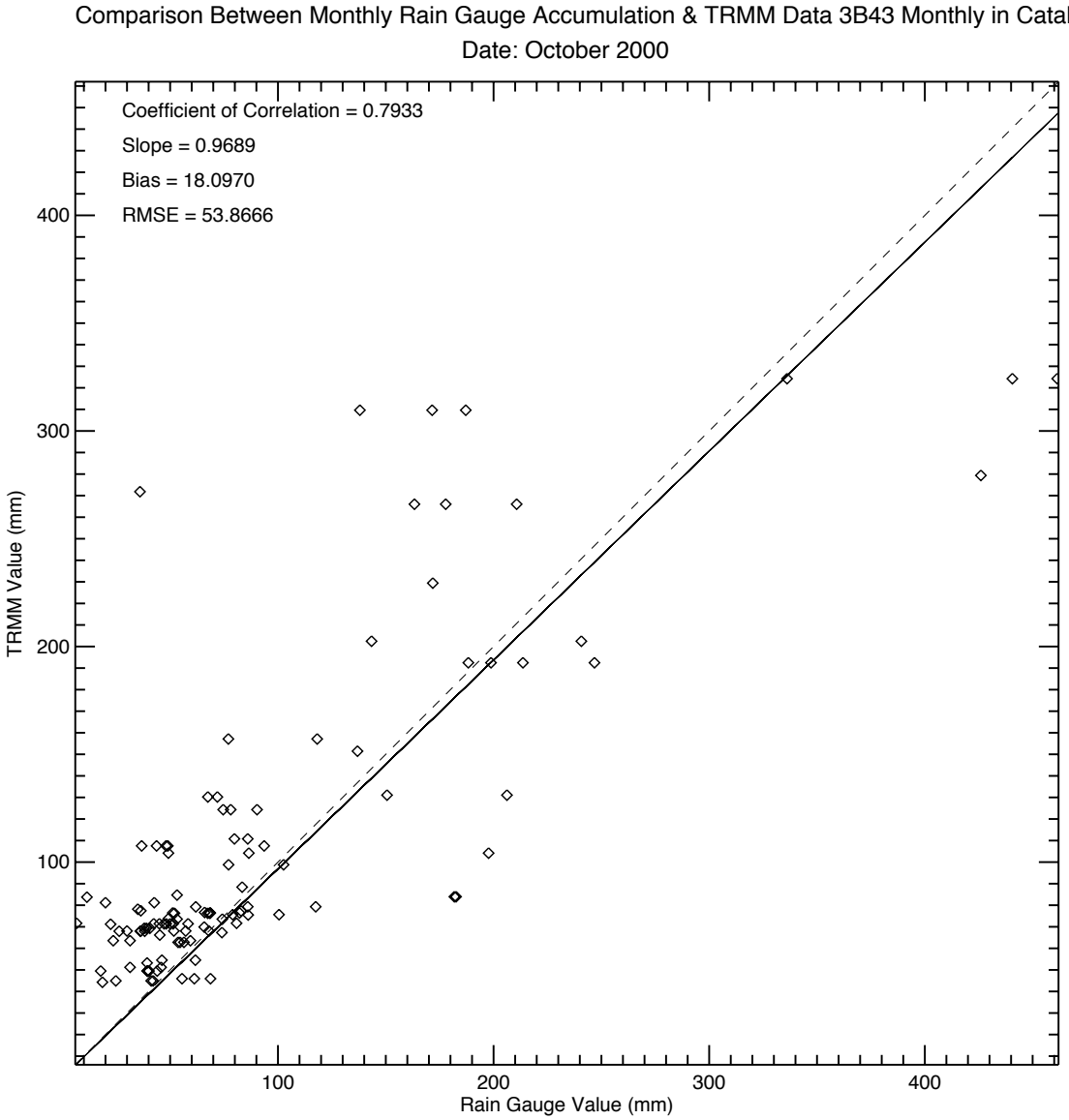

Figure 3.9: Comparison between rain gauge and TRMM estimation after discarding zero rain gauge values.

3.3.2.3 Daily statistical parameters

Daily mean rain gauge values are measured from the rain gauge stations available on that day after excluding the zero rain gauge values and mean TRMM values are also measured by

using the pixels over the corresponding rain gauge stations (Figure 3.10). Coefficient of correlation, bias, and RMSE are also calculated by using rain gauge and corresponding TRMM pixel values (Figure 3.10). Discontinuities of correlation coefficients represent the NaN (not a number). Only the bias values within the range (-30 mm < bias < 30 mm) are considered and the corresponding RMSE values are also measured (Figure 3.11).

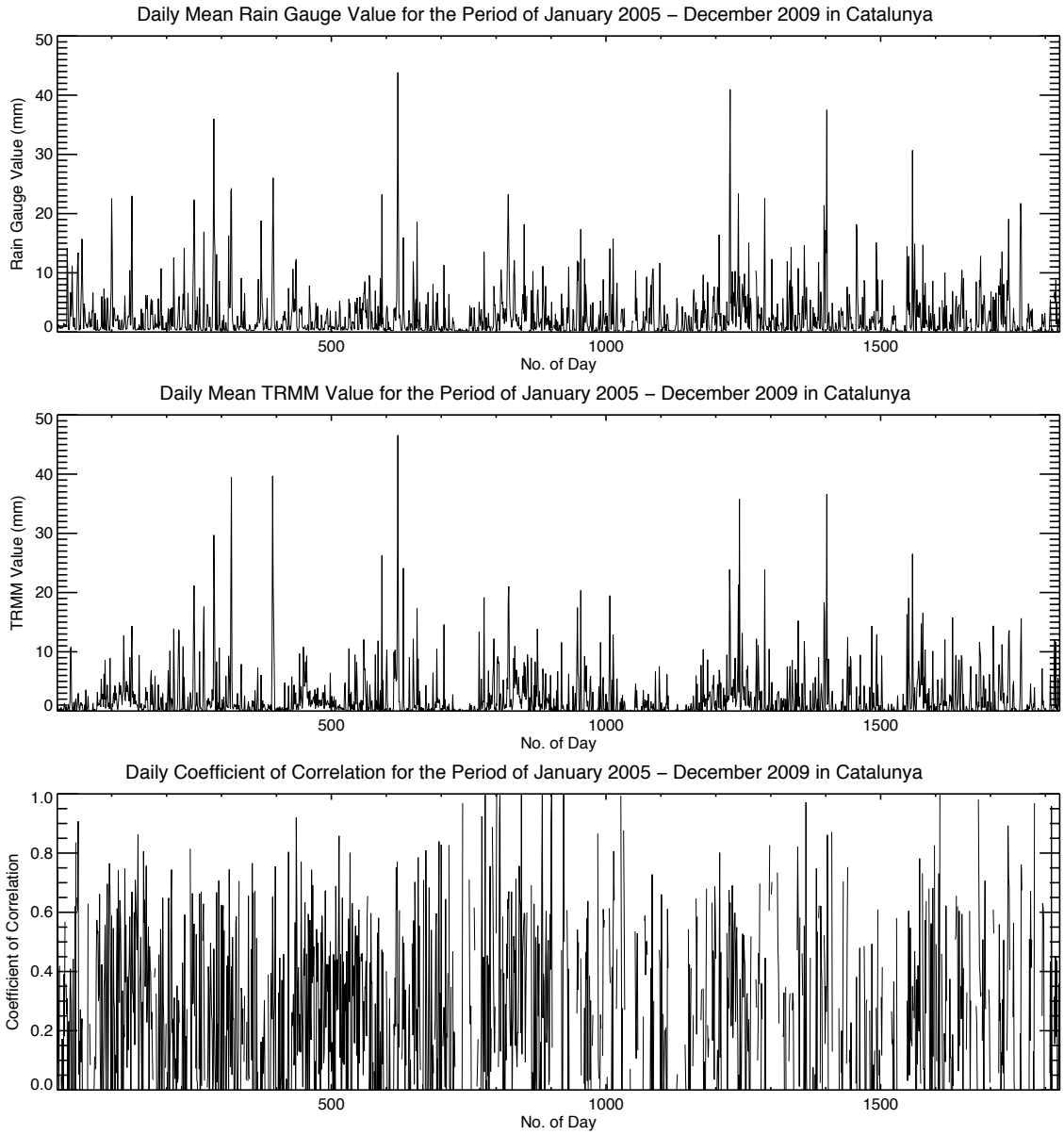

Figure 3.10: Daily mean rain gauge and TRMM values with daily coefficient of correlation for the period January 2005 – December 2009 in Catalunya.

For the specified time period of January 2005 – December 2009 there are 1826 days out of which 60 days have coefficient value greater than 0.70 and less than 0.90 (Figure 3.10). For this range bias and RMSE ranges between -8 mm and 8 mm (Figure 3.11) and between 0 mm

and 23 mm (Figure 3.11) respectively. Number of days that are showing greater than 0.90 correlation value is 5. Coefficient value varies from 0.50 to 0.70 for 203 days with getting high bias and RMSE values (RMSE ranges from 0 mm to 899 mm and bias from -123 mm to 23 mm). 417 days have correlation value between 0.20 and 0.50 with having bias values from -15 mm to 15 mm and RMSE from 0 mm to 33 mm. Finally, 642 days have correlation value less than 0.20.

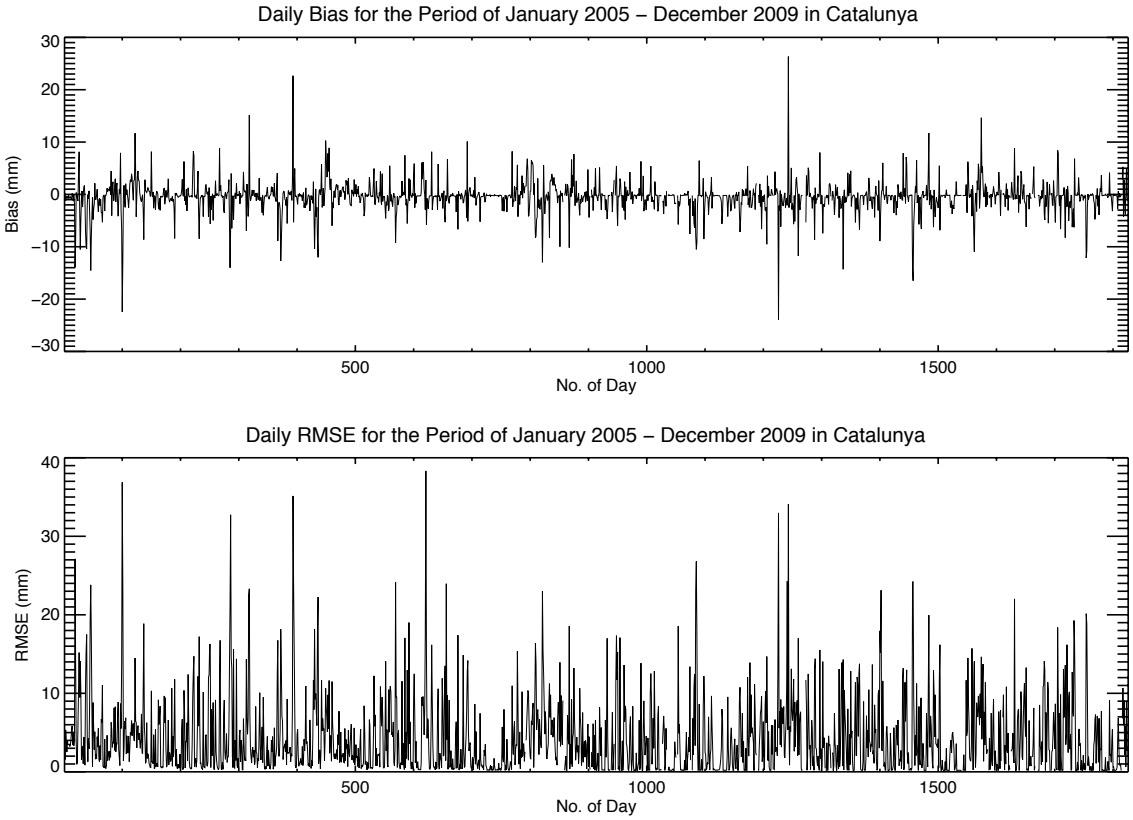

Figure 3.11: Daily bias and RMSE for the Period January 2005 – December 2009 in Catalunya.

3.3.2.4 Monthly statistical parameters

Monthly mean rain gauge and TRMM values, coefficient of correlation, bias, and RMSE are also calculated as we have done for daily events. Figure 3.12 shows the monthly coefficient of correlation along with monthly mean rain gauge and TRMM values for the study period from

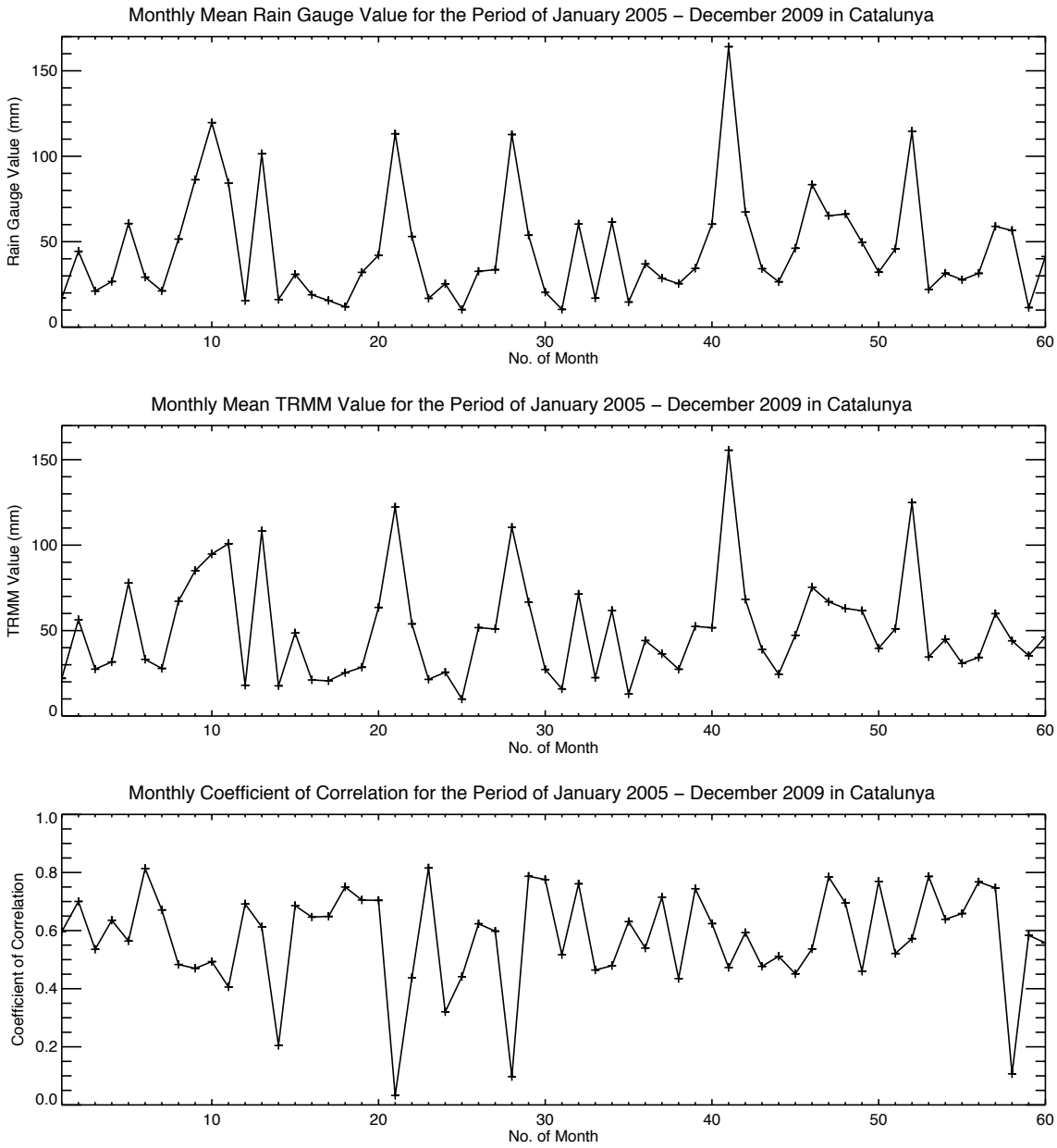

Figure 3.12: Monthly mean rain gauge and TRMM values with monthly coefficient of correlation for the period January 2005 – December 2009 in Catalunya.

January 2005 to December 2009. Except few months in the first two years, monthly mean rain gauge and TRMM values show same pattern of change at each month (Figure 3.12). From the Figure 3.12 it is shown that 12 months have correlation value less than 0.20 out of which September and October get maximum 2 times less than 0.20. For these months corresponding bias and RMSE values are also very high (Figure 3.13). 12 months out of these 60 months have correlation value greater than 0.20 and less than 0.50. January, February, September, and October get maximum 2 times coefficient value within this range. For this range maximum positive and negative bias values are 17 mm and -25 mm respectively. RMSE value ranges

between 7 mm and 63 mm for the specified range of coefficient value. 23 months have coefficient value greater than 0.50 and less than 0.70. For this range maximum positive and negative bias values are 24 mm and -9 mm respectively and the maximum and minimum RMSE values are 50 mm and 14 mm respectively. Another 13 months have coefficient value greater than 0.70 and the maximum monthly correlation value is 0.81. Bias and RMSE value vary from -4 mm to 21 mm and from 15 mm to 36 mm respectively.

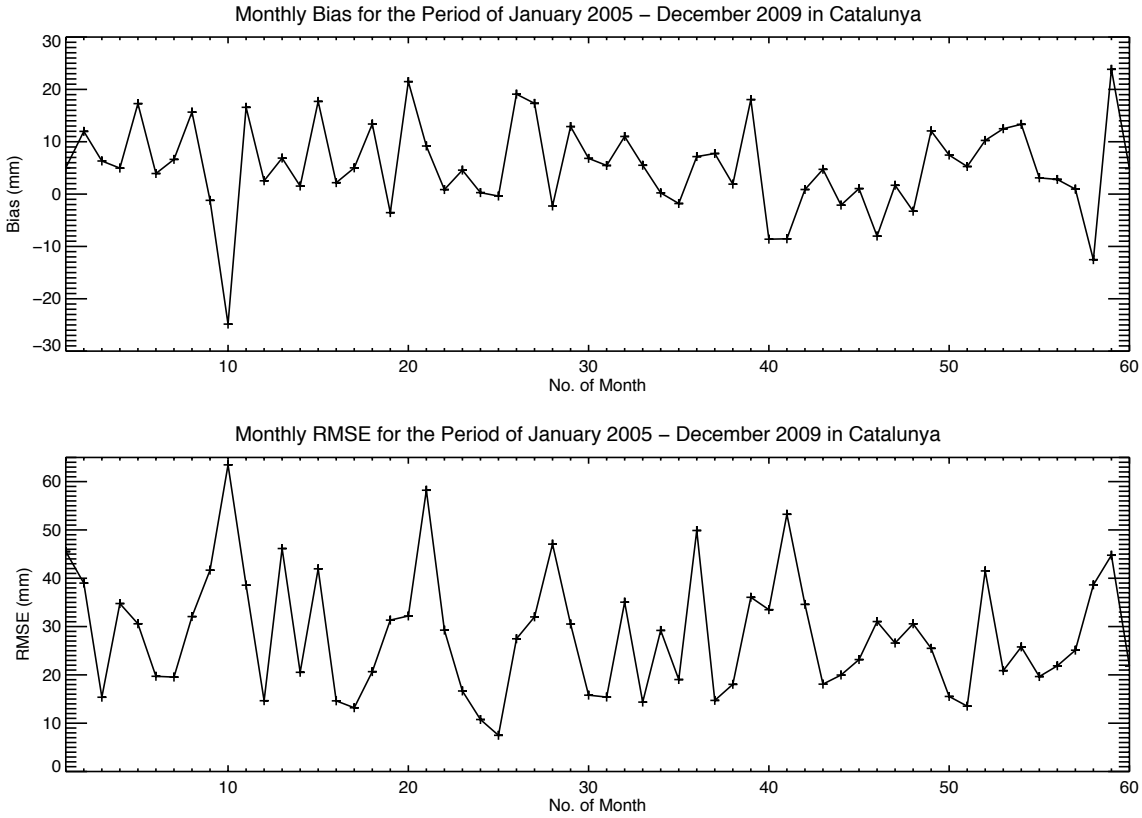

Figure 3.13: Monthly bias and RMSE for the period January 2005 – December 2009 in Catalunya.

3.3.2.5 Statistical parameters for different temporal resolutions

Daily TRMM values are accumulated over 2 day, 3 days, 5 days, 10 days, 15 days, and 30 days period and corresponding rain gauge accumulations are also estimated. By using these rain gauges and TRMM values two statistical parameters bias and RMSE are measured for different temporal resolutions i.e. 2 day, 3 days, 5 days, 10 days, 15 days, and 30 days period (Figures 3.14, 3.15, 3.16, 3.17, 3.18, and 3.19). Figures 3.14, 3.15, and 3.16 show bias for the period from January 2005 to December 2009 in Catalunya. Figures 3.17, 3.18, and 3.19 show root mean square error (RMSE) for the same area and same time period (2005-2009).

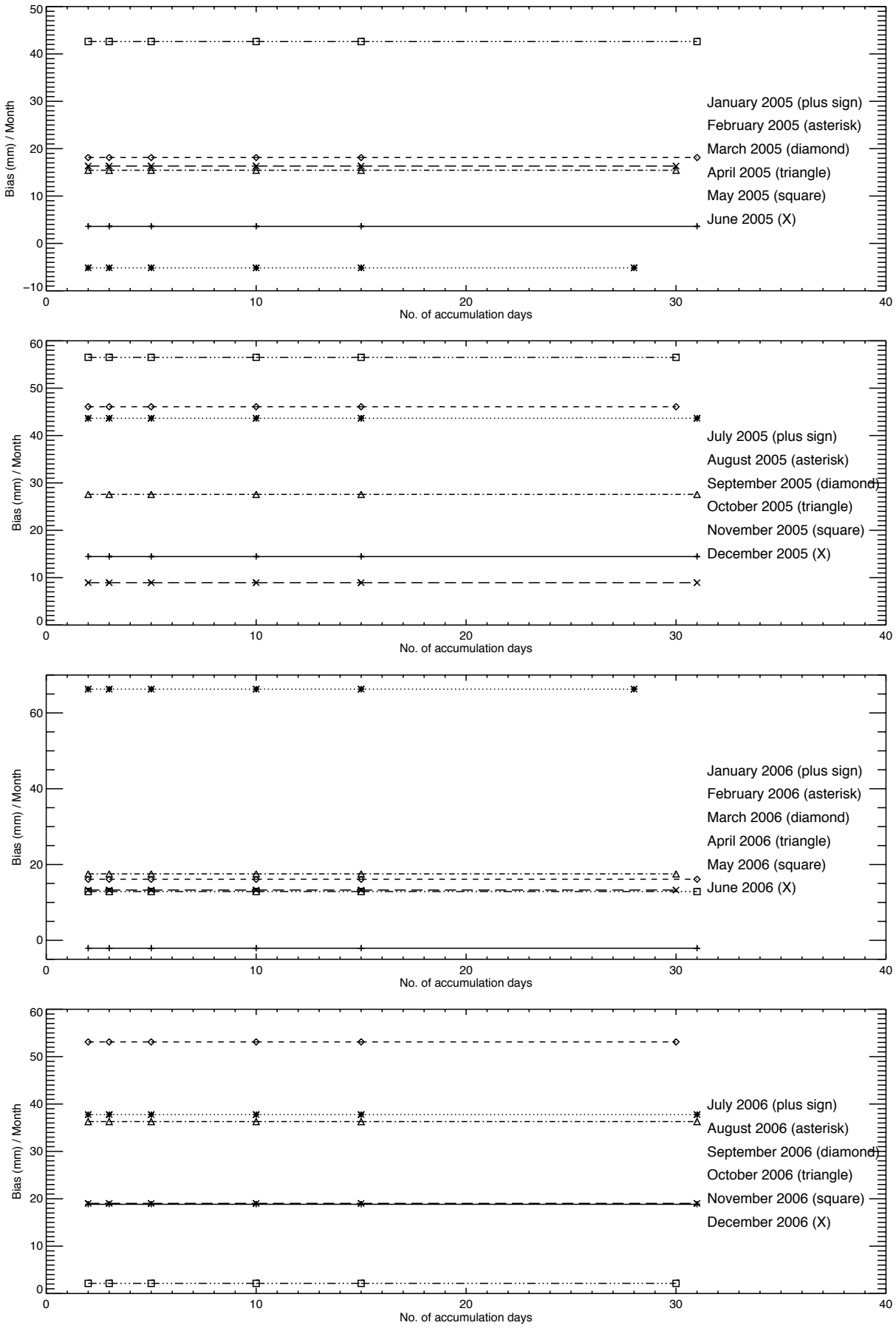

Figure 3.14: Bias for different temporal resolutions for the period 2005-2006 in Catalunya.

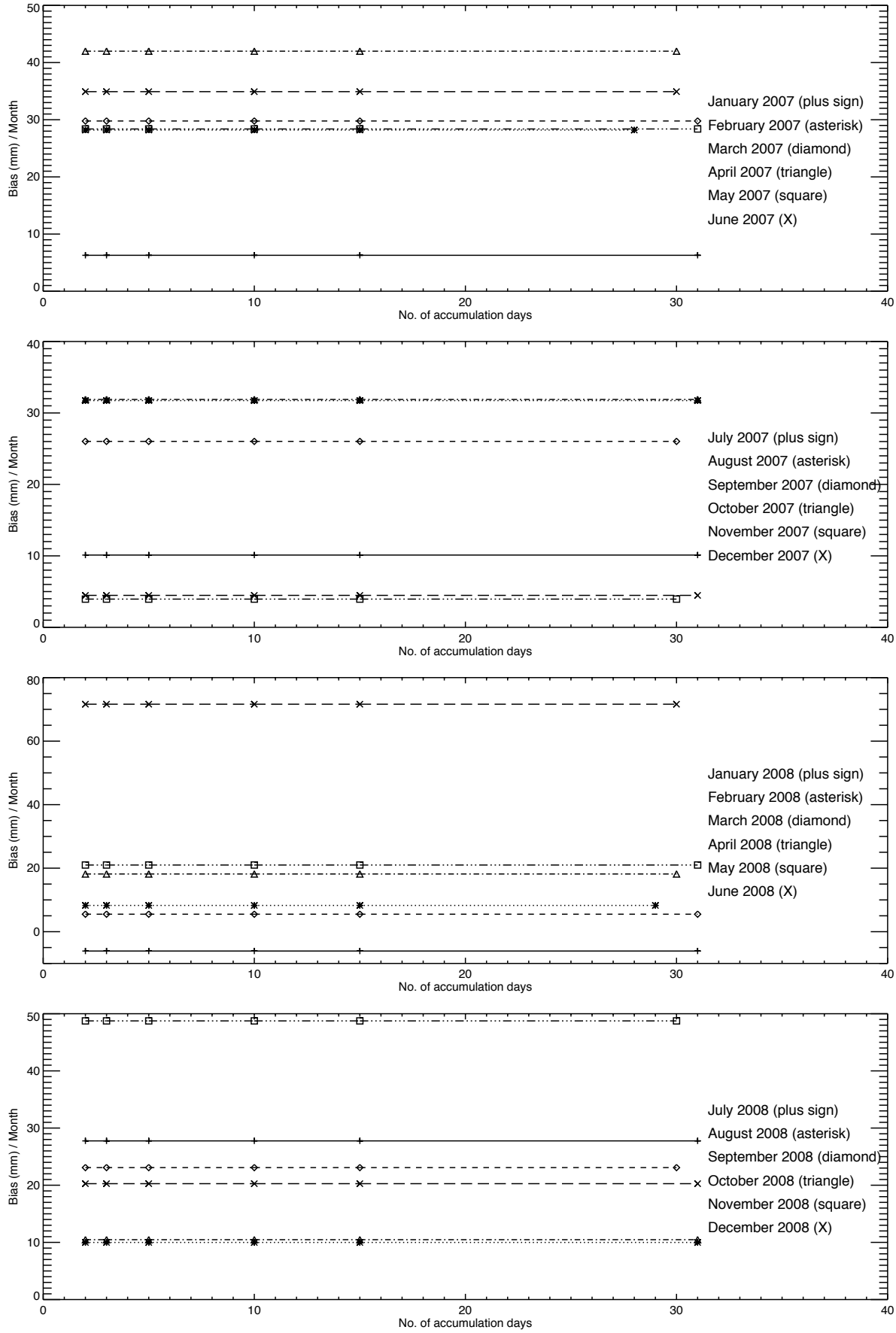

Figure 3.15: Bias for different temporal resolutions for the period 2007-2008 in Catalunya.

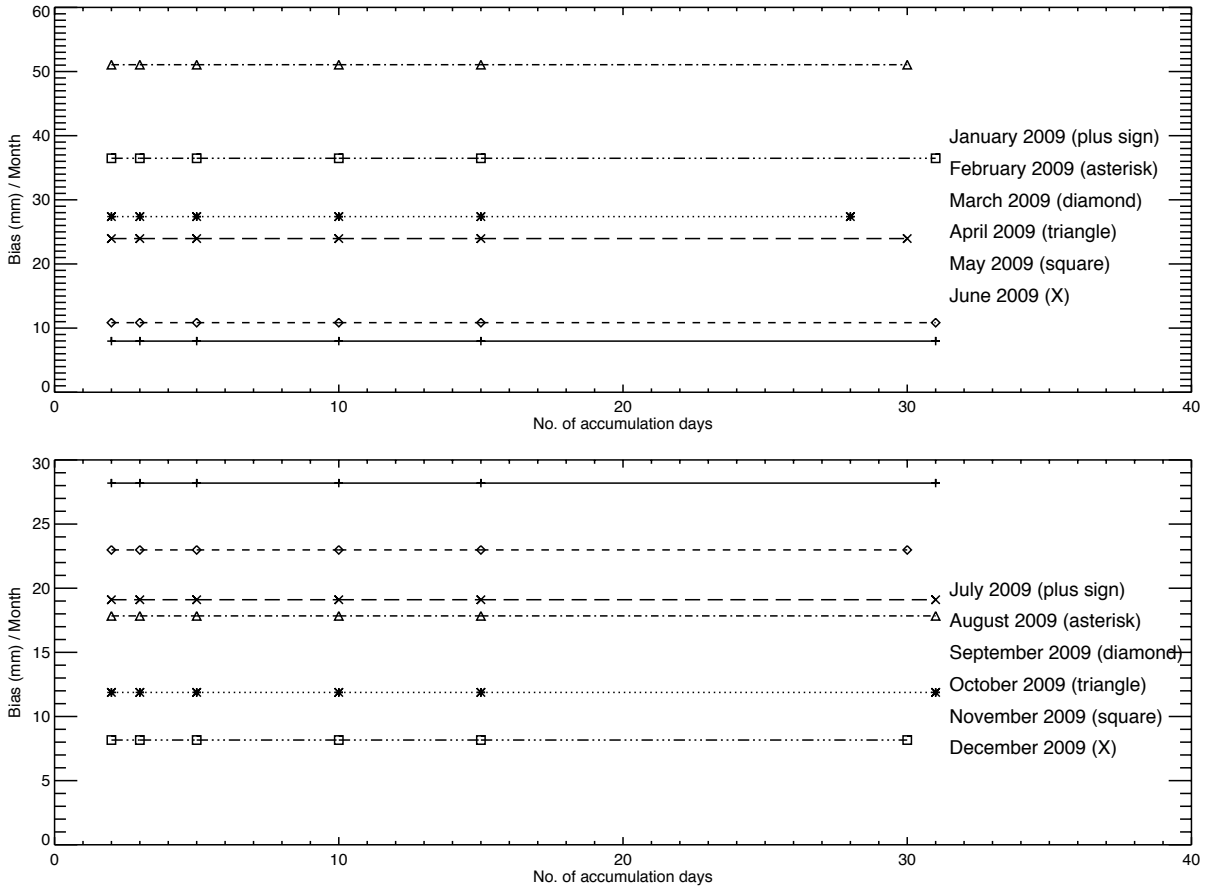

Figure 3.16: Bias for different temporal resolutions for 2009 in Catalunya.

From Figures 3.14, 3.15, and 3.16 it is shown that bias are all constant in monthly scale for all the accumulation period (2 day, 3 days, 5 days, 10 days, 15 days and 30 days) for the entire time period from January 2005 to December 2009. All months are showing positive bias except February 2005, January 2006, and January 2008. These three months are showing small negative bias.

From Figures 3.17, 3.18, and 3.19 it is showed that with increasing accumulation period RMSE decreases in Catalunya for the entire period 2005-2009. However, the rate of fall of the RMSE curve is higher for 2 day, 3 days, 5 days, and 10 days than those for 15 days and 30 days accumulation period.

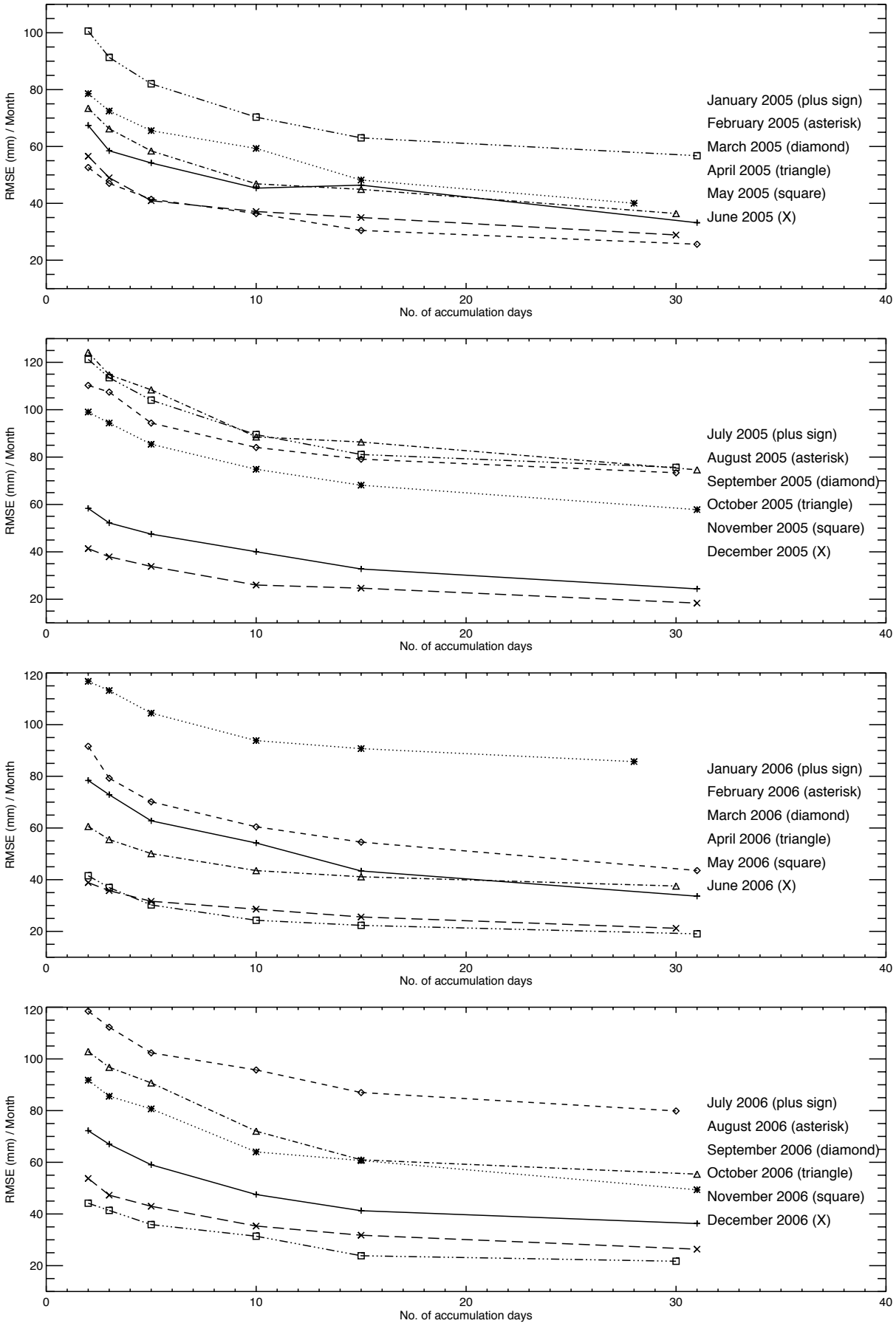

Figure 3.17: RMSE for different temporal resolutions for the period 2005-2006 in Catalunya.

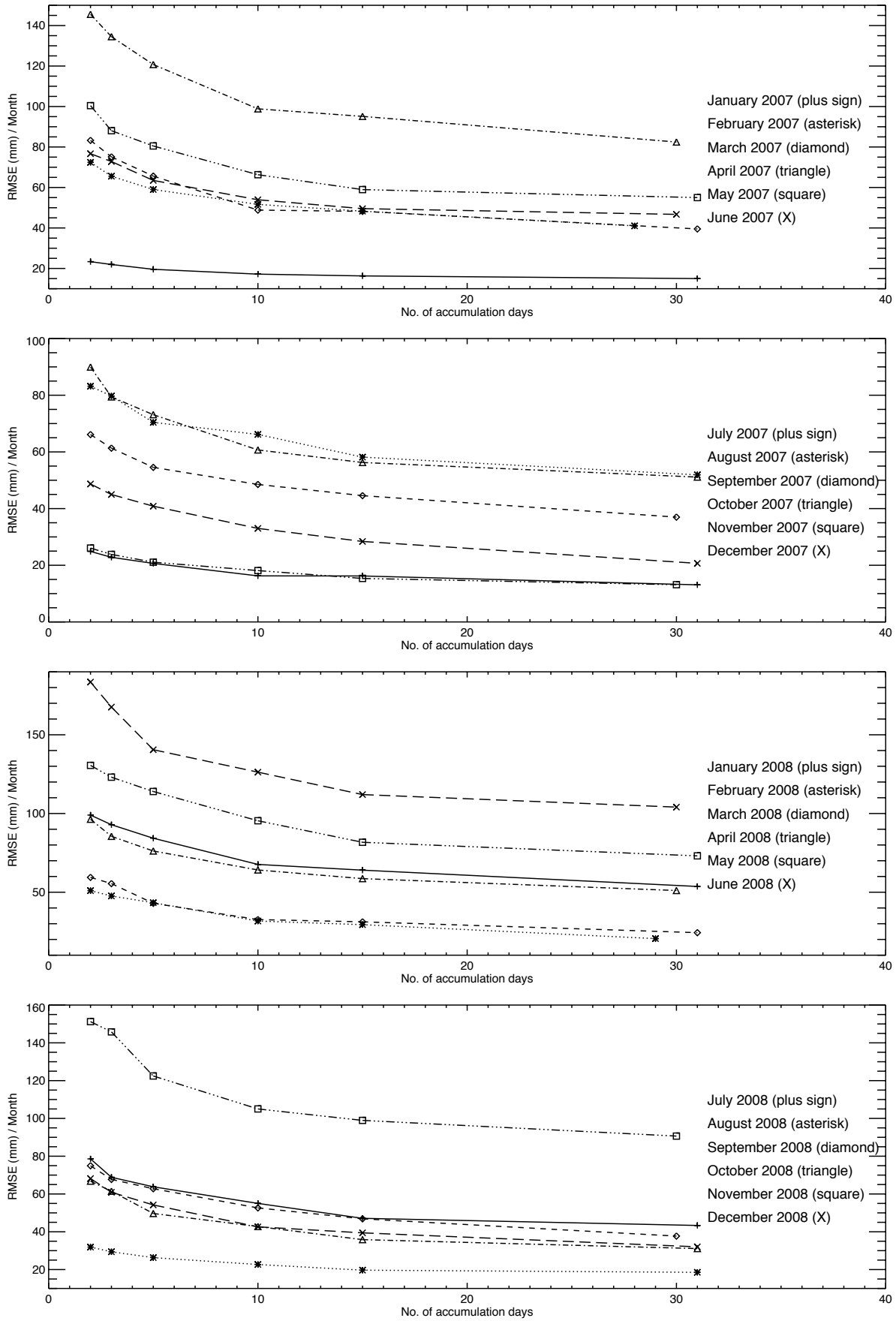

Figure 3.18: RMSE for different temporal resolutions for the period 2007-2008 in Catalunya.

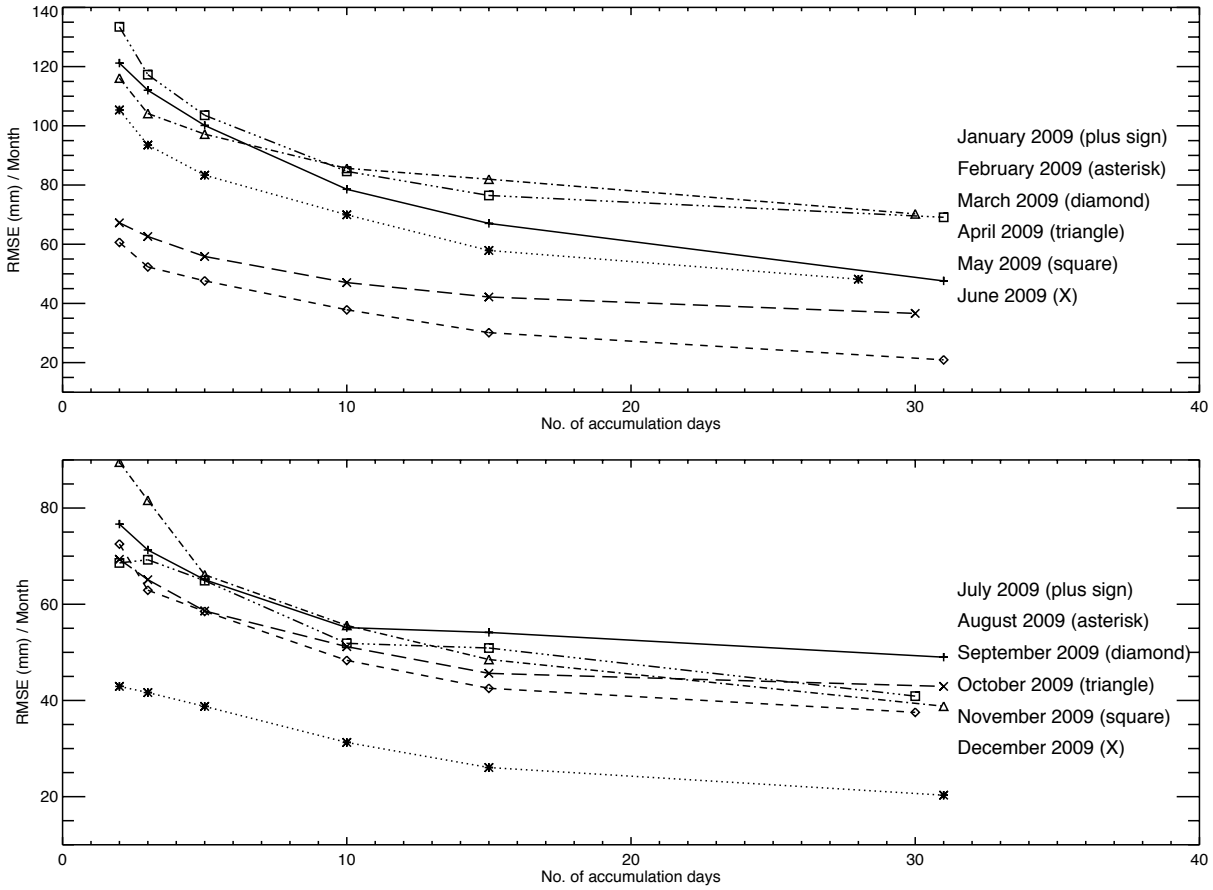

Figure 3.19: RMSE for different temporal resolutions for the period 2009 in Catalunya

3.3.3. Bangladesh

Bangladesh is well known for its natural disasters such as cyclone, storm surges, floods, droughts, and river erosions. Precipitation is the major meteorological variable which plays a significant role in the hydrological cycles as well as these extreme climatic events [Islam and Hasan (2012)]. The rain gauge network is very sparse in Bangladesh. There are only 35 rain gauge stations all over Bangladesh with different period of observations.

3.3.3.1 Daily event on 14 September 2004

We have studied several daily events over Bangladesh in different seasons of the years with large amount of rainfall. Generally, the heaviest rainfall occurs during the months from mid June to mid August, and this period of time is called rainy season (monsoon) in Bangladesh. But, here we have chosen an extraordinary daily event that happened during autumn in 2004.

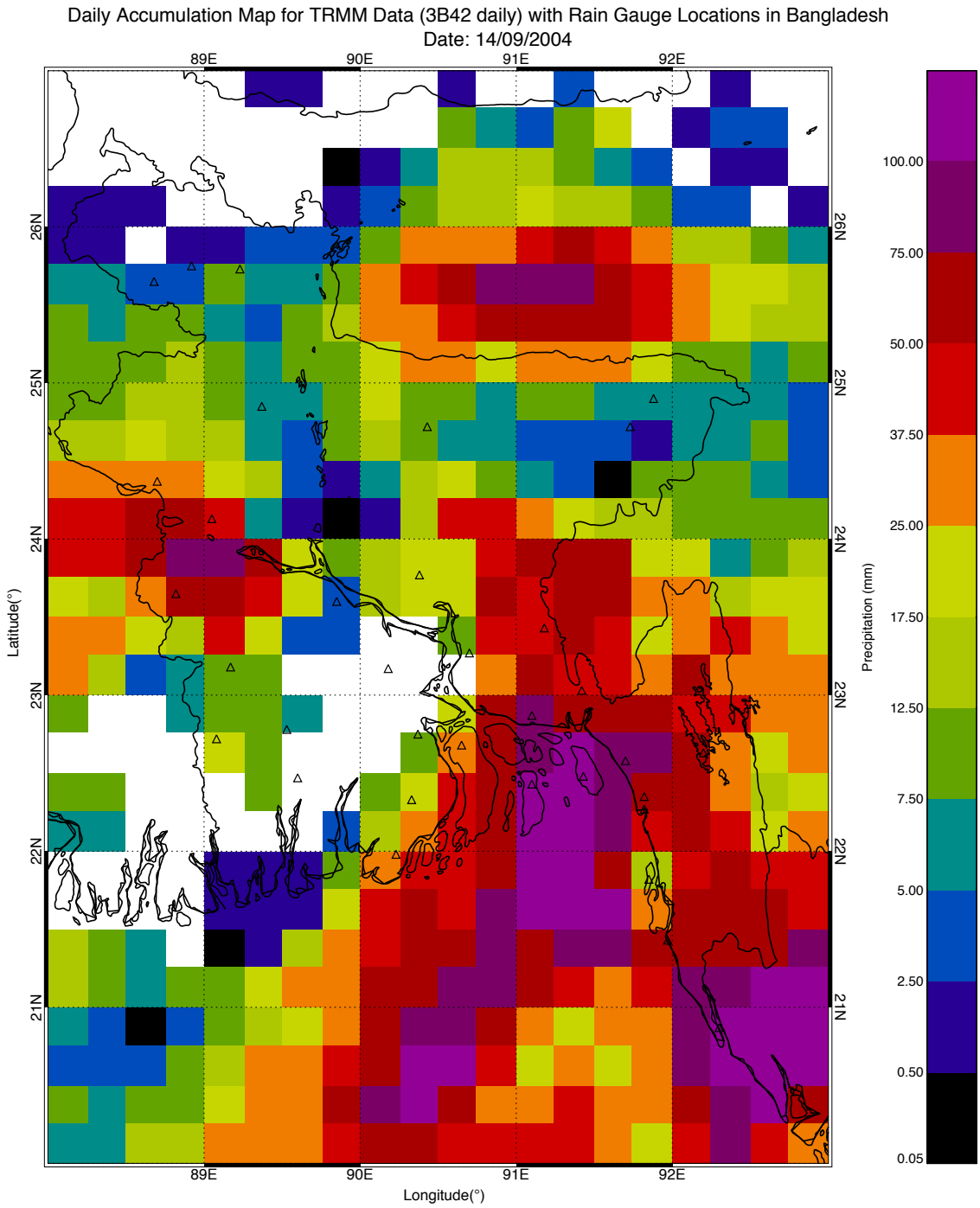

Figure 3.20: Daily accumulation map for TRMM data 3B42 daily over Bangladesh on 14 September 2004 with rain gauge locations.

On 14 September 2004, Dhaka (23.77°N, 90.38°E) the capital city of Bangladesh received unprecedented heavy rainfall and more than two-third of the city was inundated. This is an extraordinary rainfall event. The highest amount of rainfall in 24 hours was recorded at Dhaka

(341mm), which were the highest ever recorded. Due to this heavy rainfall, flash flood situation was created in Dhaka and some other parts of the country. Other nearby weather stations of Bangladesh Meteorological Department (BMD) recorded 376 mm at Maijdi Court, 422 mm at Sandwip, 234 mm at Chandpur, 179 mm at Bhola, 170 mm at Comilla, 195 mm at Faridpur, 196 mm at Hatiya, 215 mm at Jessore, and 184 mm at Tangail. This torrential rain disrupted life in the metropolitan capital city and caused flash flood situations [Ahasan et al. (2011)]. Figure 3.20 shows the daily accumulation map of TRMM 3B42 daily data over Bangladesh on 14 September 2004 with the available rain gauge locations.

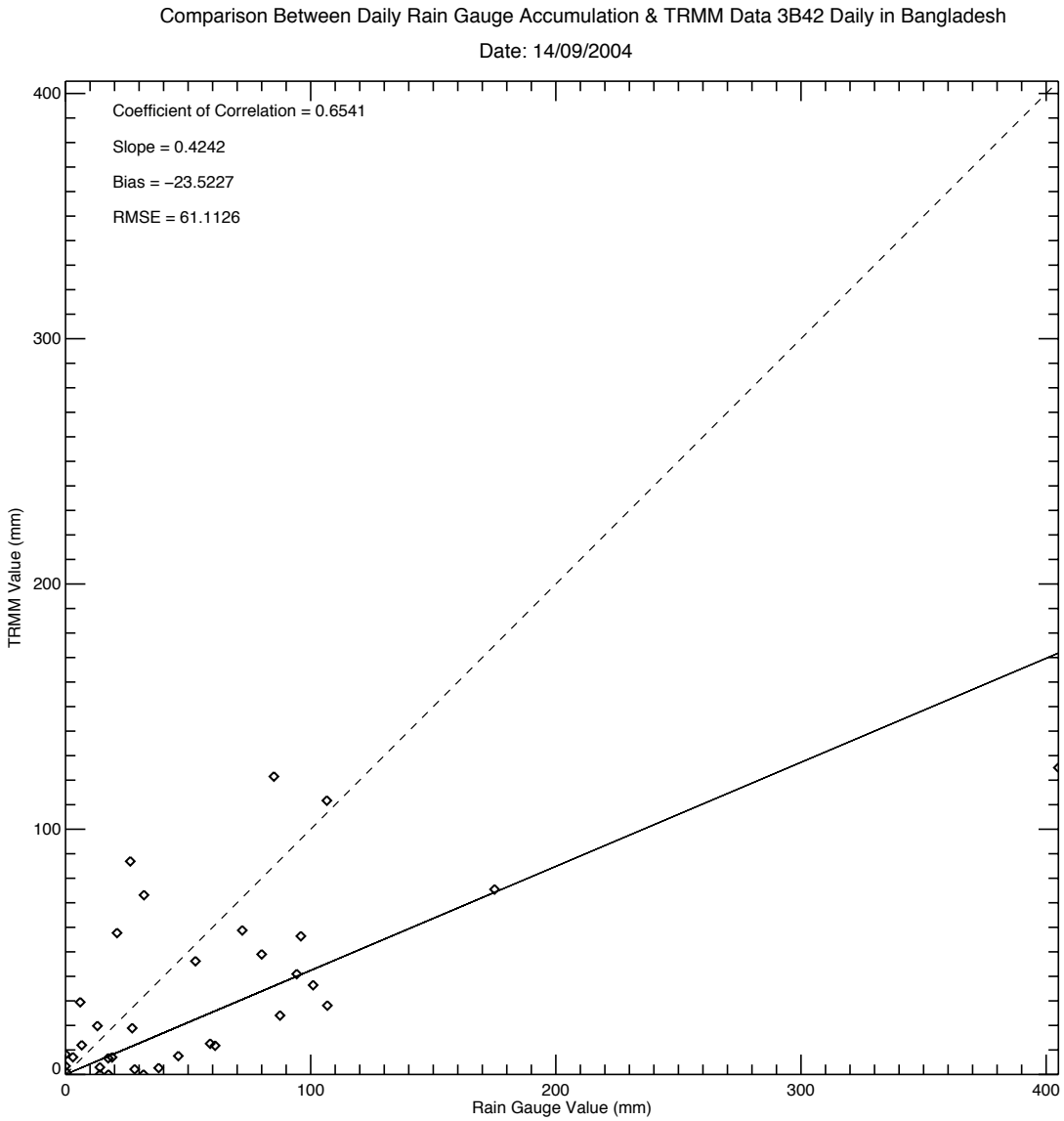

Figure 3.21: Comparison between rain gauge and TRMM estimation before discarding zero rain gauge values.

From Figure 3.20 it is showed that heavy precipitation occurred mainly over the southeastern part of Bangladesh. A Few western districts were also affected by this torrential precipitation. TRMM estimated maximum rainfall of 125 mm at Sitakunda in 24 hours period whereas rain gauge measured 405 mm at the same location and this was also the maximum rainfall observed by any rain gauge on 14 September 2004.

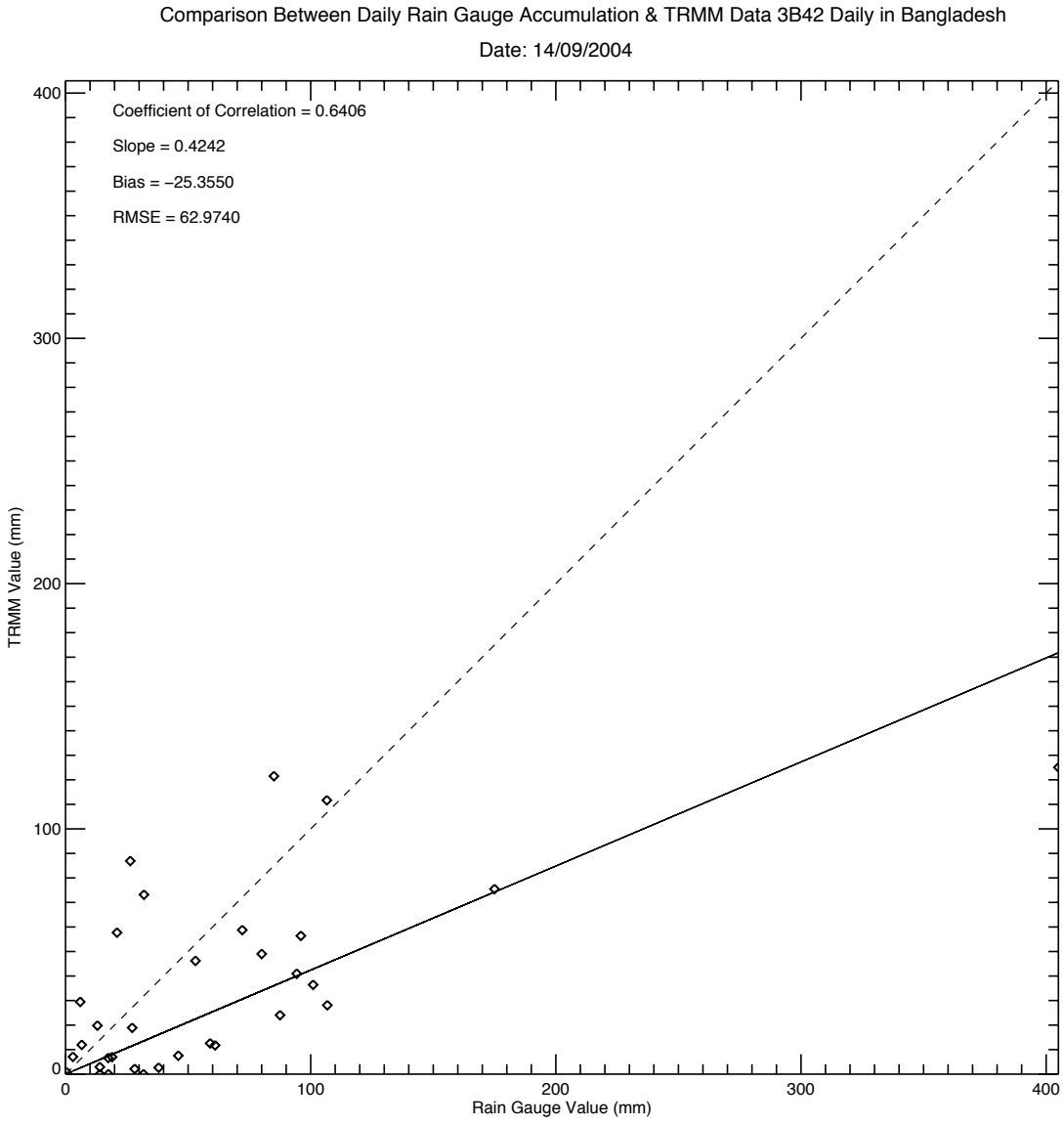

Figure 3.22: Comparison between rain gauge and TRMM estimation after discarding zero rain gauge values.

From Figures 3.21 and 3.22, it is shown that there is no significant difference between the statistical parameters before and after removing the zero values from the data set. Bias changes from -25 mm to -24 mm, which indicates serious underestimation by the satellite and slope 0.42 also implies the same. RMSE increases from 61 mm to 63 mm. On the other hand, coefficient of correlation is good (0.64 ~ 0.65).

3.3.3.2 Monthly rainfall on June 2007

June and July are the heaviest rainfall months in Bangladesh. In the following section, we will analyze monthly rainfall over Bangladesh during June 2007.

Figure 3.23 shows the monthly accumulation map using TRMM data 3B43 monthly product over Bangladesh for the month of June 2007. For this month, all rain gauge station picked up precipitation except one at Patengag and another one at Patuakhali. During this period, these two stations were not in service condition temporarily.

Figure 3.24 shows quite good results having coefficient of correlation 0.85 with slope 1.00 although bias and RMSE values are quite high 19 mm and 107 mm respectively. Maximum rainfall 979 mm was estimated by rain gauge over a period of 30 days at Chittagong (Ambagan) while TRMM estimated 748 mm over the same area although bias value 19 mm shows the over estimation by the satellites. However, the maximum precipitation 891 mm is observed by the satellites at Mymensingh while rain gauge estimated it as 863 mm.

During this period on 11 June 2007, Chittagong (22.35°N, 91.82°E), the south-eastern coastal metropolitan city of Bangladesh, received unprecedented heavy rainfall and more than one-third of the metropolitan city was inundated. This extraordinary rainfall event was localized over a region of 20-30 km. Bangladesh Meteorological Department (BMD) recorded rainfall was 425 mm within a span of 24-h on that eventful day, out of which 315 mm in just six hours (00 UTC-06 UTC). Other nearby weather stations of BMD recorded rainfalls were 225 mm at Sandwip, 146 mm at Rangamati, 110 mm at Kutubdia, and 101 mm at Cox's Bazar. This torrential rain disrupted life in the metropolitan city, caused flash flood situation. In addition to the floods, the rains triggered devastating landslides in the deforested hills on which the city is built. The citywide death toll from the floods and landslides was nearly 130

on June 12 as reported in the print media (Reuters). Most of the deaths were as a result of the landslides or from buildings collapsing due to the rain [Ahasan et al. (2011)].

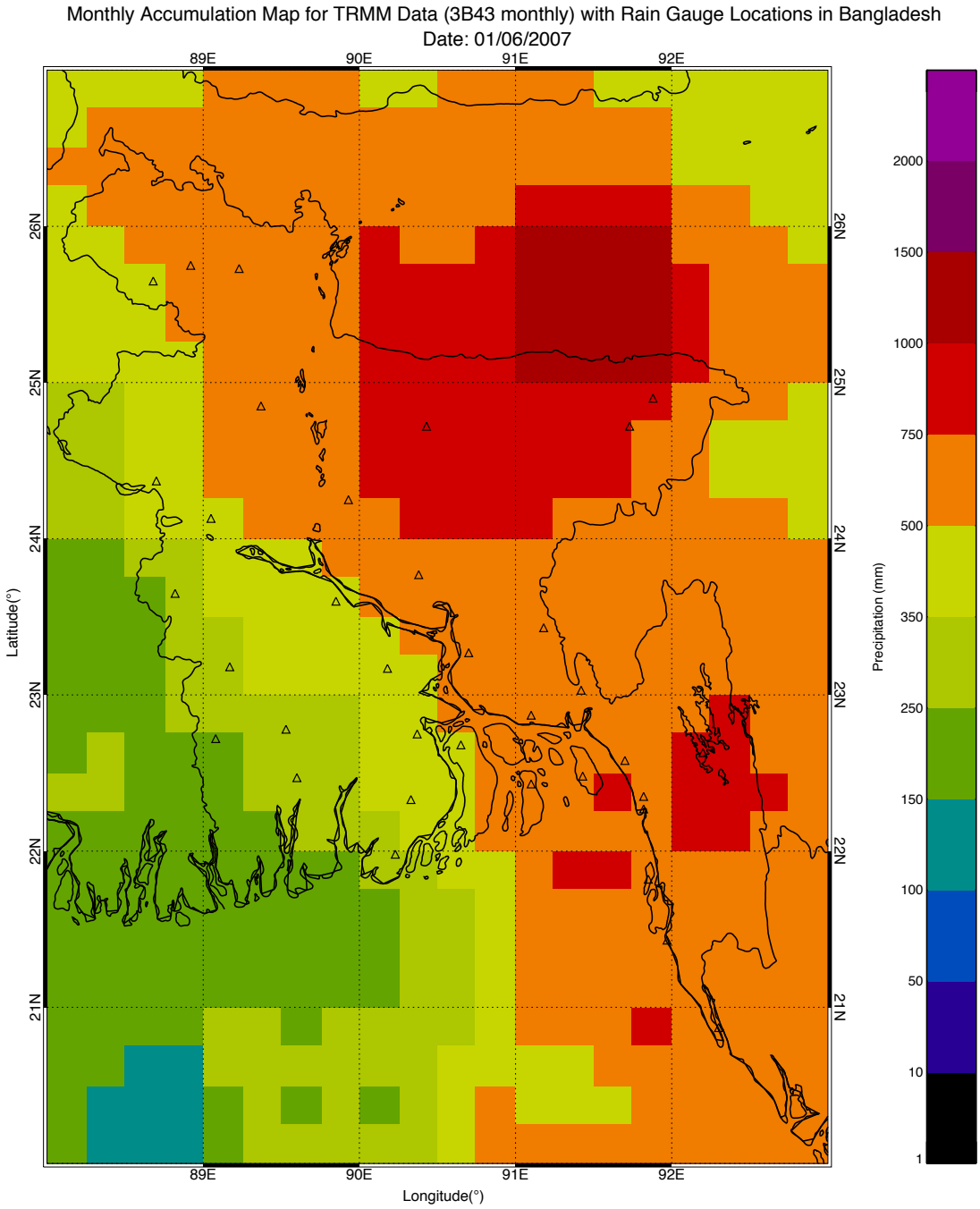

Figure 3.23: Monthly accumulation map for TRMM data 3B43 over Bangladesh on June 2007 with rain gauge locations.

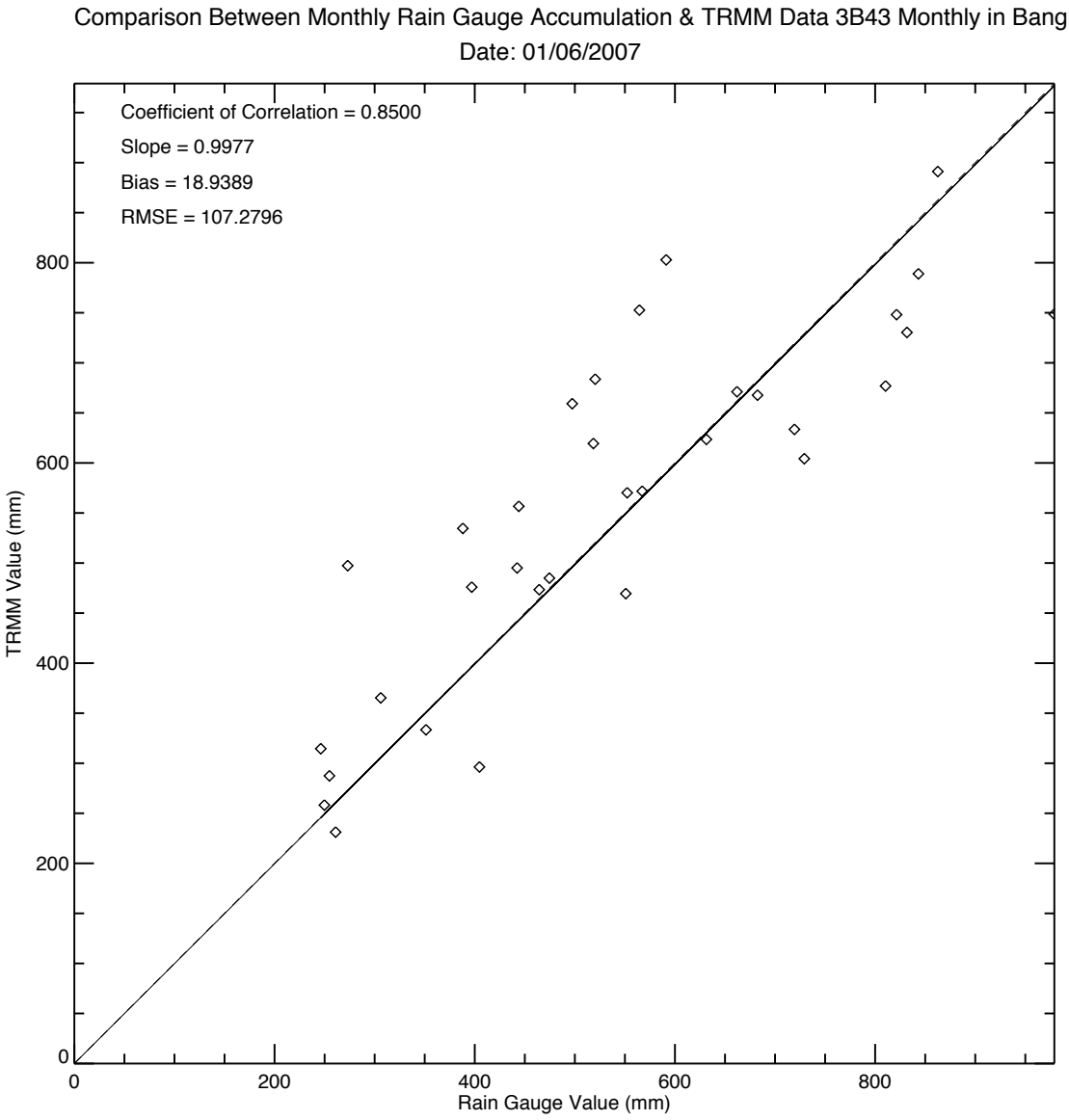

Figure 3.24: Comparison between rain gauge and TRMM estimation during June 2007 over Bangladesh.

3.3.3.3 Daily statistical parameters

Daily mean TRMM values are measured by using the pixels over the corresponding rain gauge stations (Figure 3.25) and daily mean rain gauge values are also measured by using the rain gauge stations available on that day excluding zero rain gauge values (Figure 3.25). Coefficient of correlation, bias, and RMSE are calculated by using rain gauge and TRMM values for the period January 2005 – December 2009 in Bangladesh.

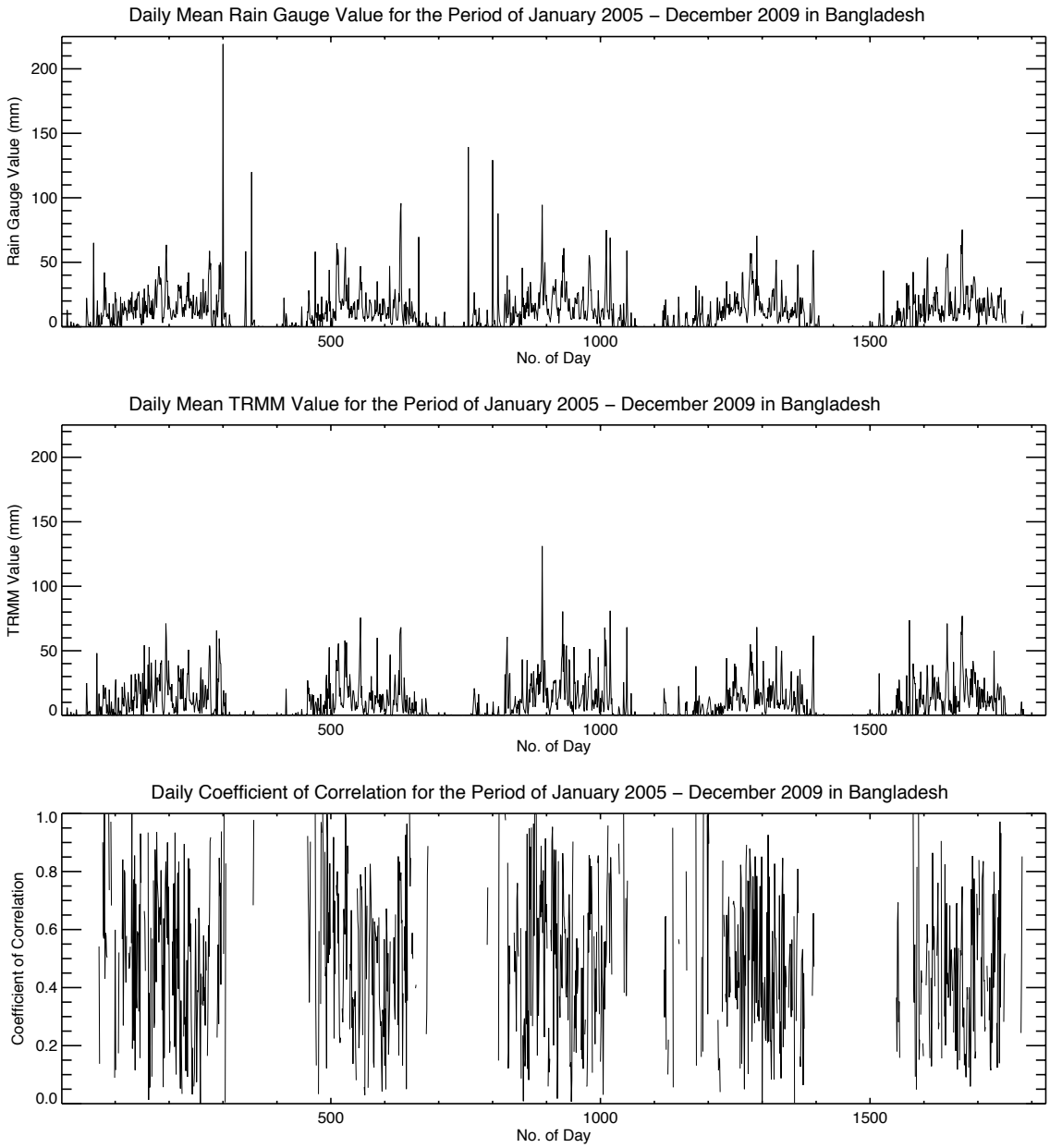

Figure 3.25: Daily mean rain gauge and TRMM values with daily coefficient of correlation for the period January 2005 – December 2009 in Bangladesh.

From Figure 3.25 it is shown that rain gauge and TRMM values moderately shows the same pattern of daily precipitation. The troughs of rain gauge and TRMM plots represent the winter period of each year because during winter period (from December to March) in Bangladesh there is almost no rainfall. Maximum coefficient of correlation values are observed during the monsoon periods when heavy rainfall events occur. Within the considered time period there are 77 days that are showing coefficient values greater than 0.90 with maximum bias and RMSE 29 mm and 76 mm respectively (Figures 3.25 and 3.26). There are also 137 days with correlation value greater than 0.70 and less than 0.90 with maximum and minimum RMSE

values are 66 mm and 2 mm respectively. For this range of correlation, positive and negative bias varies from 0 mm to 29 mm and from 0 mm to 28 mm respectively. 226 days range from 0.50 to 0.70 correlation with maximum bias and RMSE 29 mm and 72 mm respectively. However, 301 and 134 days have correlation value from 0.20 to 0.50 and less than 0.20 respectively.

The observed maximum RMSE is 76 mm for the condition -30 mm < bias < 30 mm (Figure 3.26). Figure 3.26 also shows distinct pattern in dry and wet periods. During dry periods both bias and RMSE show approximately zero values while those values during rainy season display abrupt changes (up and down).

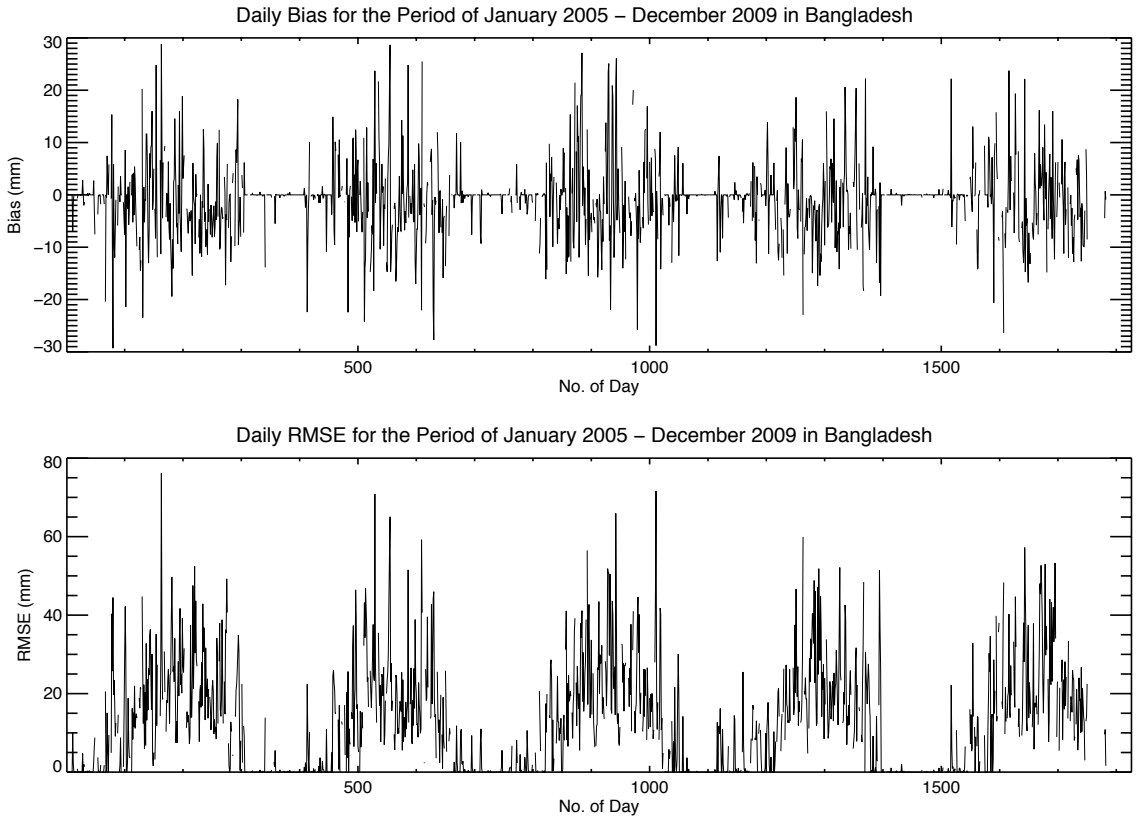

Figure 3.26: Daily bias and RMSE for the period January 2005 – December 2009 in Bangladesh.

3.3.3.4 Monthly statistical parameters

Monthly mean rain gauge and TRMM values show the same pattern of monthly rainfall for the period January 2005 – December 2009 (Figure 3.27), also display definite boundary for

dry period and rainy season. Here, we have considered the condition -30 mm < bias < 30 mm for Figure 3.28.

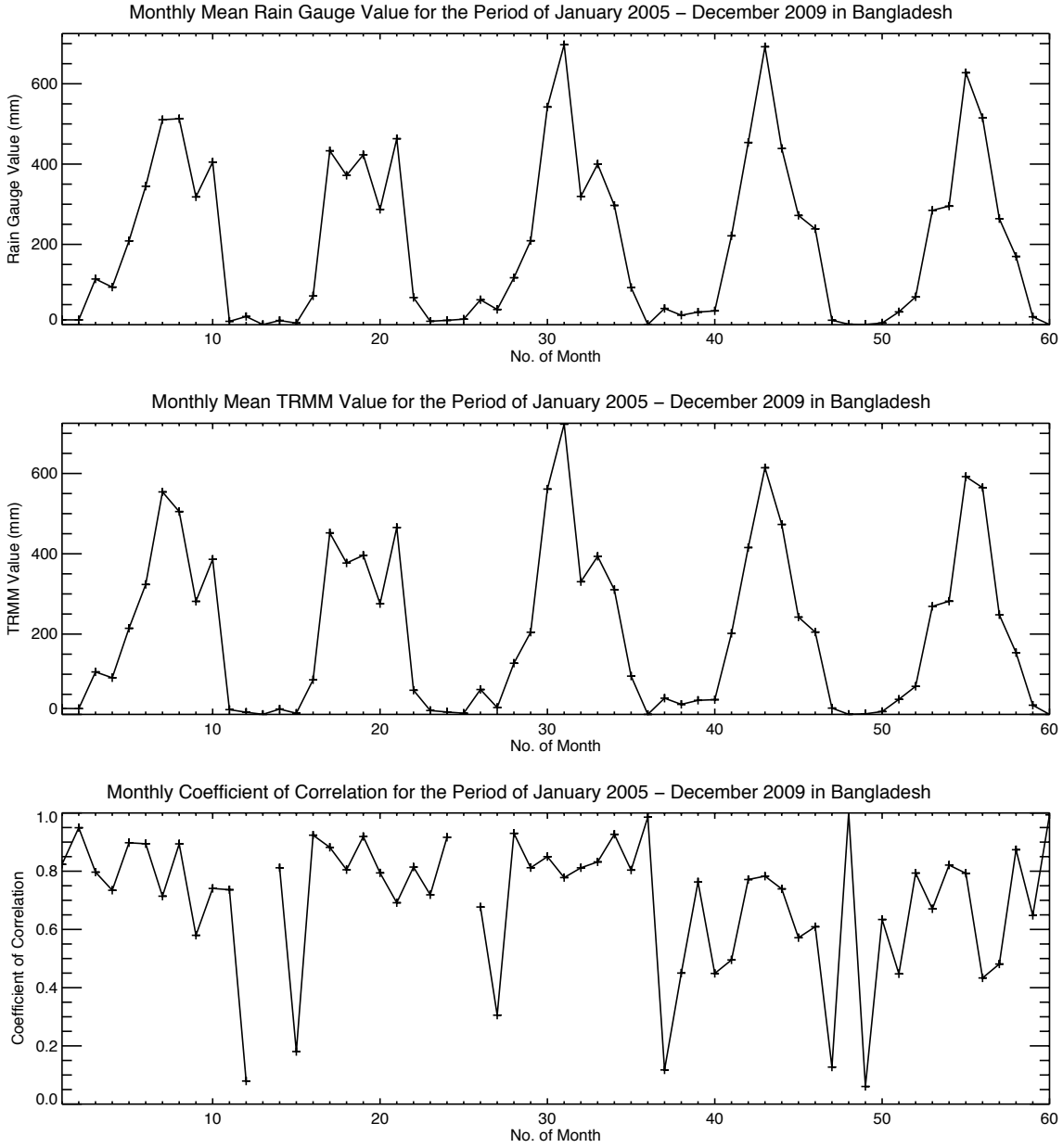

Figure 3.27: Monthly mean rain gauge and TRMM values with monthly coefficient of correlation for the period January 2005 – December 2009 in Bangladesh.

From Figures 3.27 and 3.28 it is showed that 7 months have correlation value less than 0.20 with bias and RMSE value ranges from -15 mm to 5 mm and from 0 mm to 40 mm respectively. 6 of these 7 months occurred during winter (from December to March) when precipitation is rare. Similarly, another 7 months ranges between 0.20 and 0.50 coefficient value having RMSE and bias values from 22 mm to 158 mm and from -21 mm to 50 mm

respectively. Out of these 7 months, 3 months occurred during winter. 8 months (2 months occurred during winter) have correlation value between 0.50 and 0.70 with bias and RMSE values from -37 mm to 3 mm and from 8 mm to 129 mm respectively. Maximum 29 (4 months occurred during winter) months have correlation value from 0.70 and 0.90 while for this range bias and RMSE ranges from -78 mm to 44 mm and from 7 mm to 264 mm respectively. 9 months have very high correlation value over 0.90. The minimum and maximum bias for these 9 months are -27 mm and 14 mm and RMSE are 0 mm and 91 mm. Out of these 9 events 5 events occurred during winter.

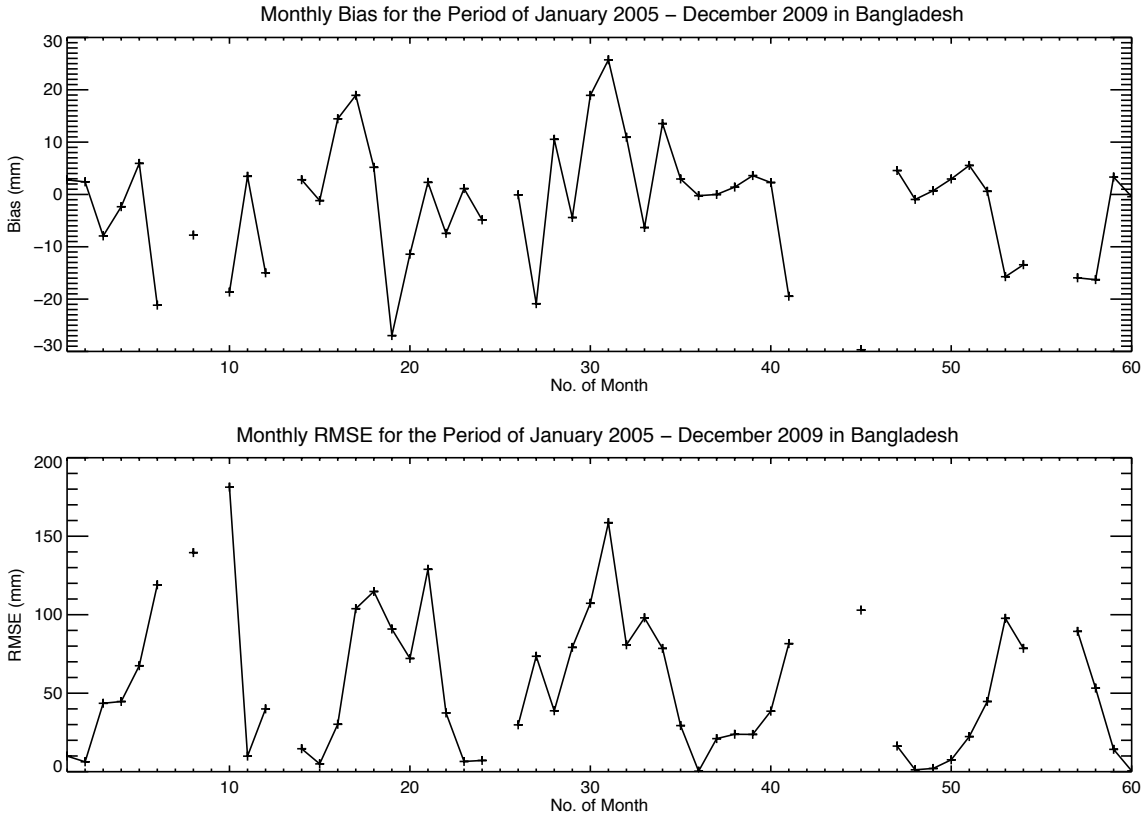

Figure 3.28: Monthly bias and RMSE for the period January 2005 – December 2009 in Bangladesh.

3.3.3.5 Statistical parameters for different temporal resolutions

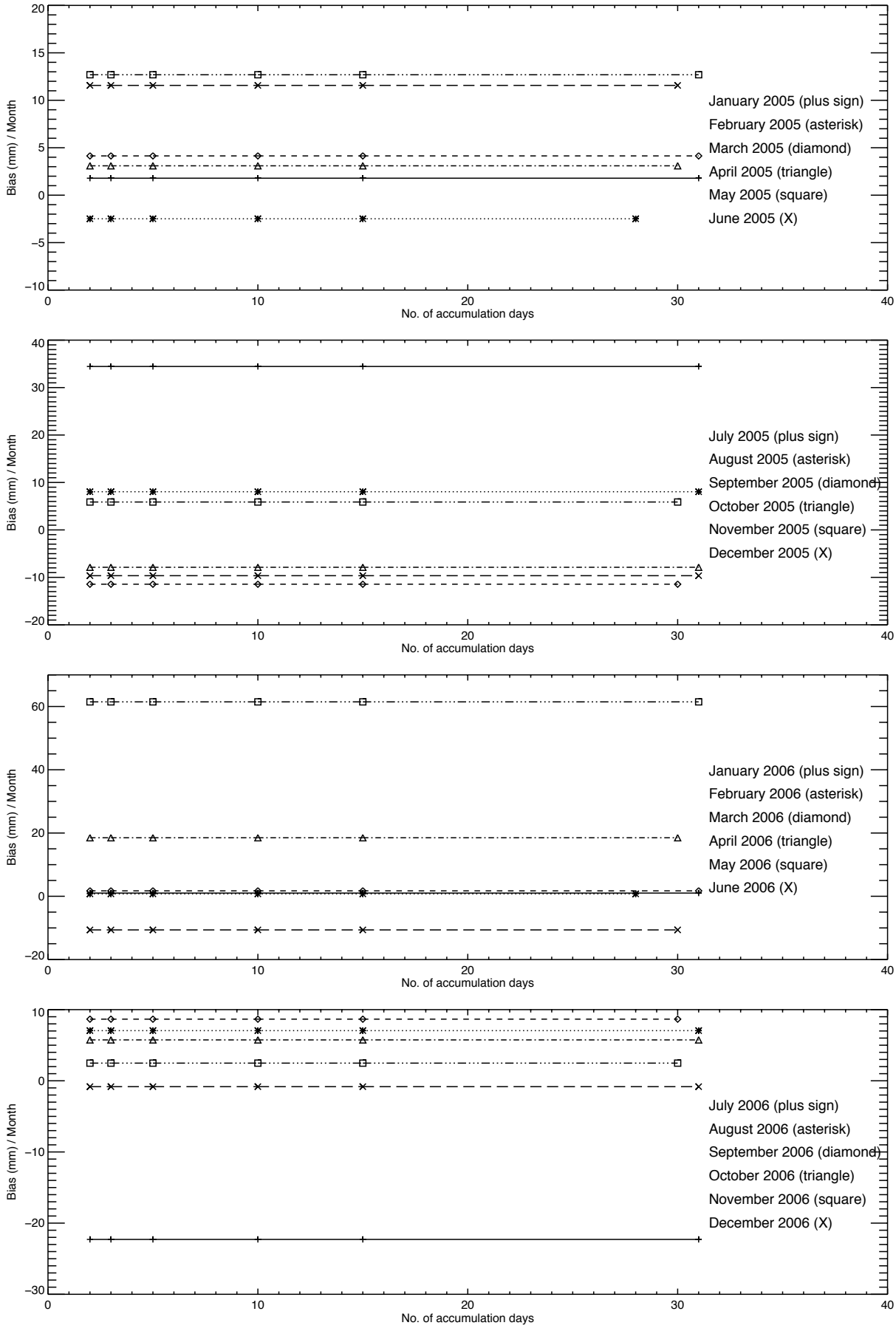

Figure 3.29: Bias for different temporal resolutions for the period 2005-2006 in Bangladesh.

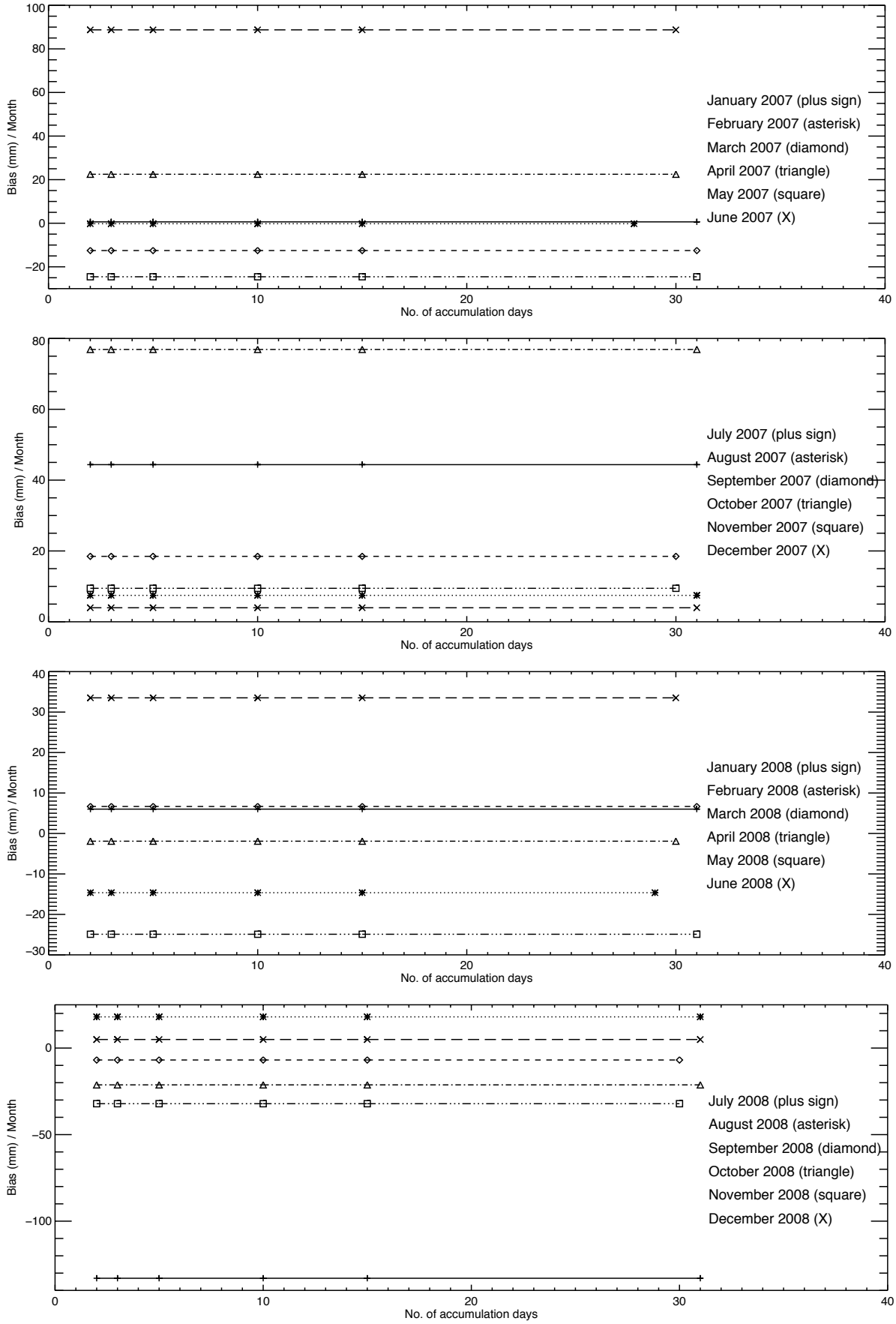

Figure 3.30: Bias for different temporal resolutions for the period 2007-2008 in Bangladesh.

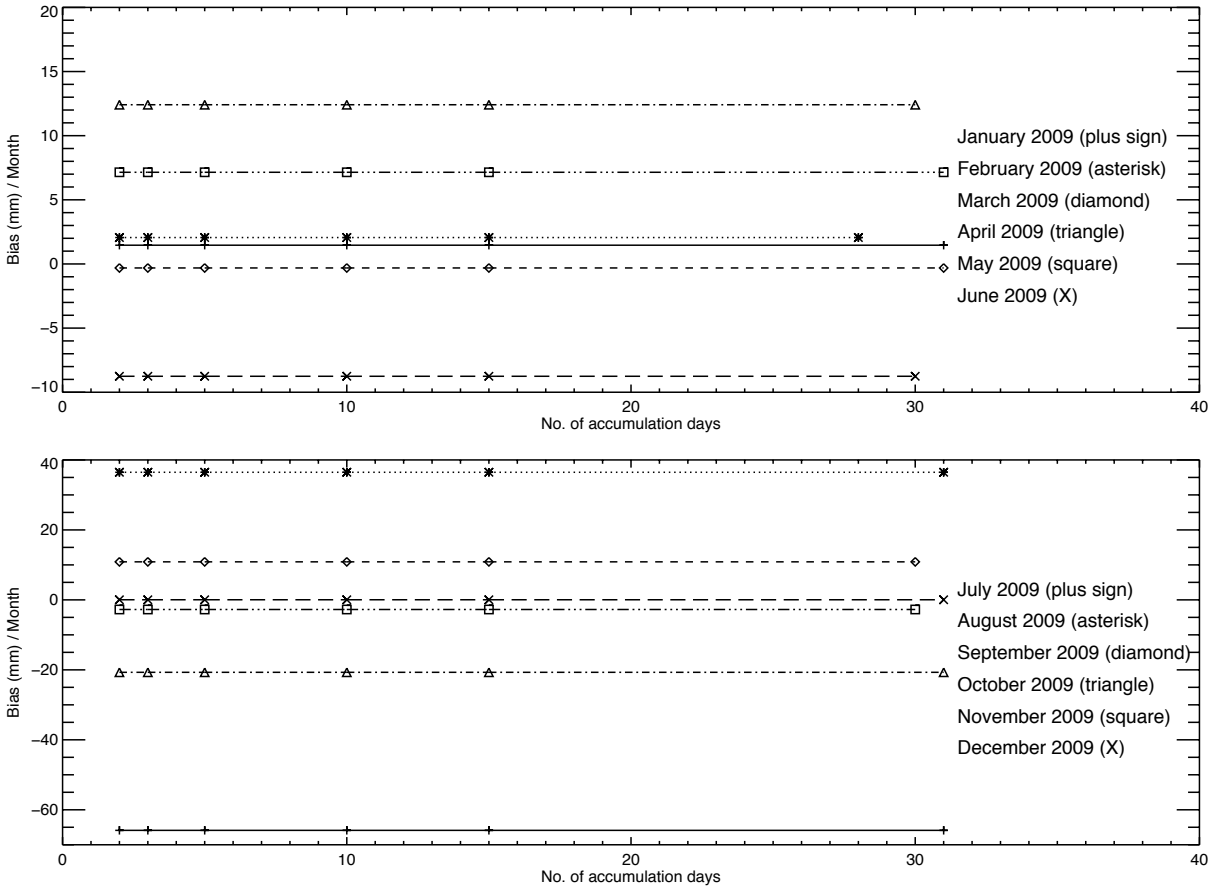

Figure 3.31: Bias for different temporal resolutions for 2009 in Bangladesh.

Figures 3.29, 3.30, and 3.31 show bias for the whole period 2005-2009 in Bangladesh. From the Figures it is shown that bias are constant for all temporal accumulation for the whole time duration from January 2005 to December 2009. The months that are showing large bias for monthly products (3B43) mainly during high rainfall period (June-August).

Figures 3.32, 3.33, and 3.34 show RMSE for the period from January 2005 to December 2009 in Bangladesh. From the Figures it is showed that RMSE decreases with increase the accumulation period and the rate of decrease is higher for 2 day, 3days, 5 days, and 10 days accumulation than those for 15 days and 30 days in Bangladesh same as Catalunya.

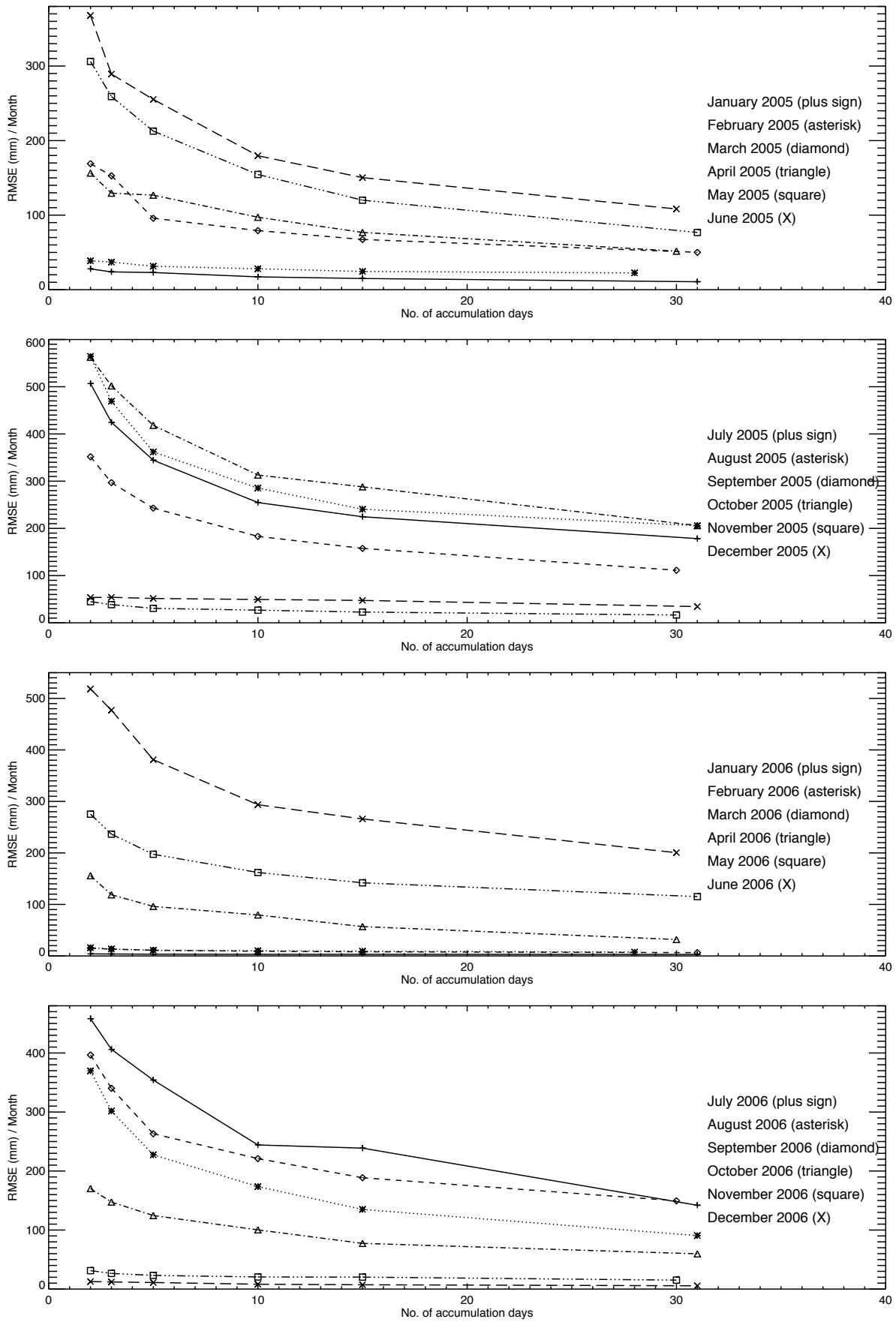

Figure 3.32: RMSE for different temporal resolutions for the period 2005-2006 in Bangladesh.

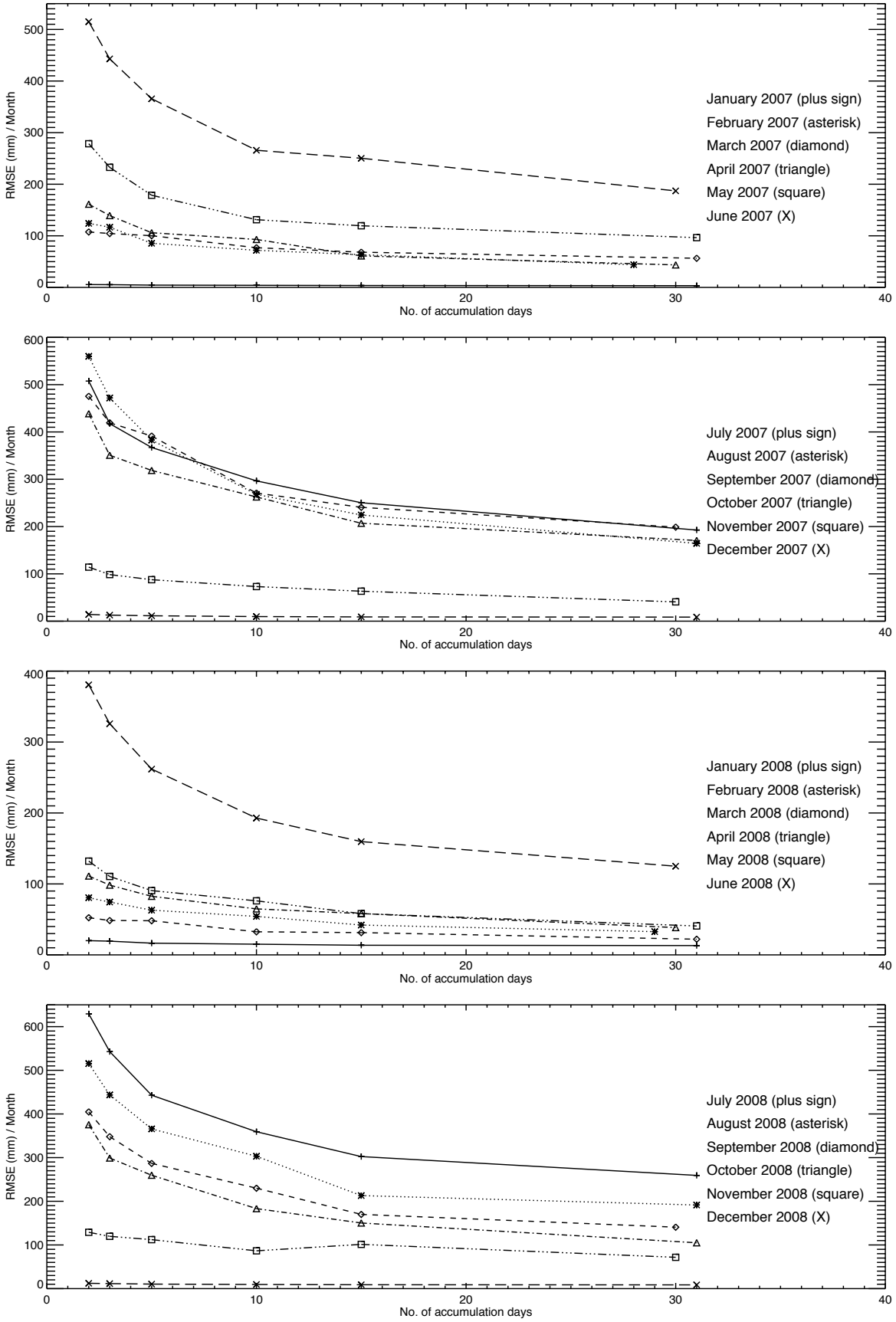

Figure 3.33: RMSE for different temporal resolutions for the period 2007-2008 in Bangladesh.

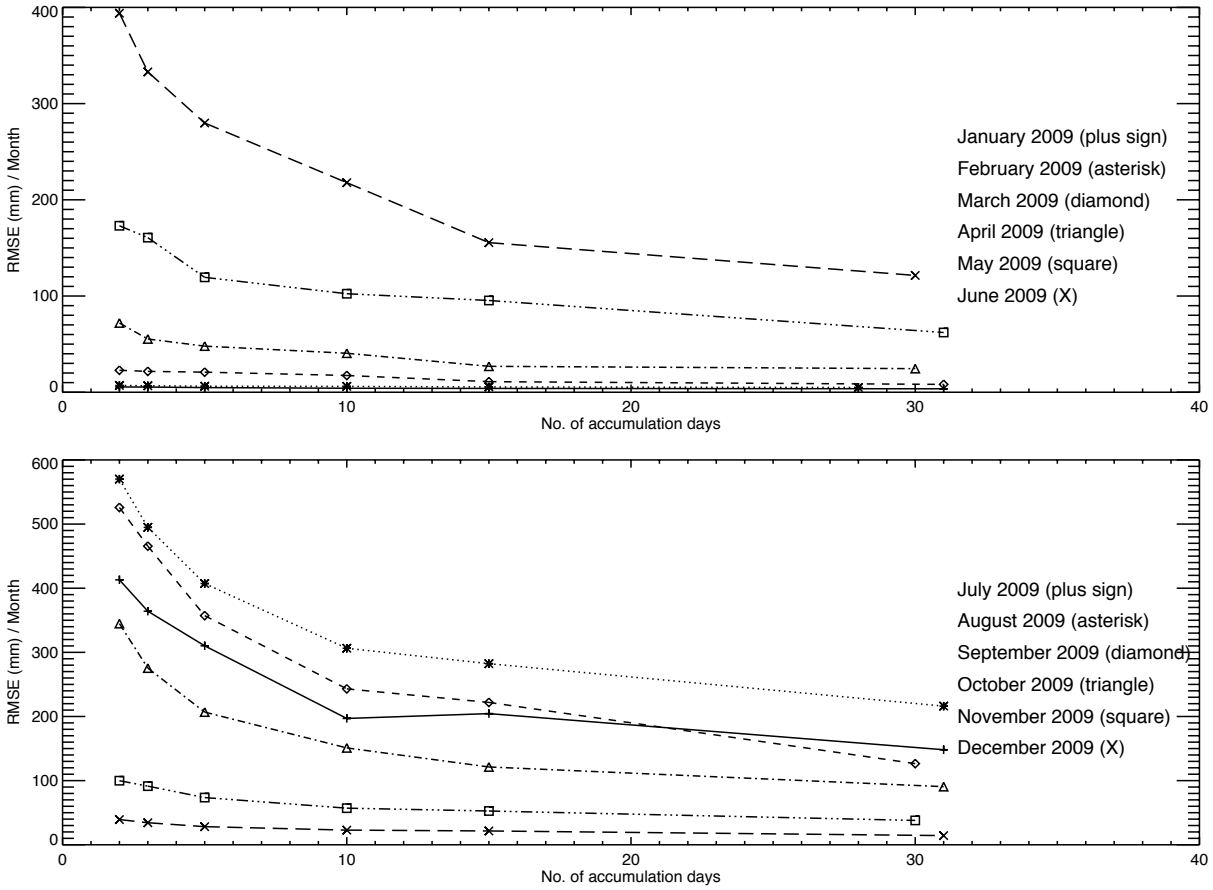

Figure 3.34: RMSE for different temporal resolutions for 2009 in Bangladesh.

3.3.4. South Africa

Although much of southern Africa lies within arid to semi-arid climatic regions, extreme rainfall events in the region are relatively frequent [Lindesay and Jury (1991); Mason and Jury (1997)]. South Africa (SA), south of 15°S**,** is a semi-arid region mainly experiencing its larger rainfall amounts in austral summer between November and February [Crétat et al. (2012)]. Because of the predominance of rain-fed agriculture over SA, large departures from the average seasonal cycle (either floods or droughts) may have detrimental effects on the economies and societies of the region. The southern African rainfall field is known to show strong spatio-temporal variability at different scales, materializing the influence of distinct rain-bearing processes that themselves depend on various modes of atmospheric variability [Crétat et al. (2012)]. There are 4012 rain gauge stations all over South Africa with different collection period. We have selected 2185 stations on the basis of collection period from January 2001 to last.

3.3.4.1 Daily rainfall on 2 August 2006

South Africa receives most of its rainfall in austral summer except for a region in the southwest that experiences austral winter rainfall [Philippon et al. (2012)]. Rainfall maxima are recorded from May to August when the track of the temperate weather systems (i.e. extratropical cyclones, cold fronts and cutoff lows) is shifted northward [Rouault and Richard (2003)]. That southwestern region which encompasses part of the Western and Northern Cape Provinces is bordered in the east by the cold Benguela upwelling system, and to the south, at a distance, by the warm Agulhas Current [Philippon et al. (2012)]. Orography plays an important role. In particular, the Cape Folded Mountains which stretch northward to the west and east–west to the south favour high (low) rainfall on their seaward (landward) side [Philippon et al. (2012)].

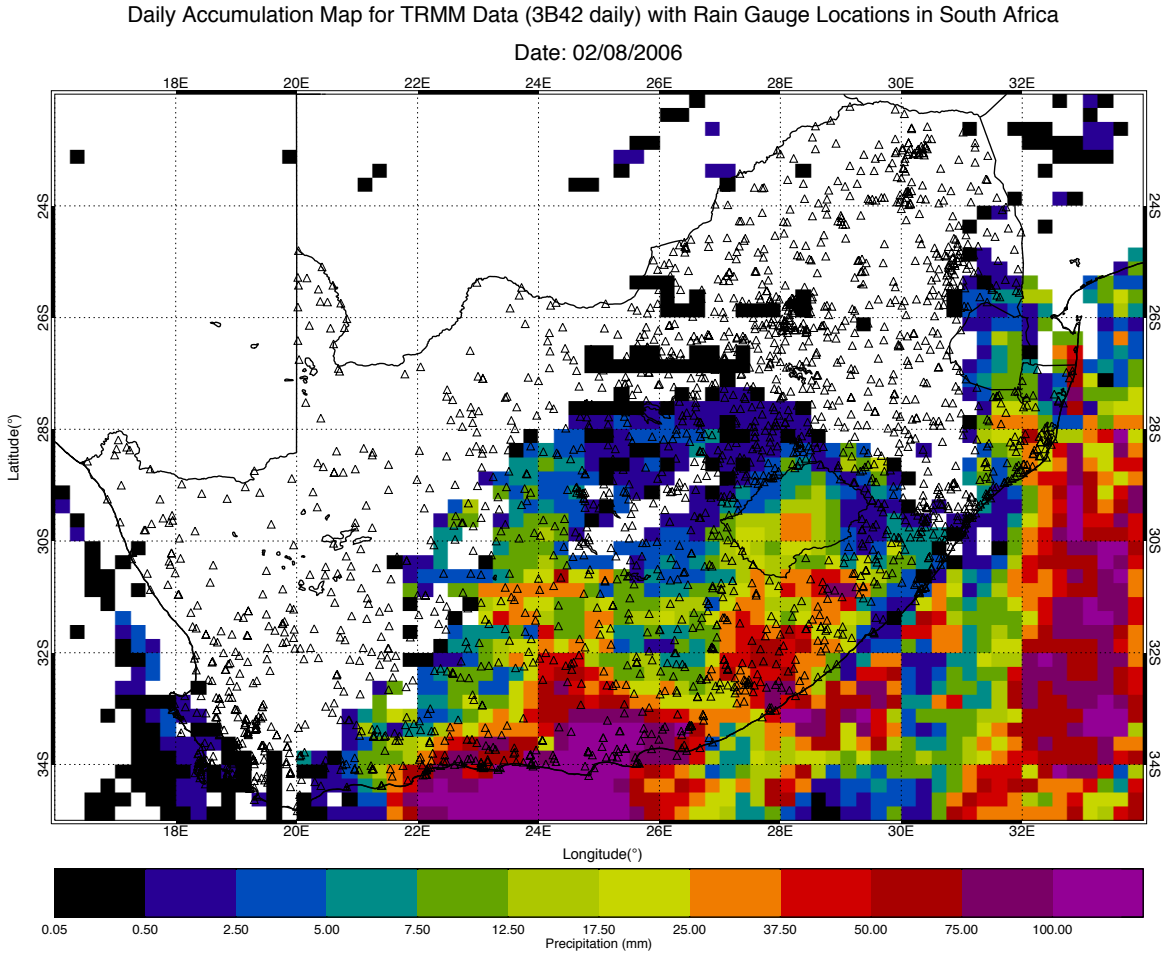

Figure 3.35: Daily accumulation map for TRMM data 3B42 over South Africa on 2 August 2006 with rain gauge locations.

Like the above two case study areas, we have studied several days with large amount of precipitation over South Africa. Since, it is a large country, it is very hard to find an event occurring over the entire country at a time.

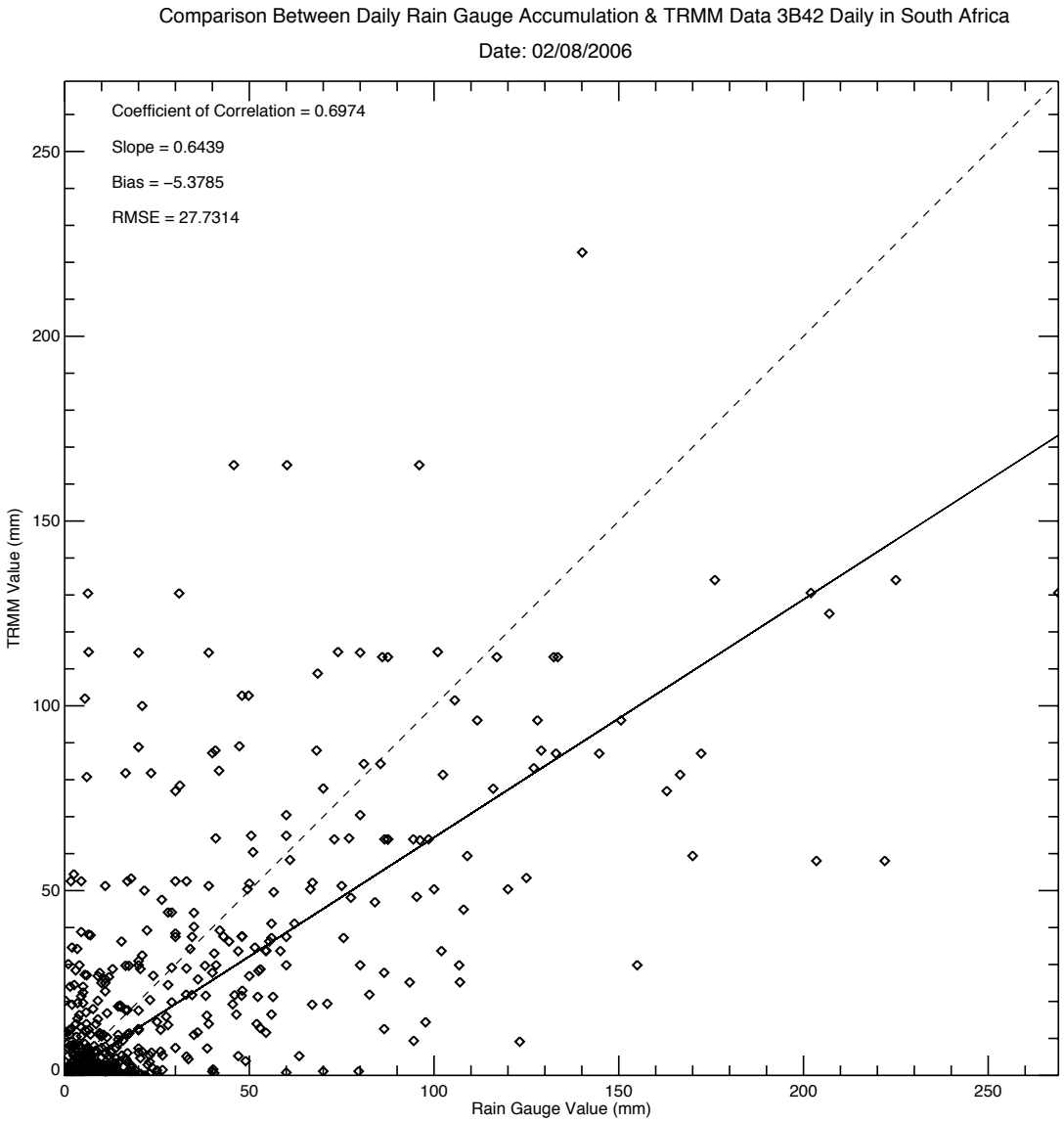

Figure 3.36: Comparison between rain gauge and TRMM estimation on 2 August 2006 over South Africa.

Figure 3.35 shows a daily rainfall over South Africa on 2 August 2006 that mainly occurred over southwestern part of eastern Cape Province including Port Elizabeth one of the major port cities in South Africa. 664 rain gauge stations (out of 2185 stations) have values greater than zero. Maximum rainfall recorded 269 mm in 24 hours period while TRMM estimated

131 mm at the same location. Likewise, TRMM observed maximum rainfall 223 mm while rain gauge measured 140 mm in 24 hours period at the same location. Figure 3.36 shows the scatter plot between rain gauge and TRMM estimates on 2 August 2006. Coefficient of correlation is 0.70 with slope 0.64. Bias -5 mm indicates underestimation by the satellite and RMSE is 28 mm.

3.3.4.2 Monthly rainfall on October 2007

During October 2007 rainfall occurred over entire South Africa although heavy precipitation mostly occurred over the eastern part (KwaZulu-Natal, Free State, North West, Gauteng, Mpumalanga, Limpopo, and part of Eastern Cape and Northern Cape provinces, Figure 3.37).

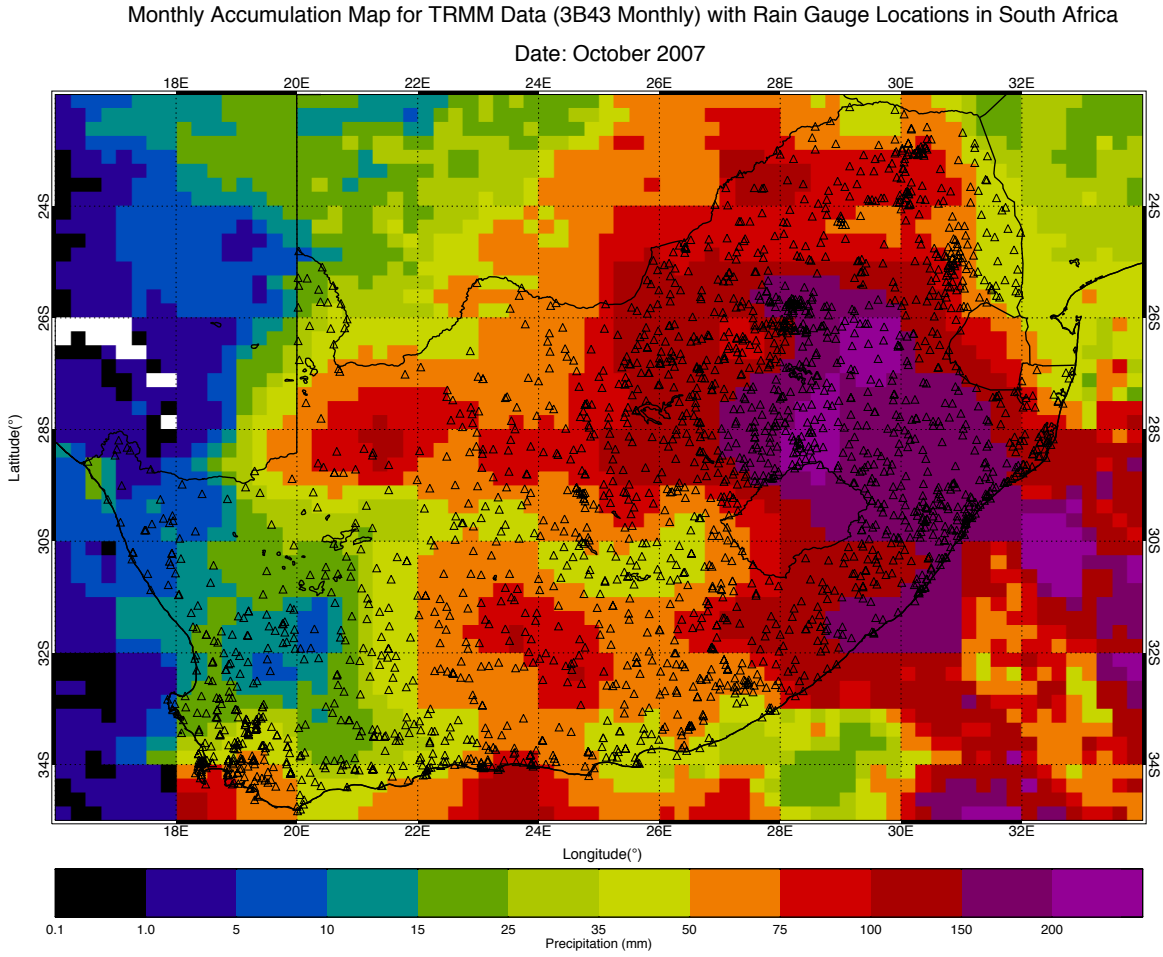

Figure 3.37: Monthly accumulation map for TRMM data 3B43 over South Africa during October 2007 with rain gauge locations.

During this month there were 1,453 rain gauge stations all over South Africa that received precipitation greater than zero. Maximum rainfall 403 mm was estimated by rain gauge over the entire month whereas satellite estimated it as 145 mm at the same location during October 2007. Similarly, satellite estimated maximum rainfall 275 mm during October 2007 while rain gauge estimated 311 mm rainfall at the same location and over the same duration. Coefficient of correlation for this month is measured 0.80 with slope 0.98, which indicates little underestimation by the satellites (Figure 3.38). On the other hand, bias 9 mm shows overestimation by the satellites. RMSE is found as 38 mm.

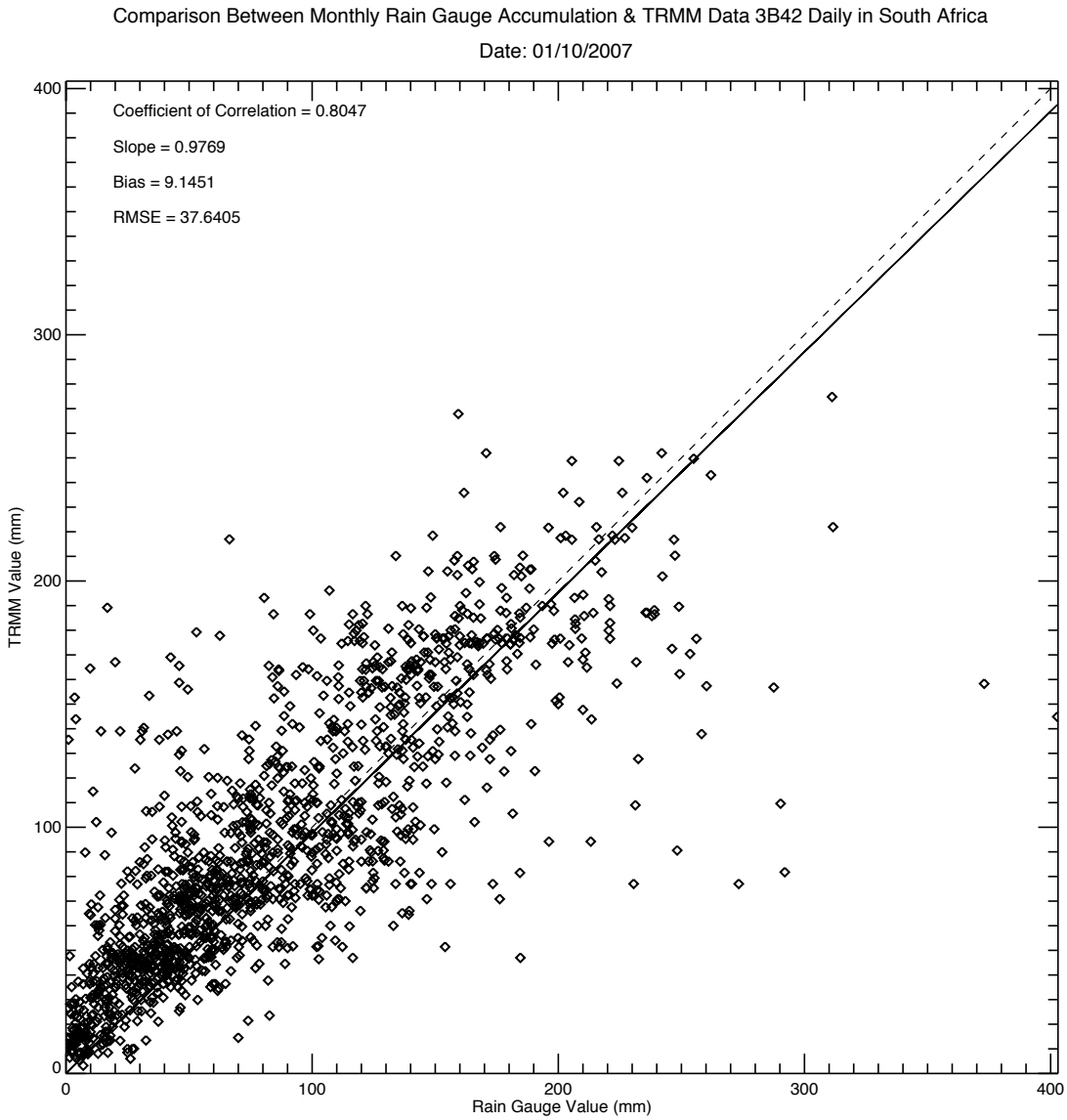

Figure 3.38: Comparison between rain gauge and TRMM estimation during October 2007 over South Africa.

3.3.4.3 Daily statistical parameters

Daily mean TRMM, daily mean rain gauge, coefficient of correlation, bias, and RMSE are all calculated in the same way as we have done for Catalunya and Bangladesh for the period from January 2005 to December 2009. Here, all bias and RMSE values are presented without any limit (Figure 3.40). Figure 3.39 shows mean TRMM, mean rain gauge, and correlation values in South Africa.

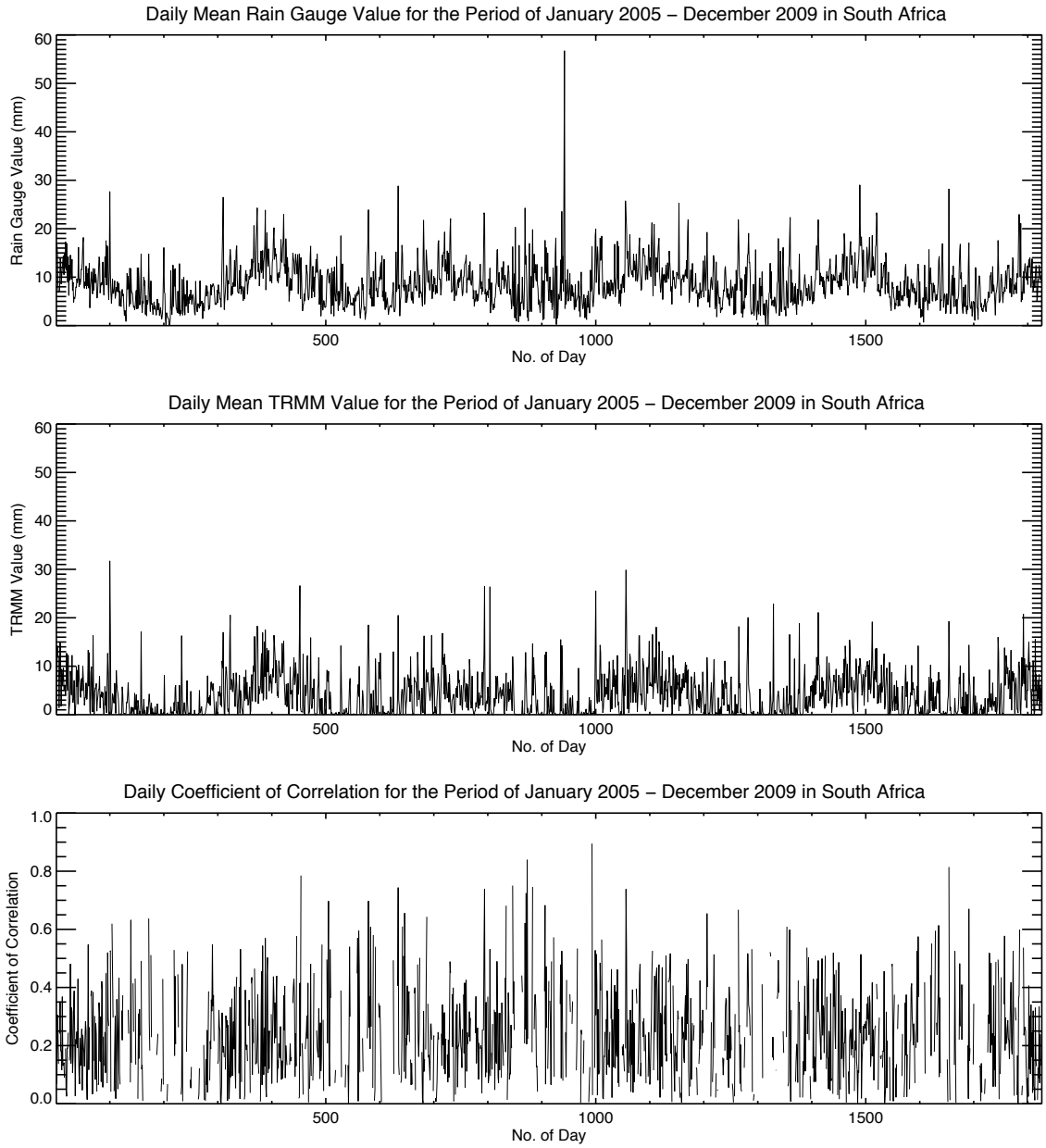

Figure 3.39: Daily mean rain gauge and TRMM values with daily coefficient of correlation for the period January 2005 – December 2009 in South Africa.

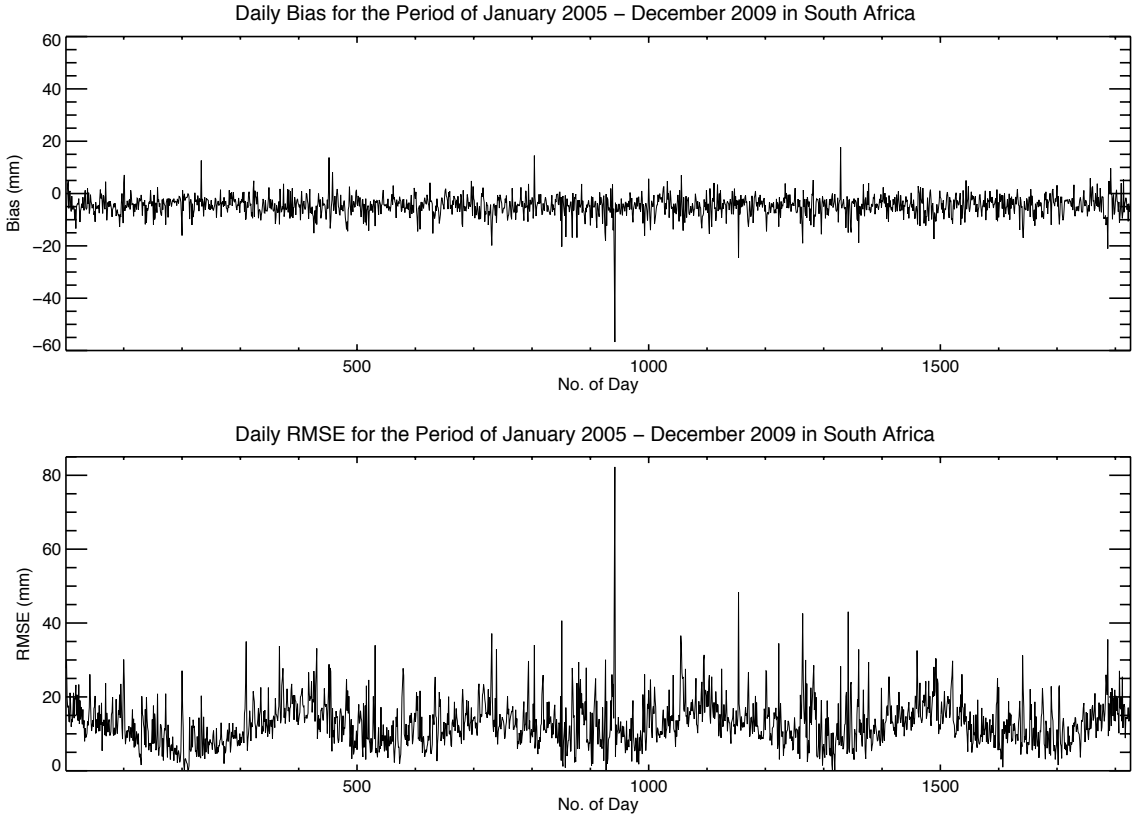

Figure 3.40: Daily bias and RMSE for the Period January 2005 – December 2009 in South Africa.

Out of 1826 days 3 days have correlation value greater than 0.90 with maximum bias and RMSE -6 mm and 10 mm respectively. 13 days have coefficient value greater than 0.70 and less than 0.90 having maximum bias -16 mm and maximum RMSE 34 mm. Correlation value varies between 0.50 and 0.70 for 79 days and maximum RMSE and bias are 43 mm and -19 mm respectively. For 587 days correlation value ranges between 0.20 and 0.5 and for the corresponding range maximum bias is -20 mm and maximum RMSE is 37 mm. 573 days show coefficient of correlation less than 0.20.

3.3.4.4 Monthly statistical parameters

From Figure 3.41 it is shown that maximum monthly mean rain gauge rainfall 139 mm was recorded in January 2006 and TRMM also estimated maximum monthly mean rainfall 156 mm in January 2006. It also follows the same trend for minimum monthly mean precipitation for both rain gauge and TRMM. TRMM (17 mm) and rain gauge (17 mm) both recorded minimum monthly mean rainfall in July 2005. Actually, both curve shows same pattern of

change of rainfall in each month for the considered period of study from January 2005 to December 2009. Moreover, maximum and minimum coefficient of correlation is found 0.86 and 0.48 during July 2007 and April 2009 respectively. 2 monthly out of these 60 months have coefficient value less than 0.60 and 41 months have correlation value greater than 0.70.

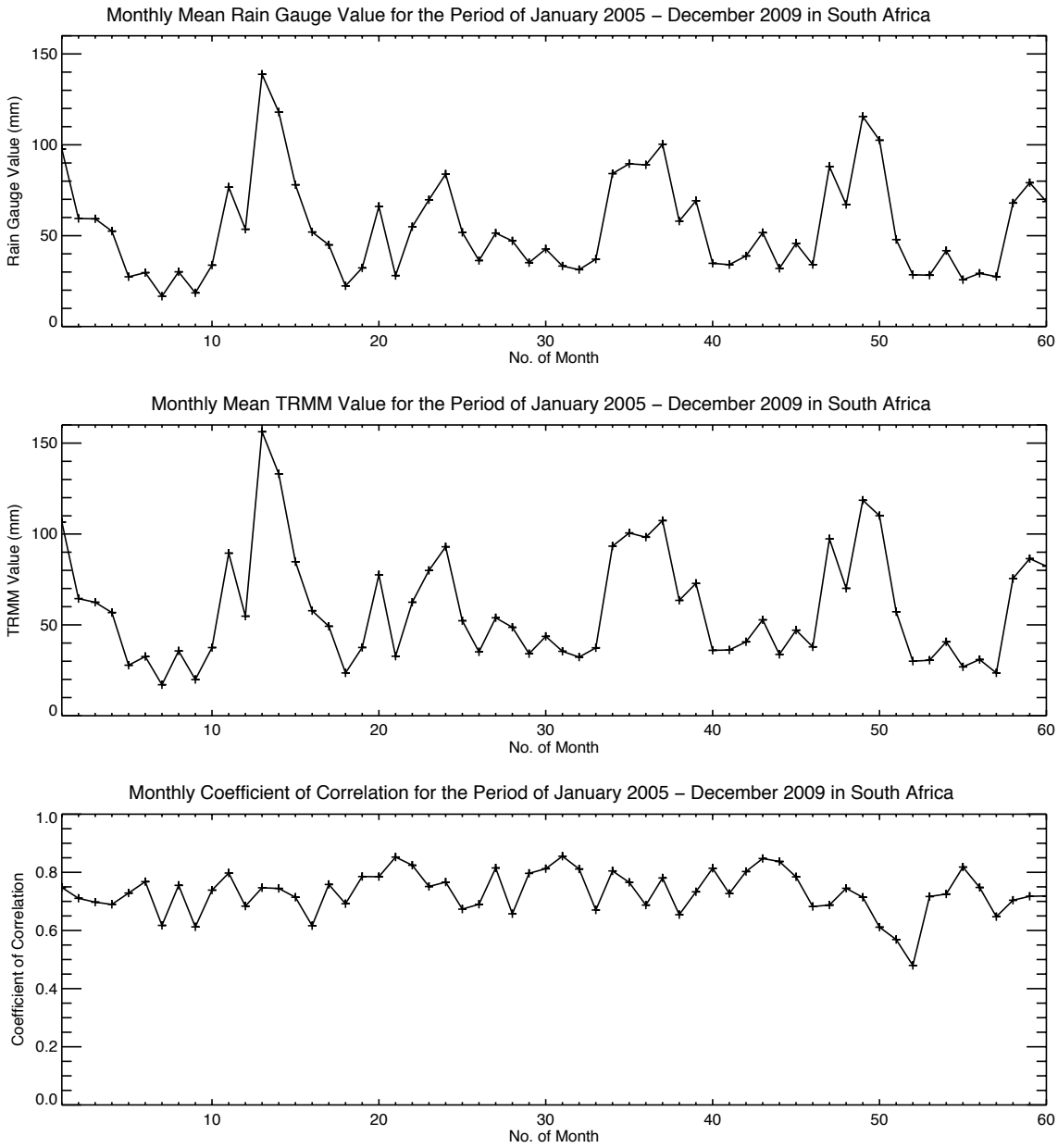

Figure 3.41: Monthly mean rain gauge and TRMM values with monthly coefficient of correlation for the period January 2005 – December 2009 in South Africa.

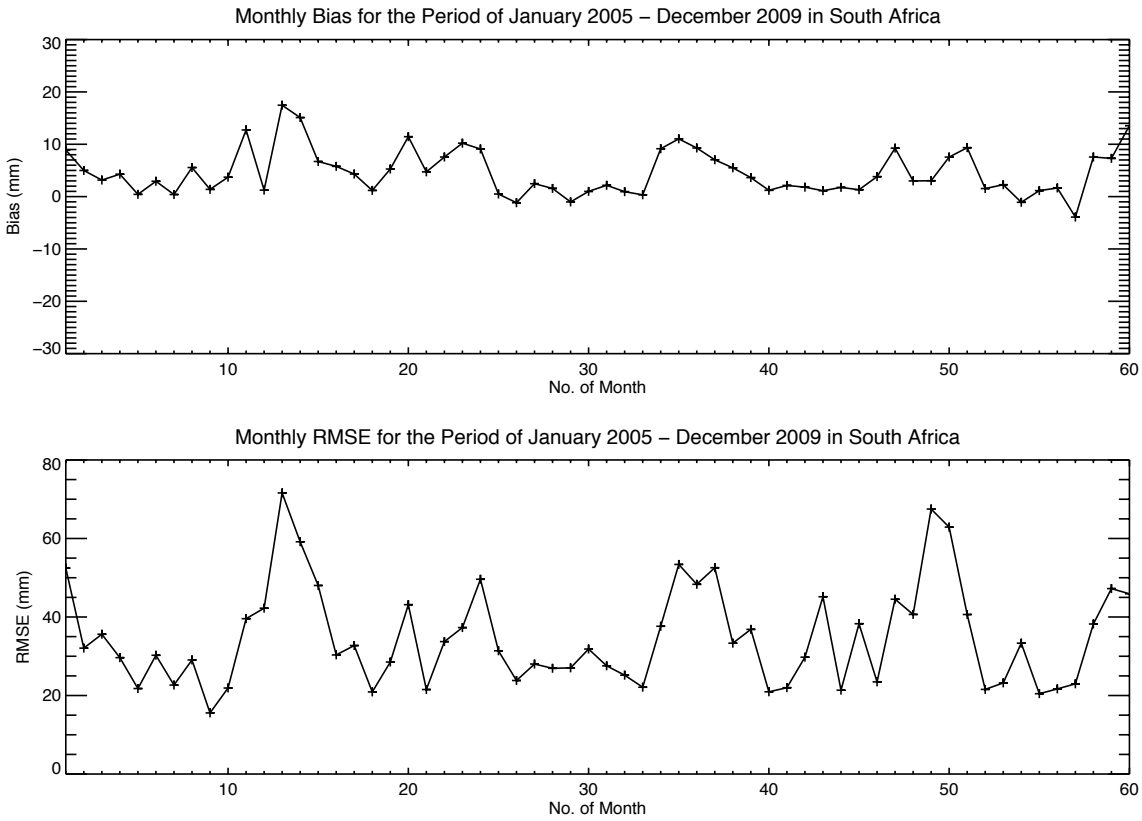

Figure 3.42: Monthly Bias and RMSE for the Period January 2005 – December 2009 in South Africa.

From Figure 3.42 it is found that minimum and maximum positive bias values are 0 mm (September 2007) and 17 mm (January 2006) respectively whereas negative bias are -1 mm (May 2007) and -4 mm (September 2009) respectively. Minimum RMSE 16 mm is found in September 2005 while maximum RMSE 72 mm is observed in January 2006. It is worthwhile to mention that maximum precipitation, maximum positive bias, and maximum RMSE are all measured in January 2006. The coefficient of correlation for this month is found as 0.75.

3.3.4.5 Statistical parameters for different temporal resolutions

Figures 3.43 and 3.44 show bias and RMSE for 2005 in South Africa. From the Figure 3.43 it is shown that bias is constant for all temporal accumulation for the year 2005. From the Figure 3.44 it is showed that RMSE decreases with increase the accumulation period and the rate of decrease is higher for 2 day, 3days, 5 days, and 10 days accumulation than those for 15 days and 30 days same as Catalunya and Bangladesh.

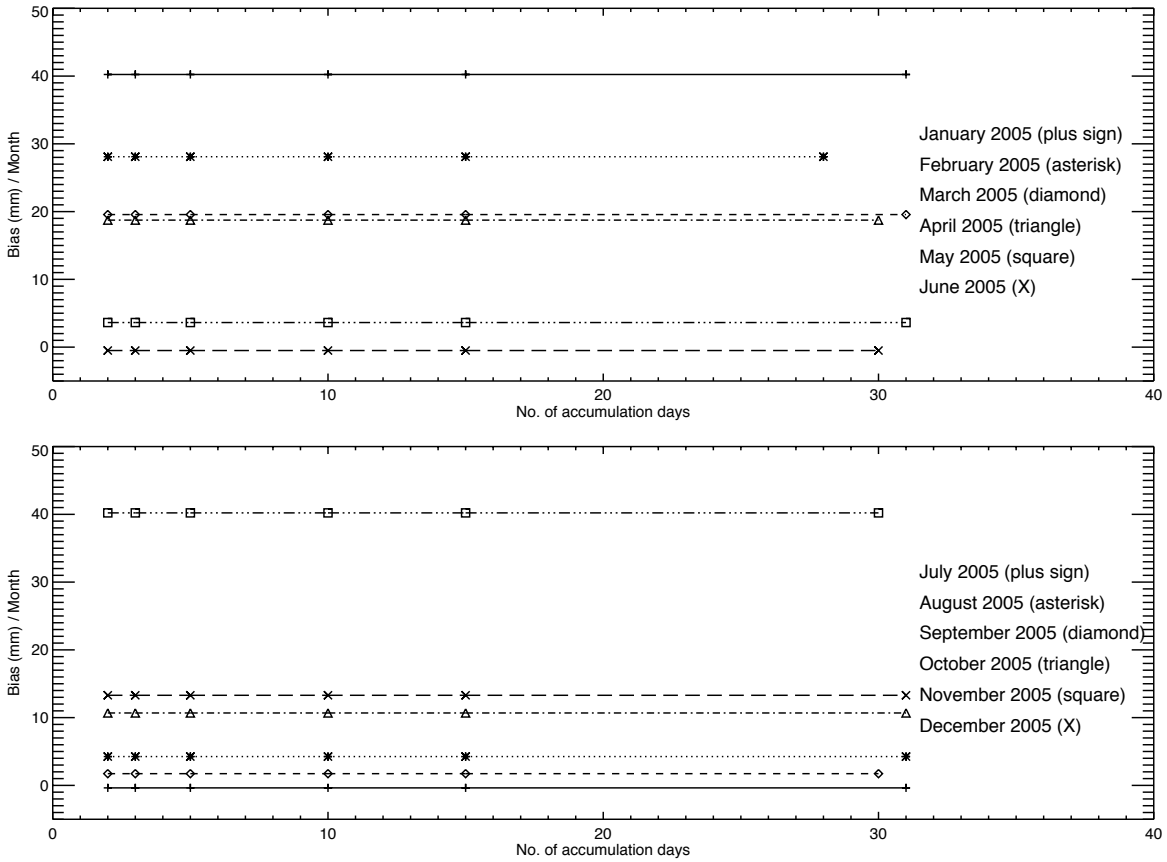

Figure 3.43: Bias for different temporal resolutions for 2005 in South Africa.

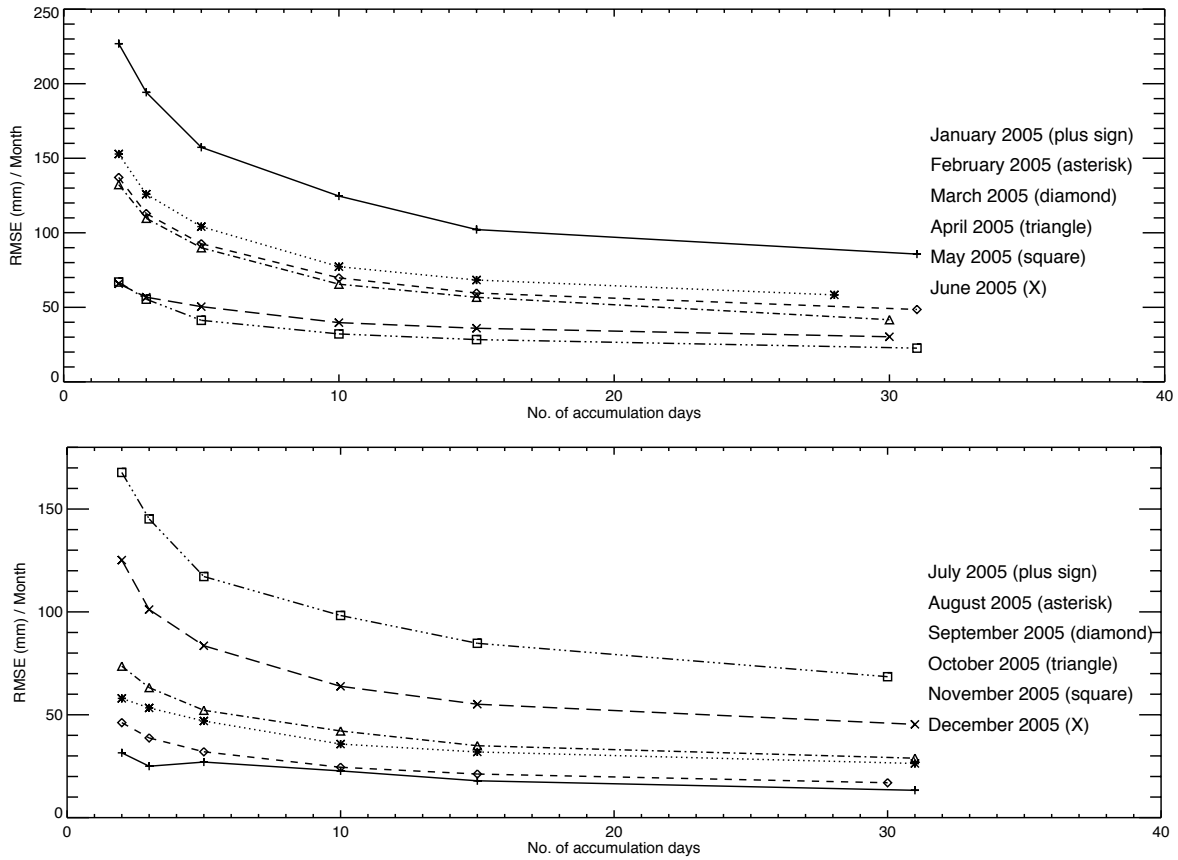

Figure 3.44: RMSE for different temporal resolutions for 2005 in South Africa.

3.4. Comparison between mean rain gauge and TRMM estimation

Table 3.2 shows coefficient of correlation, bias, and RMSE for three case study areas in daily and monthly temporal scale using mean rain gauge and TRMM value. Catalunya, Bangladesh, and South Africa all three case study areas show very good results in monthly scale and at the same time all case study areas also show good results in daily scale.

Table 3:2 Correlation coefficient, bias, and RMSE are measured using mean rain gauge and TRMM value for the three case study areas

	Daily			Monthly		
	Catalunya	Bangladesh	South Africa	Catalunya	Bangladesh	South Africa
Corr. Coeff.	0.74	0.62	0.60	0.96	1.00	1.00
Bias (mm)	-0.47 (-0.39*)	-1.98 (-1.12*)	-4.62 (-4.62*)	5.25 (5.25*)	-3.45 (-3.38*)	4.60 (4.60*)
RMSE (mm)	3.02 (5.68*)	13.49 (21.42*)	6.10 (12.94*)	10.07 (28.46*)	19.96 (69.79*)	6.34 (34.78*)

(….*) means average bias and RMSE from Figures 3.11 and 3.13, 3.26 and 3.28, and 3.40 and 3.42 for Catalunya, Bangladesh, and South Africa respectively

3.5. Summary of results

In this chapter, we have presented the areal distribution of precipitation over the three case study areas namely Catalunya, Bangladesh, and South Africa. We have also studied several extraordinary rainfall events in daily and monthly scale over the areas. Later on, three statistical parameters coefficient of correlation, bias. and RMSE have been determined in daily and monthly scale for the entire study period (from January 2005 to December 2009) at the case study areas. The results show significant spatial and seasonal variation of performance of TRMM satellite rainfall products such as in Bangladesh the TRMM satellite identified the dry and wet period very well.

We have studied the variation of performance of TRMM rainfall products at different temporal resolutions for the entire study period in Catalunya and Bangladesh and for 2005 in South Africa. Bias is constant for all temporal accumulation and RMSE decreases with increase the accumulation period and the rate of decrease is higher for 2 day, 3 days, 5 days, and 10 days accumulation than those for 15 days and 30 days in all case study areas. At the end of this chapter, we have determined the statistical parameters using mean rain gauge and mean TRMM values, which show very good results in monthly scale. The results in daily scale are not as good as in monthly scale. It is worthwhile to mention that mean TRMM value shows same pattern as like mean rain gauge value in both daily and monthly scale at all case study areas.

CHAPTER 4. BLENDING OF TRMM AND RAIN GAUGES

4.1. Introduction

Rainfall is one of the most important inputs in hydrological models and rain gauges and weather radars are probably the two sensors that are most widely used in rainfall measurement. Unfortunately, typical densities of operational rain gauge networks are usually unable to fulfill the requirements for hydrological modeling, flood forecasting, and weather observations. There are also large areas with no rain gauge coverage (e.g. over the oceans). Previous works suggested that radar data are essential information in providing accurate flow estimates using a rainfall runoff model, even when a dense rain gauge network exists [Sempere-Torres et al. (1999); Seo (1998)]. These results have led to the development of diverse methodologies for estimating rainfall fields by merging radar and rain gauge data.

According to Velasco-Forero et al. (2009) these merging techniques range from the simplest formulation, i.e. finding a constant multiplicative calibration factor [Harrold and Austin (1974); Wilson and Brandes (1979); Chumchean et al. (2006)], to statistical approaches based on multivariate analysis [Hevesi et al. (1992); Hevesi et al. (1992)], radar-rain gauge probability distribution analysis [Calheiros and Zawadzki (1987); Rosenfeld et al. (1994)], geostatistical estimators [Seo (1998); Creutin et al. (1988); Seo et al. (1990); Seo (1998); Sinclair and Pegram (2005); Schiemann et al. (2011)], or Bayesian methods [Todini (1999)].

In this chapter a blending technique is applied to estimate the rainfall field using rain gauge data and introducing satellite information as supporting data in the three case study areas. Li and Shao (2010) used a nonparametric kernel smoothing method to merge TRMM data with rain gauge observations. Scheel et al. (2011) proposed an ordinary cokriging algorithm that uses rain gauge values as the variate and the TMPA as the covariate. In this study, we have applied a approach to implement the technique proposed by Velasco-Forero et al. (2009) and Schiemann et al. (2011) [originally used for radar-rain gauge blending] to combine TRMM estimates with rain gauge records. This technique is based on the concepts of kriging [see e.g Goovaerts (1997); Isaaks and Srivastava (1989)] to interpolate rain gauge records using TRMM estimates as a secondary variable. This is a first attempt to do the blending and this is not the first work in this topic. The performance of the blending technique is also evaluated using two statistical parameters namely bias and root mean square error.

4.2. Ordinary kriging

Ordinary kriging is the most widely used geostatistical method to estimate a value at a point from the optimal linear combination of point observations in the neighborhood area, provided that the variogram is known; and probably the best unbiased linear combination [Isaaks and Srivastava (1989); Goovaerts (1997); Velasco-Forero et al. (2009); Li and Shao (2010)]. It is also a well-established reference to assess the improvements of new advance technique.

Suppose, we have (x_1, x_2, x_3,……, x_n) n locations in two dimensional space with rain gauge rainfall values as R(x_1), R(x_2), R(x_3),……R(x_n) and x_0 is the location at which the rainfall value is unknown. Then, the rainfall value R(x_0) at location x_0 is estimated by ordinary kriging (OK) method as a linear combination of the n observations through the following equation:

$$R(x_0) = \sum_{i=1}^{n} w_i R(x_i) \tag{4}$$

where, $R(x_i)$ are the observed rainfall values and w_i are the corresponding weights. If, the target location changes, the corresponding weight of the available rainfall data also changes accordingly.

The optimal weights for a specific unknown location are computed from the kriging equation system by minimizing the estimation error variance with the constraint of unbiased estimates

$$\begin{cases} \sum_{i=1}^{n} w_i \gamma(s_i - s_j) + \mu = \gamma(s - s_j) \qquad for\ j = 1,2,3, \dots \dots, n \\ \sum_{i=1}^{n} w_i = 1 \end{cases} \tag{5}$$

where, $\gamma(s_i - s_j)$ is the semivariogram value between points separated by $S_i - S_j$ and μ is the auxiliary Lagrange multiplier, the last equation represents the null bias constraint of the estimation.

4.3. The semi-variogram

The semi-variogram is the traditional tool for modeling the spatial dependence in geostatistical applications [Schiemann et al. (2011)]. The semi-variogram function, $\gamma(h)$, was originally named by Matheron (1963) as half the variance of the difference between points separated by a distance h. The semivariogram is calculated as

$$\gamma(h) = \frac{1}{2|N(h)|} \sum_{N(h)} \left(z_i - z_j\right)^2 \tag{6}$$

where $N(h)$ is the set of all pairwise Euclidean distances $i - j = h$, $|N(h)|$ is the number of distinct pairs in $N(h)$, and z_i and z_i are data values at spatial locations i and j, respectively. In this formulation h represents a distance measure with magnitude only. Sometimes, it might be desirable to consider direction in addition to distance. In such cases, h will be represented as the vector ***h*,** having both magnitude and direction.

The terms semi-variogram and variogram are often used interchangeably. By definition, $\gamma(h)$ is the semi-variogram and the variogram is $2\gamma(h)$.

The main goal of a semi-variogram analysis is to construct a semi-variogram that best estimates the autocorrelation structure of the underlying stochastic process. Most semi-variograms are defined through several parameters; namely, the nugget effect, sill, and range. These parameters are shown in Figure 4.1 and are defined as follows:

- nugget effect – represents micro-scale variation or measurement error. It is estimated from the empirical semi-variogram as the value of $\gamma(h)$ for $h = 0$.
- sill – the $\lim_{h\to\infty} \gamma\,(h)$ representing the variance of the random field.
- range – the distance (if any) at which data are no longer autocorrelated.

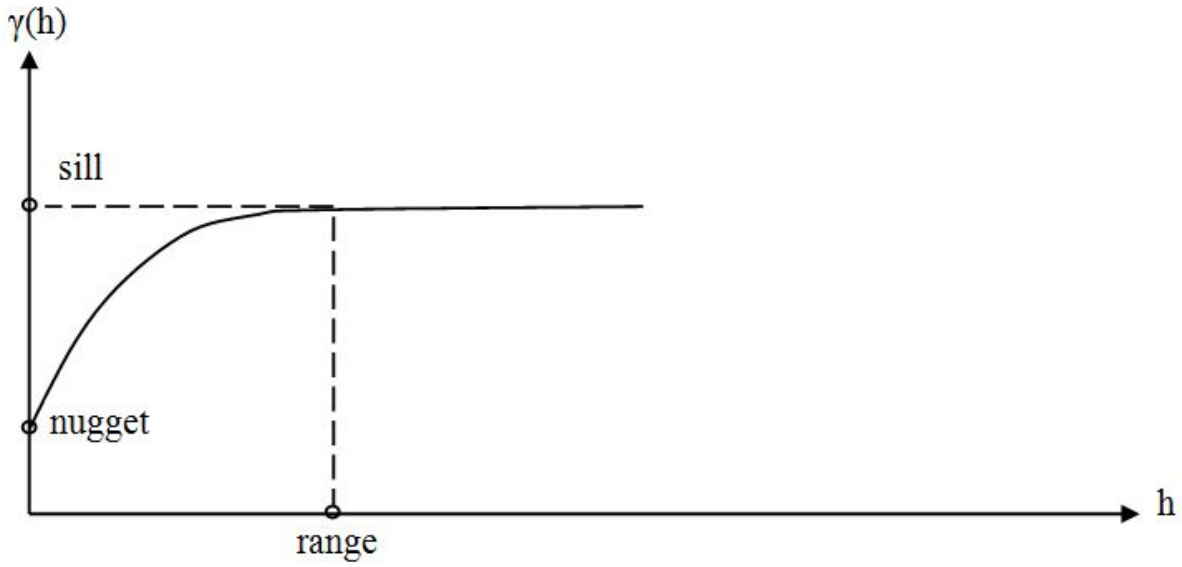

Figure 4.1: A generic semi-variogram showing the sill and range parameters along with a nugget effect.

Depending on the properties of the measure taken and the right fit of the data set, there are different types of semi-variogram model such as linear, spherical, exponential, Gaussian etc. Schuurmans et al. (2007) have determined spherical semi-variogram model for radar rain gauge combination to estimate high-resolution daily rainfall fields. The parameters of the models are fitted automatically with nonlinear regression, using weights $N(h)/h^2$ with $N(h)$ as the number of point pairs and h as the distance. This criterion is partly suggested by theory, and partly by practice [Pebesma (2004)]. When it was not possible to fit a unique semi-variogram model, the range was forced to be beyond the extent. Alternatively, Velasco-Forero et al. (2009) and Schiemann et al. (2011) used a sample 2-dimensional semi-variogram computed from radar rainfall products. The use of radar data allows to determine a dense semi-variogram (unlike rain-gauges, which require interpolation) and to consider the anisotropy of the rainfall field in the blending; that is, it allows considering the preferential directions of correlation.

4.4. Kriging with external drift

If extensive auxiliary information (e.g. radar, satellite or topographical data) is available and correlated with the target variable (e.g. rainfall), kriging with external drift is a simple method for including an external variable in the estimation process [Velasco-Forero et al. (2009)]. In

this thesis, kriging with external drift allows us to drive the rainfall. Kriging with external drift (KED) assumes that estimations are modeled as a drift term plus a residual term. The drift term is an unknown linear function defined externally through the auxiliary variable. Previous works have estimated rainfall fields using KED merging ground radar rainfall estimates and rain gauges [Cassiraga et al. (2002); Raspa et al. (1997); Velasco-Forero et al. (2009); Schiemann et al. (2011)] or rain gauge and satellite data [Grimes et al. (1999)]. A full description of KED equations can be found in the literature [Wackernagel (1995); Goovaerts (1997); Hengl et al. (2003)].

If only one secondary variable $Z_2(x)$ is available, KED assumes that the mean of the main / principle variable is linearly related to the tendencies of the secondary variable, such that

$$E\big(Z_1(x)\big) = m_1(x) = a_0 + a_1.Z_2(x), \tag{6}$$

where $E\big(Z_1(x)\big)$ and $m_1(x)$ are the expected and mean values respectively of the principal variable at the point x, $Z_2(x)$ is the value of the secondary variable at the same location, and a_0, and a_1 are unknown coefficients (which do not need to be estimated). Rainfall estimations using KED [Equation (7)] are computed using the same expression as in the OK (ordinary kriging) estimator [Equation (4)]

$$Z^*_{KED}(x_0) = \sum_{i=1}^{n} w_i^{KED} Z_G(x_i). \tag{7}$$

However, KED weights, w_i^{KED}, are unlike those used in the OK technique because the equation system of KED estimator [Equation (8)] has an additional constraint to satisfy the new drift hypothesis and there is a second auxiliary Lagrange multiplier, μ_1

$$\begin{cases} \sum_{j=1}^{n} w_i^{KED} C_R(x_i, x_j) + \mu_0 + \mu_1 Z_R(x_i) = C_R(x_i, x_0), & i = 1,2, \dots \dots, n \\ \sum_{j=1}^{n} w_j^{KED} = 1 \\ \sum_{j=1}^{n} w_j^{KED} Z_R(x_j) = Z_R(x_0) \end{cases} \quad (8)$$

where $Z_G(.)$ and $Z_R(.)$ are rain gauge and satellite observations at a given location respectively and C_R is the covariance of the residuals $Z_G(x) - m_G(x)$, where $m_G(x)$ is the gauge drift field. The covariance of the residuals have been estimated from TRMM data using the method proposed by Velasco-Forero et al. (2009). As discussed above, the sample 2-dimensional semi-variogram is estimated from TRMM data, and the validity of the semi-variogram is guaranteed with the method of Yao and Journel (1998).

The final constraint of the equation system [Equation (8)] introduces the variability of the satellite data into the interpolation process of the rain gauge values. This constraint means that rain gauge data are weighted using the set of weights that add in the effect of estimating the satellite value at the target point as the satellite values at rain gauge locations were interpolated.

4.5. Testing of TRMM-rain gauge blending rainfall products

The verification of the blended products has been based on a cross-validation technique: rain gauge measurements in a TRMM cells have not been used in the blending, and the blending estimate is compared against rain gauge measurements. In this way, the rain gauge measurements in that cell (not used in the blending) are an independent reference that can be used to evaluate the blended product. We have repeated this testing procedure for several cells at each case study areas using TRMM 3B43 monthly products.

4.5.1. Catalunya, Spain

In Catalunya, we have chosen seven cells at different latitude and longitude (see Table 4.1) to test the blended rainfall products against the rain gauge rainfall data. Table 4.1 also shows the number of rain gauges inside each cell. Figure 4.2 shows the location of the cells where we considered for testing the blending rainfall products.

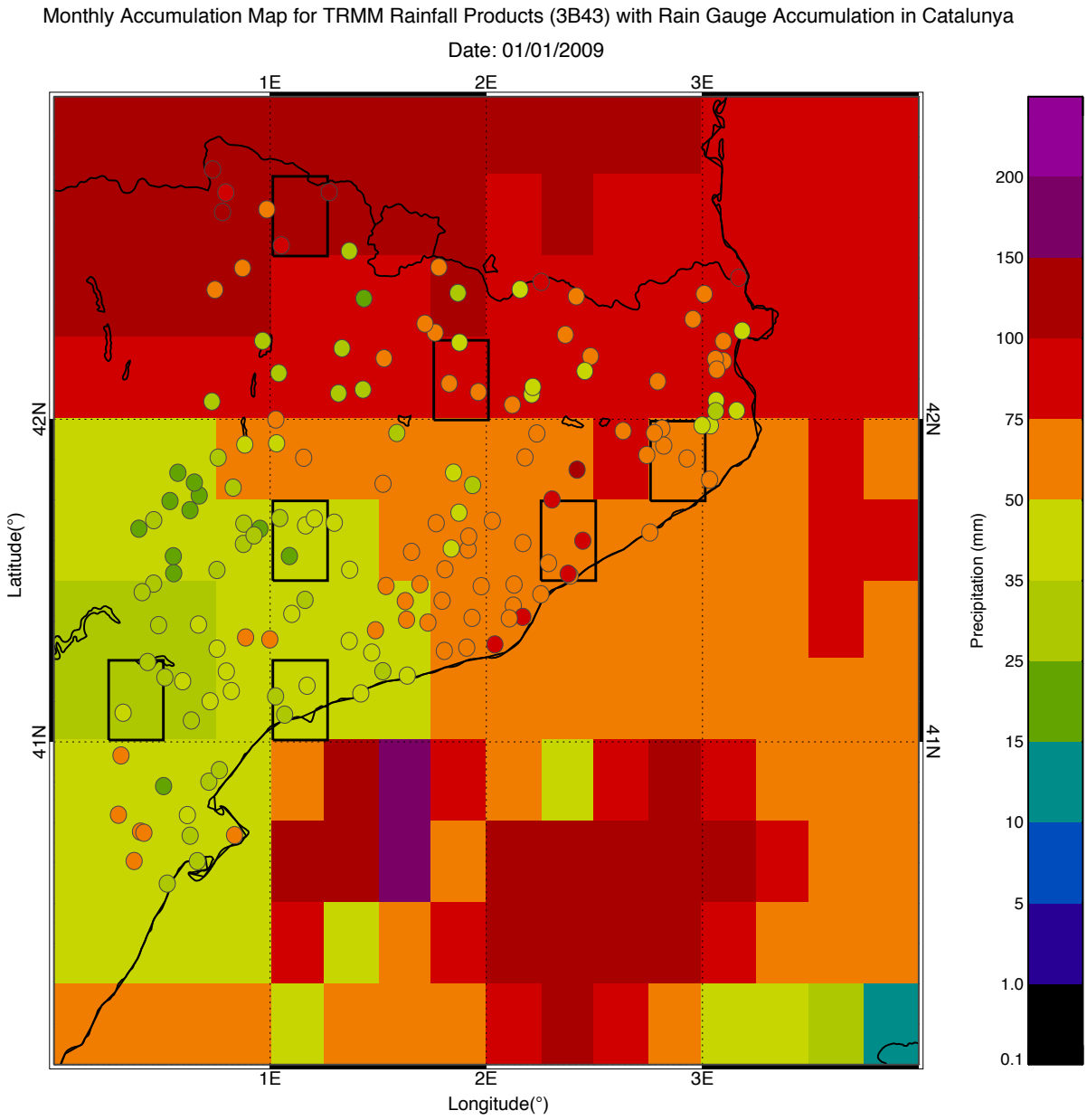

Figure 4.2: Monthly accumulation map of TRMM 3B43 in January 2009 with location of all the cells (shown by rectangles) in Catalunya to test the blended TRMM rainfall products (circles represent corresponding monthly accumulations of rain gauges).

To verify the improvement of the blended rainfall products, we have compared the blended and original TRMM rainfall products with rain gauge data (those rain gauges we removed while blending technique is implemented) for each cell separately for the time period from January 2005 to December 2009. In this case, we have applied TRMM 3B43 monthly rainfall products. Figures 4.3 and 4.4 show the scatter plots of the cells (4,6) and (11,7) respectively and all the results are summarized in Table 4.2.

Table 4.1: Latitude and longitude of the testing cells or pixels with the number of rain gauges inside the cells in Catalunya

Cell / Pixel	**Column No. (starts from zero)**	**Row No. (starts from zero)**	**Latitude (Degree)**	**Longitude (Degree)**	**No. of rain gauges inside the cells**
Cell (1,4)	1	4	41.125 N	0.375 E	2
Cell (4,4)	4	4	41.125 N	1.125 E	3
Cell (4,6)	4	6	41.625 N	1.125 E	4
Cell (7,8)	7	8	42.125 N	1.875 E	3
Cell (9,6)	9	6	41.625 N	2.375 E	4
Cell (11,7)	11	7	41.875 N	2.875 E	5
Cell (4,10)	4	10	42.625 N	1.125 E	1

All cells / pixels are showing good correlation (above 0.85) before and after blending except cell (4,10) and cell (7,8) [see Table 4.2]. Cell (4,10) is showing 0.43 and 0.64 before and after blending respectively. However, for cell (7,8) correlation value increases from 0.65 to 0.90 after blending. After blending for cells (1,4), (4,6), (7,8), (9,6), and (4,10) correlation values are increased and bias and RMSE values are decreased. Alternatively, for cells (4,4) and (11,7) bias and RMSE values are increased and correlation values are decreased after blending.

From the bias values of Table 4.2, it is shown that TRMM 3B43 values were overestimated before applying the blending technique and it remains the same after blending for cells (1,4), (4,6), (7,8), and (9,6). Cells (4,4) and (4,10) were under estimated by TRMM satellite before blending and after blending it persists the same. Before blending, cell (11,7) was overestimated whereas after blending it is under estimated. Out of all cells (4,10) was

seriously under estimated by TRMM satellite (-24 mm bias) and the blending procedure applied here does not reduce the under estimation (-24 mm bias).

Before blending, maximum and minimum RMSE were observed as 68 mm [for cell (4,10)] and 16 mm [for cell (11,7)] respectively. Likewise, after blending maximum and minimum RMSE were determined 57 mm [for cell (4,10)] and 13 mm [for cell (4,6)] respectively [see Table 4.2].

Table 4.2: Results of the testing cells before and after blending in Catalunya

	Cell / Pixel	**No. of rain gauges inside the cells**	**Correlation**	**Bias (mm)**	**RMSE (mm)**	**Slope**
After blending	Cell (1,4)	2	0.95	6	15	1.17
	Cell (4,4)	3	0.90	-4	22	0.84
	Cell (4,6)	4	0.93	5	13	1.10
	Cell (7,8)	3	0.90	6	19	1.02
	Cell (9,6)	4	0.94	3	15	1.00
	Cell (11,7)	5	0.87	-1	21	0.99
	Cell (4,10)	1	0.64	-24	57	0.70
Before blending	Cell (1,4)	2	0.90	7	16	1.07
	Cell (4,4)	3	0.96	-4	21	0.77
	Cell (4,6)	4	0.88	16	23	1.27
	Cell (7,8)	3	0.65	11	34	0.95
	Cell (9,6)	4	0.86	7	22	0.96
	Cell (11,7)	5	0.91	0	16	0.96
	Cell (4,10)	1	0.43	-24	68	0.65

From the above analysis (Table 4.2), it can be concluded that cell (4,10) is showing the worst results out of the seven cells, due to the fact that the number of rain gauges around the cell (4,10) is lesser than those of other cells.

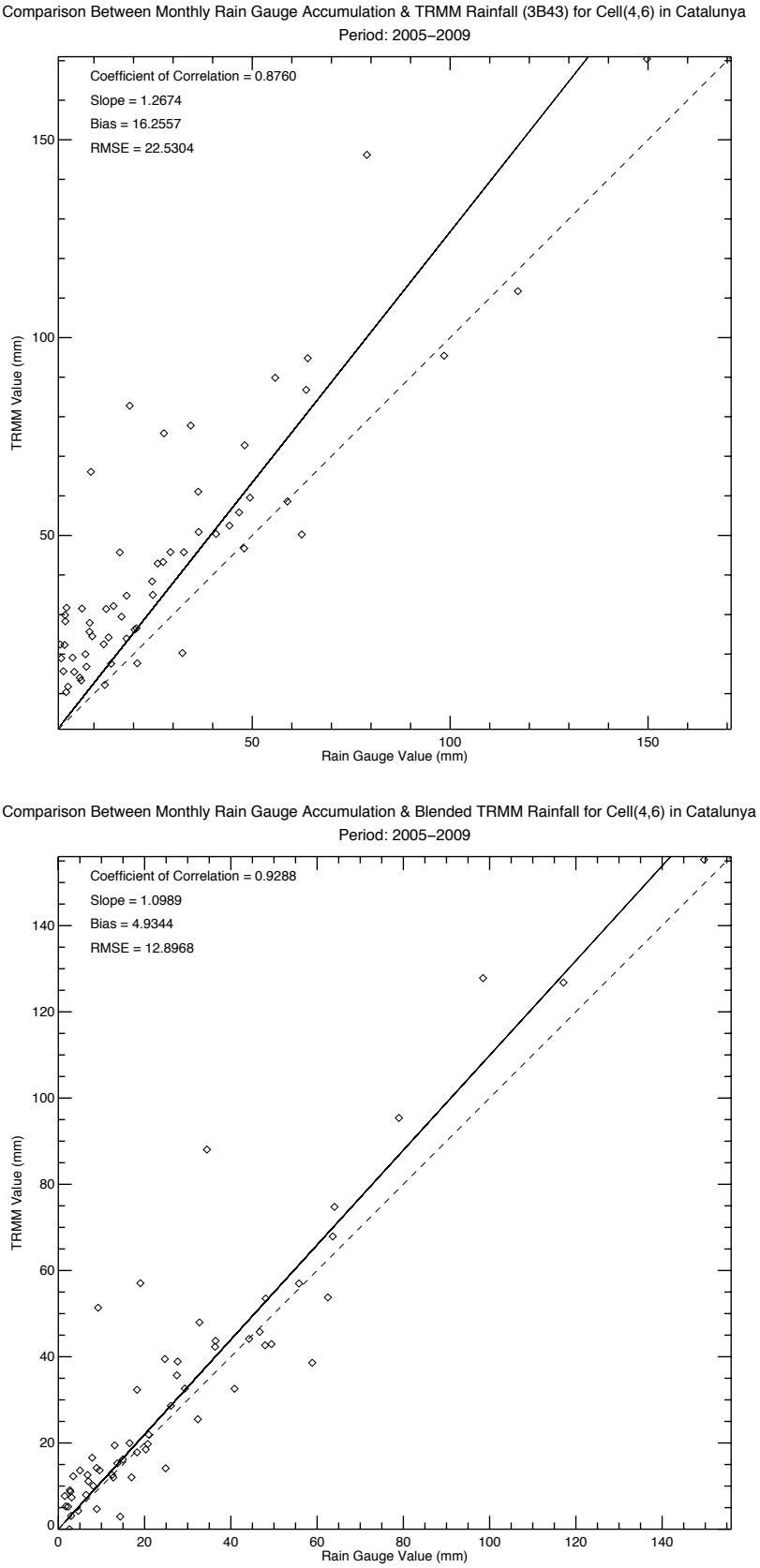

Figure 4.3: Comparison of original TRMM and blended TRMM rainfall products with rain gauge records cell (4,6).

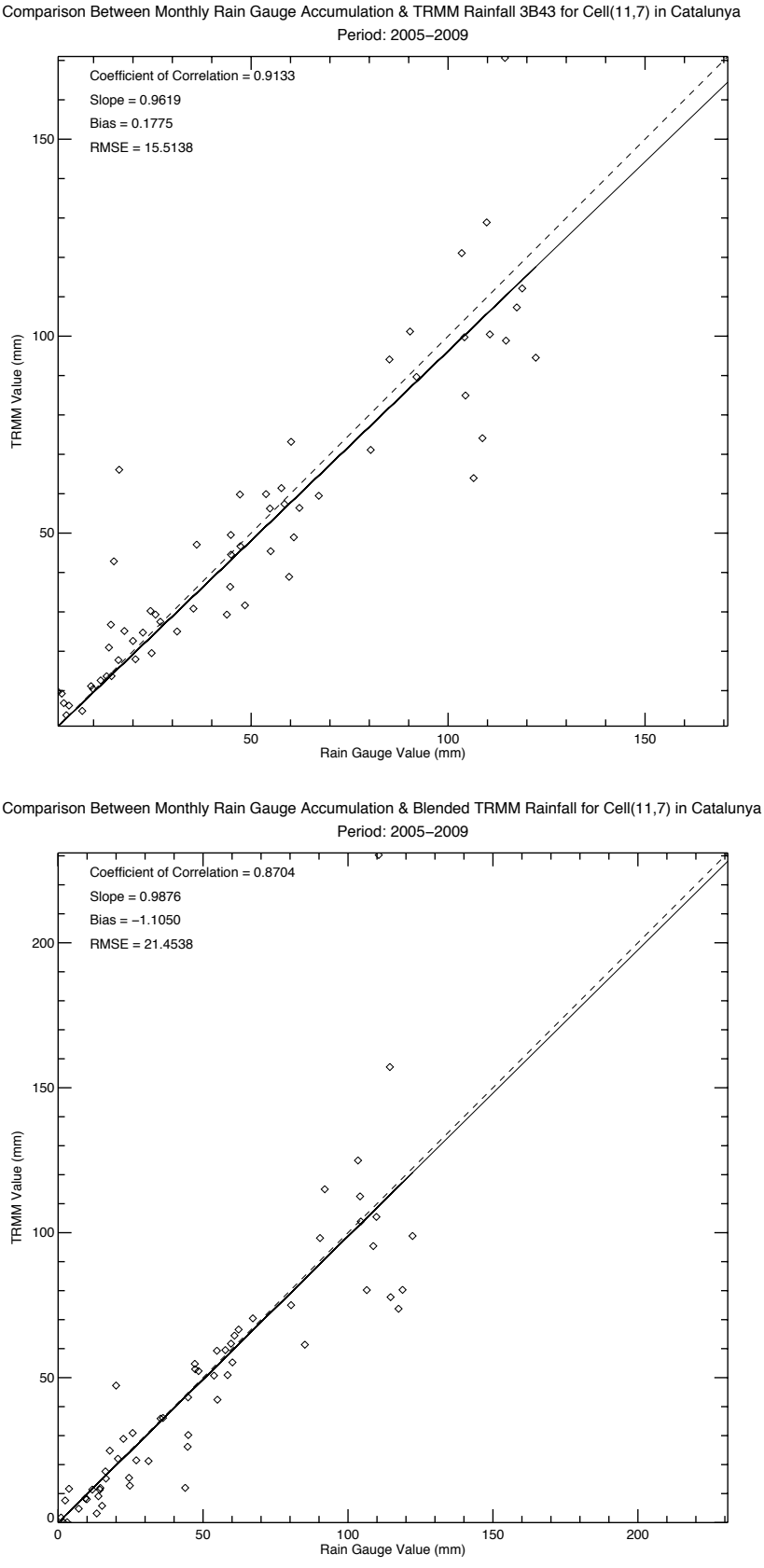

Figure 4.4: Comparison of original TRMM and blended TRMM rainfall products with rain gauge records for cell (11,7).

4.5.2. Bangladesh

In Bangladesh, we have chosen six cells at different latitude and longitude (see Table 4.3) to test the blended rainfall products against the rain gauge rainfall data. Table 4.3 also shows the number of rain gauges inside each cell. Figure 4.5 shows the location of the cells where we considered for testing the blending rainfall products.

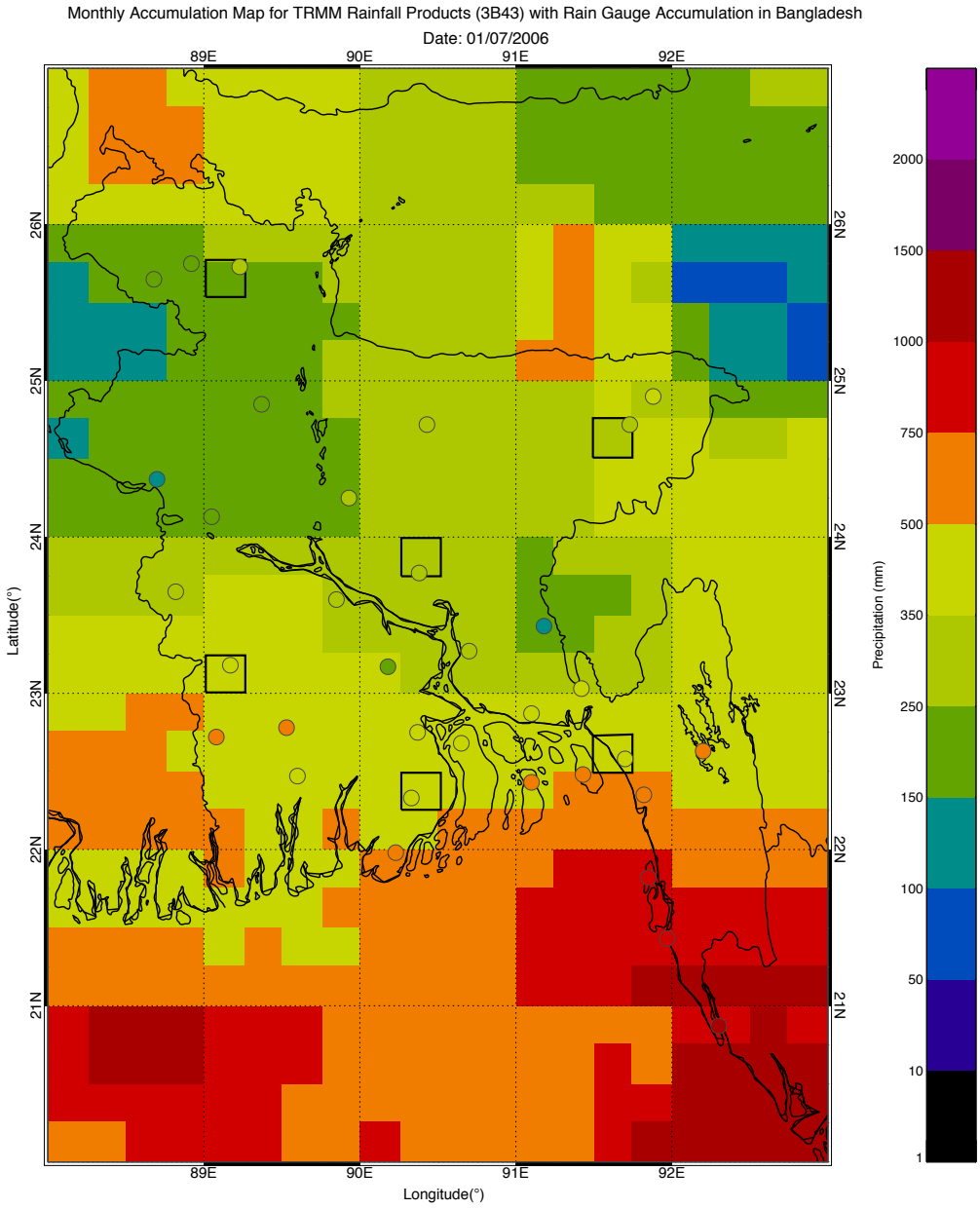

Figure 4.5: Monthly accumulation map of TRMM 3B43 in July 2006 with location of all the cells (shown by rectangles) in Bangladesh to test the blended TRMM rainfall products (circles represent corresponding monthly accumulations of rain gauges).

For these six cells we have done the same analysis in Bangladesh as we did for seven cells in Catalunya. Figures 4.6 and 4.7 show the scatter plots of the cells (9,9) and (4,22) respectively. We have summarized all the results in Table 4.4.

Table 4.3: Latitude and longitude of the testing cells or pixels with the number of rain gauges inside the cells in Bangladesh

Cell / Pixel	**Column No. (starts from zero)**	**Row No. (starts from zero)**	**Latitude (Degree)**	**Longitude (Degree)**	**No. of rain gauges inside the cells**
Cell (9,9)	9	9	22.375 N	90.375 E	1
Cell (4,12)	4	12	23.125 N	89.125 E	1
Cell (4,22)	4	22	25.625 N	89.125 E	1
Cell (9,15)	9	15	23.875 N	90.375 E	1
Cell (14,10)	14	10	22.625 N	91.625 E	1
Cell (14,18)	14	18	24.625 N	91.625 E	1

Four cells / pixels are showing very good correlation (above 0.90) before and after blending except cells (4,12) and (14,18). Cell (4,12) is showing 0.61 and 0.41 before and after blending respectively [see Table 4.4]. Moreover, cell (14,18) is showing 0.78 and 0.82 before and after blending respectively. Only for cell (14,18) correlation value is increased after blending while for other five cells correlation values are decreased after blending. Furthermore, RMSE values are increased after blending for all cells. Perhaps, the number of rain gauges plays a very important role to get better estimates.

From the Table 4.4, it is shown that TRMM 3B43 values were under estimated before applying the blending technique for all cells except cell (14,18) and it remains the same after blending for cells (9,9), (4,12), and (9,15). Cells (4,22) and (4,10) get 0 mm and 1 mm bias respectively after blending. Before blending, maximum positive bias was 64 mm [for cell (14,18)] whereas maximum negative bias was 51 mm [for cell (4,12)]. After blending, maximum and minimum negative bias are 56 mm [for cell (9,9)] and 31 mm [for cell (4,12)] respectively while maximum and minimum positive bias are 101 mm [for cell (14,18)] and 0 mm [for cell (4,22)] respectively.

Before blending, maximum and minimum RMSE were observed as 225 mm [for cell (4,12)] and 43 mm [for cell (4,22)] respectively. Likewise, after blending maximum and minimum RMSE were determined 270 mm [for cell (4,12)] and 97 mm [for cell (9,15)] respectively [see Table 4.4].

Table 4.4: Results of the testing cells before and after blending in Bangladesh

	Cell / Pixel	**No. of rain gauges inside the cells**	**Correlation**	**Bias (mm)**	**RMSE (mm)**	**Slope**
After blending	Cell (9,9)	1	0.90	-56	160	0.69
	Cell (4,12)	1	0.41	-31	270	0.51
	Cell (4,22)	1	0.92	0	78	0.98
	Cell (9,15)	1	0.92	-44	97	0.77
	Cell (14,10)	1	0.93	1	112	0.95
	Cell (14,18)	1	0.82	101	191	1.41
Before blending	Cell (9,9)	1	0.90	-35	142	0.78
	Cell (4,12)	1	0.61	-51	225	0.52
	Cell (4,22)	1	0.98	0	43	1.00
	Cell (9,15)	1	0.95	-14	65	0.90
	Cell (14,10)	1	0.94	-29	112	0.84
	Cell (14,18)	1	0.78	64	169	1.23

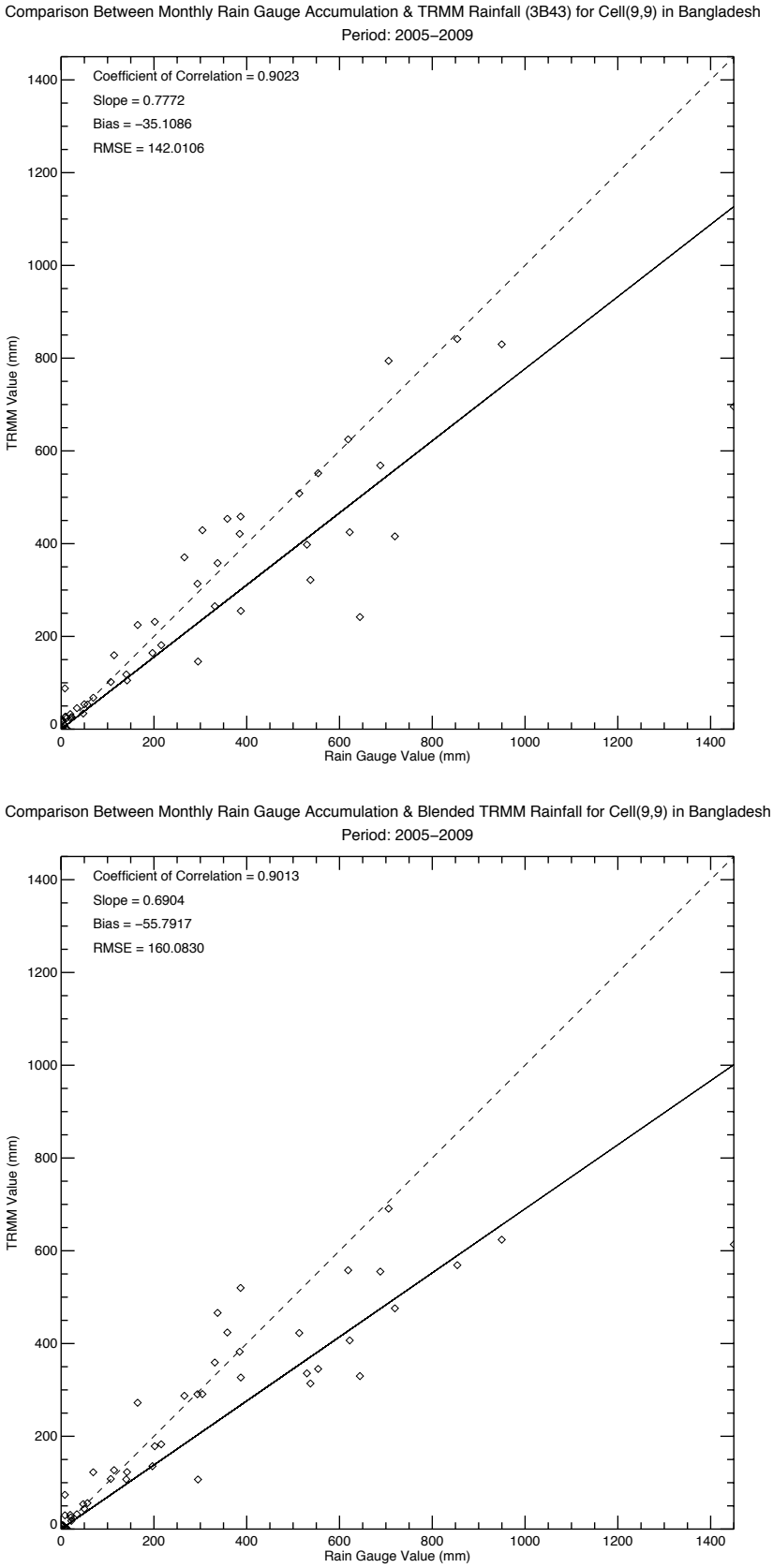

Figure 4.6: Comparison of original TRMM and blended TRMM rainfall products with rain gauge records cell (9,9).

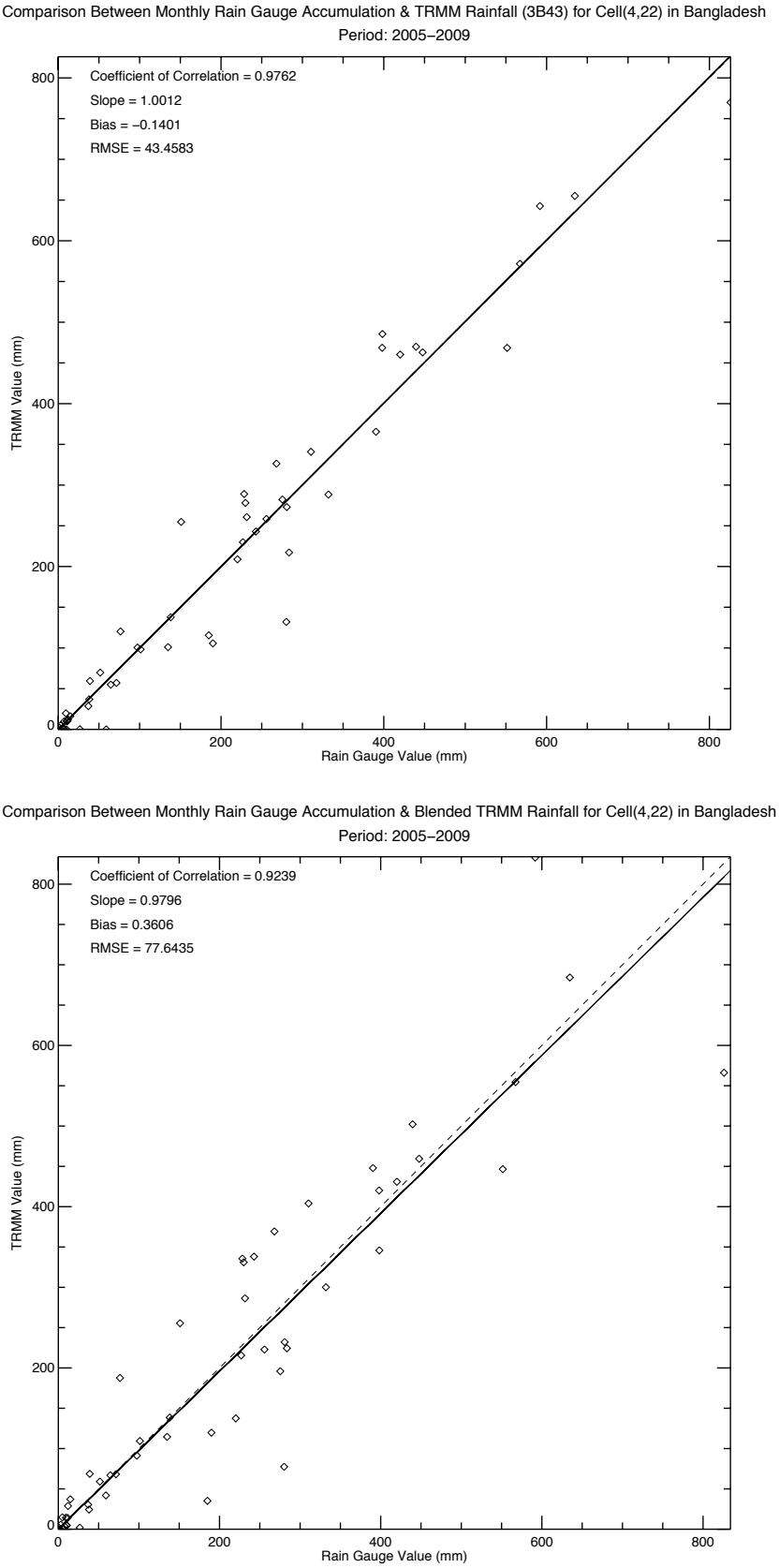

Figure 4.7: Comparison of original TRMM and blended TRMM rainfall products with rain gauge records cell (4,22).

4.5.3. South Africa

In South Africa, we have chosen six cells at different latitude and longitude (see Table 4.5) to test the blended rainfall products against the rain gauge rainfall data. Table 4.5 also shows the number of rain gauges inside each cell. Figure 4.8 shows the location of the cells where we considered for testing the blending rainfall products (The rectangles does not indicate the pixel or cell size in Figure 4.8, it simply represents the location of the cells. Here, cells or pixels are smaller than the size of the rectangles representing those cells).

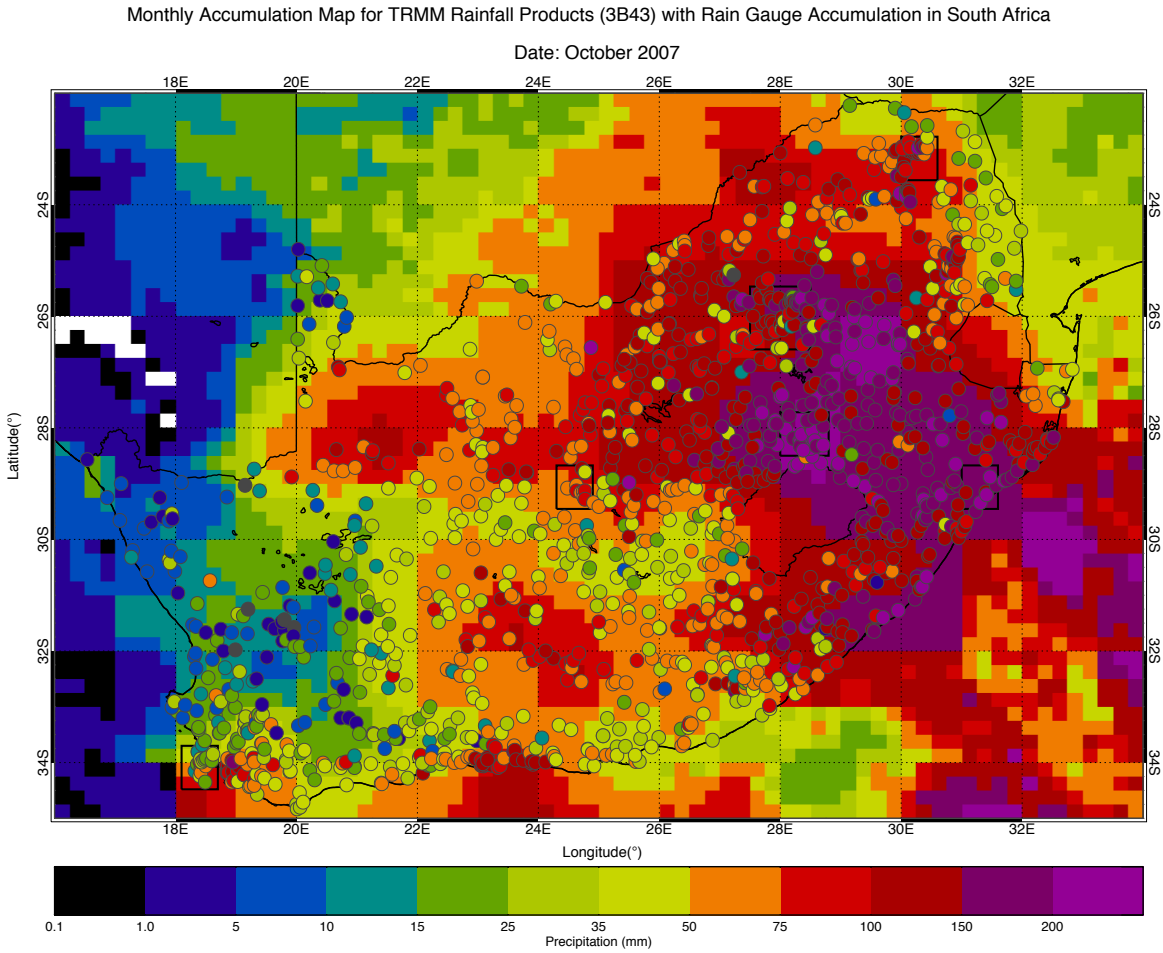

Figure 4.8: Monthly accumulation map of TRMM 3B43 in October 2007 with location of all the cells (shown by rectangles) in South Africa to test the blended TRMM rainfall products (circles represent corresponding monthly accumulations of rain gauges).

Six cells / pixels of distinct climatology have been analyzed in South Africa as we have done in Catalunya and Bangladesh. Figures 4.9 and 4.10 show the scatter plots of the cells (9,3) and (48,35) respectively. We have summarized all the results in Table 4.6.

Table 4.5: Latitude and longitude of the testing cells or pixels with the number of rain gauges inside the cells in South Africa

Cell / Pixel	**Column No. (starts from zero)**	**Row No. (starts from zero)**	**Latitude (Degree)**	**Longitude (Degree)**	**No. of rain gauges inside the cells**
Cell (9,3)	9	3	34.125 S	18.375 E	6
Cell (34,23)	34	23	29.125 S	24.625 E	4
Cell (48,35)	48	35	26.125 S	28.125 E	10
Cell (49,27)	49	27	28.125 S	28.375 E	3
Cell (57,47)	57	47	23.125 S	30.375 E	4
Cell (61,23)	61	23	29.125 S	31.375 E	3

All cells / pixels are showing good correlation (above 0.80) before and after blending except cell (34,23) which is showing 0.77 after blending [see Table 4.6]. After blending for cells (9,3), (48,35), and (49,27) correlation values are increased and bias and RMSE values are decreased. Alternatively, for cells (34,23), (57,47), and (61,23) correlation values are decreased and RMSE values are increased after blending; bias is decreased for (34,23) and (57,47) and increased for (61,23). However, from Figure 4.8 it can be showed that the number of rain gauges around the cells (9,3), (48,35), and (49,27) are higher than those of cells (34,23), (57,47), and (61,23).

From the Table 4.6, it is shown that TRMM 3B43 values were overestimated for cells (9,3), (34,23), (48,35), (49,27), and (61,23) while cell (57,47) was under estimated before blending. After applying the blending technique cells (34,23) and (61,23) remain the same as overestimated whereas cells (9,3), (48,35), and (49,27) changes to under estimation. Moreover, cell (57,47) changes from under estimation to a little overestimation. Out of all cells (9,3) was seriously overestimated by TRMM satellite (30 mm bias) and the blending procedure applied here reduces the overestimation (-5 mm bias).

Before blending, maximum and minimum RMSE were observed as 44 mm [for cell (9,3)] and 21 mm [for cell (49,27) and (34,23)] respectively. Likewise, after blending maximum and minimum RMSE were determined 38 mm [for cell (57,47)] and 15 mm [for cell (49,27)] respectively [see Table 4.6].

Table 4.6: Results of the testing cells before and after blending in South Africa

	Cell / Pixel	**No. of rain gauges inside the cells**	**Correlation**	**Bias (mm)**	**RMSE (mm)**	**Slope**
After blending	Cell (9,3)	6	0.95	-5	18	0.87
	Cell (34,23)	4	0.77	4	22	0.98
	Cell (48,35)	10	0.95	-2	17	0.94
	Cell (49,27)	3	0.97	-1	15	0.94
	Cell (57,47)	4	0.84	0	38	0.86
	Cell (61,23)	3	0.84	13	35	1.11
Before blending	Cell (9,3)	6	0.88	30	44	1.31
	Cell (34,23)	4	0.81	6	21	1.07
	Cell (48,35)	10	0.94	4	23	1.09
	Cell (49,27)	3	0.96	10	21	1.11
	Cell (57,47)	4	0.89	-1	33	0.94
	Cell (61,23)	3	0.87	9	28	1.02

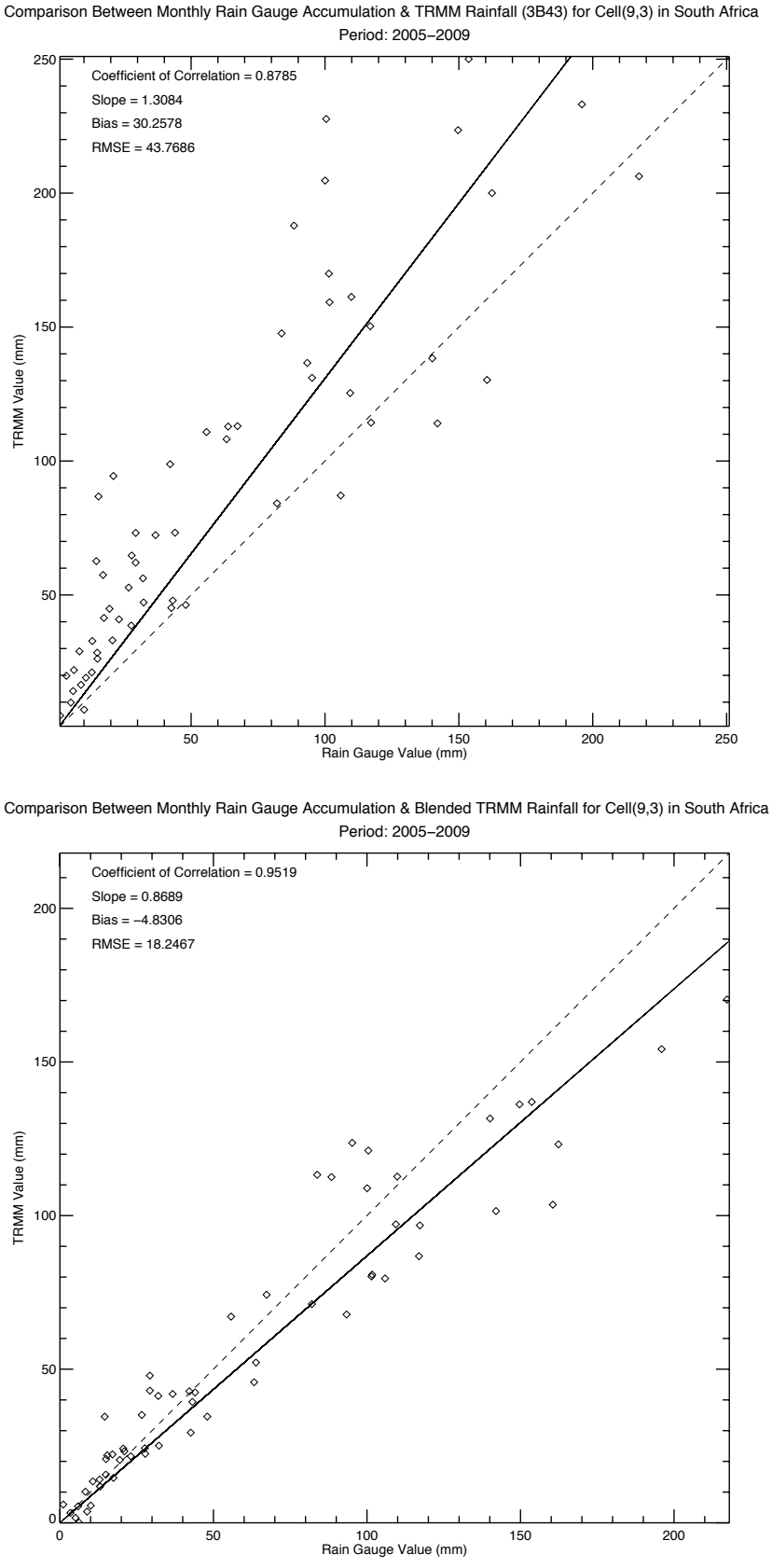

Figure 4.9: Comparison of original TRMM and blended TRMM rainfall products with rain gauge records cell (9,3).

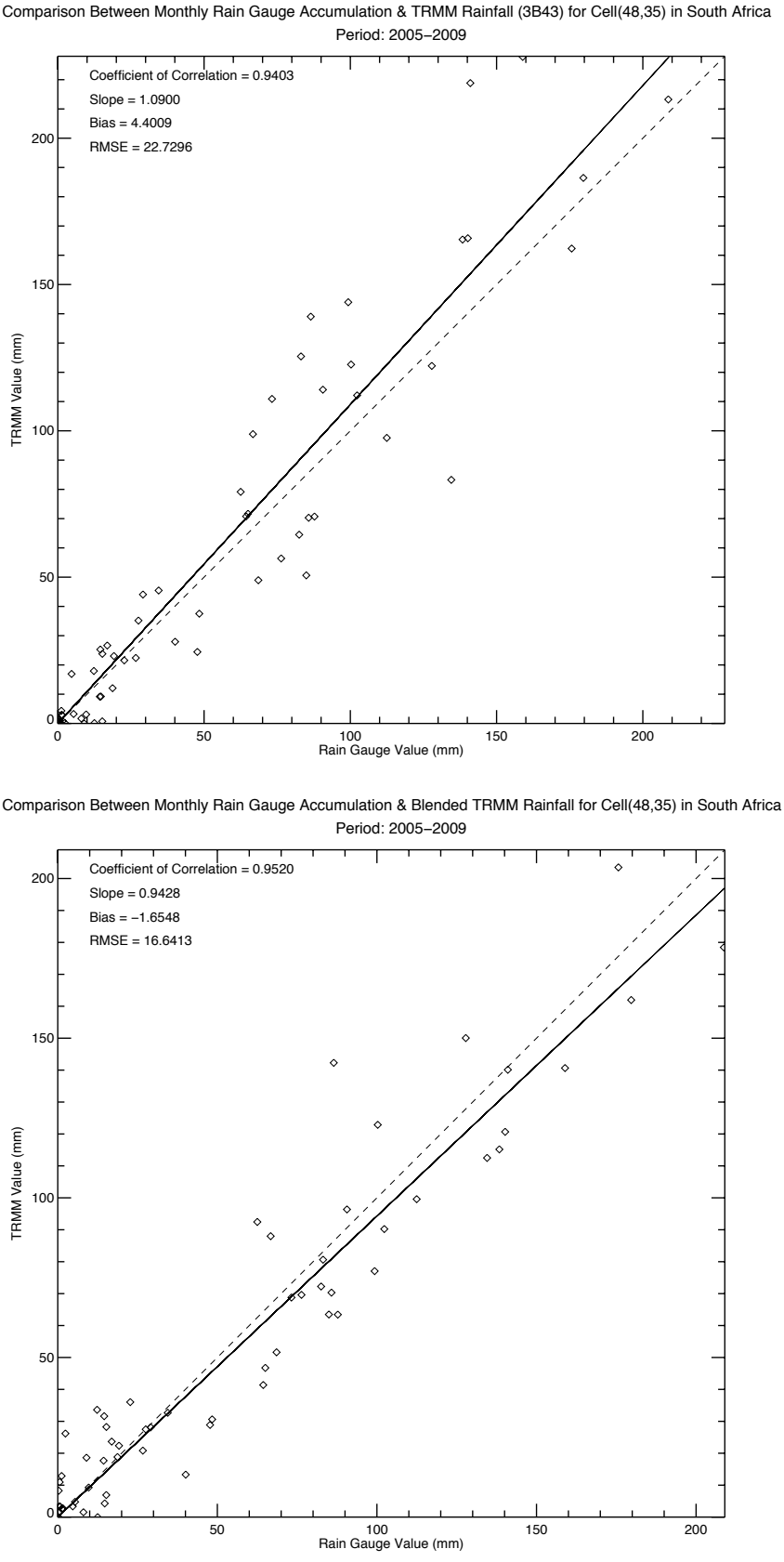

Figure 4.10: Comparison of original TRMM and blended TRMM rainfall products with rain gauge records cell (48,35).

4.6. Summary of results

In this chapter, we have applied a blending technique (originally used for radar-rain gauge blending) to combine TRMM rainfall products with rain gauge records. The verification of blending rainfall products has also been performed. The TRMM rainfall products are showing good results before and after the application of blending technique in all case study areas, however the performance of blended rainfall products highly depends on the number of rain gauges surrounding the cell / pixel. Out of the three case study areas, the performance of blended products is decreased in Bangladesh. The reason could be the sparse rain gauge network of Bangladesh. However, original TRMM rainfall products are showing very good results before blending in Bangladesh.

CHAPTER 5. CONCLUSIONS

In recent years, many efforts have been made to use the spaceborne radar rainfall products for hydrological purposes where areal precipitation estimation is essential and operational rain gauge network is sparse or absent. In this study, we have studied the accuracy of the TMPA rainfall products at three climatologically distinctive places. We have also merged the TRMM satellite rainfall data and available rain gauge observations to generate a better and more realistic precipitation estimation.

5.1. Summary

In chapter two, we have presented the three case study areas along with their general geographical and climatological features and also learned about the two TMPA rainfall products 3B42 and 3B43 version 7. Estimation procedure and other important characteristics of 3B42 and 3B43 version 7 rainfall products were analysed including their dissimilarities at corresponding scales. These products were also compared with each other to find the estimation differences at global scale.

In chapter three, we have shown the precipitation pattern over the three case study areas for the time period from January 2005 to December 2009. Some extraordinary rainfall events over those case study areas were also analysed at daily and monthly scales. We have determined three statistical parameters e.g. coefficient of correlation, bias, and RMSE at daily and monthly scales to identify the seasonal variation of the parameters and differences between satellite rainfall products and rain gauge records. Moreover, bias and RMSE were estimated at different temporal resolutions e.g. 2 day, 3 days, 5 days, 10 days, 15 days, and 30 days to find the variation of the parameters at different accumulation periods. Finally, we have determined the three statistical parameters using mean rain gauge and TRMM value at daily and monthly scales.

In chapter four, we have implemented a blending technique that is originally applied for the combination of ground based radar rainfall products and rain gauge records. These blended rainfall products were also verified to find the improvements over the original TRMM rainfall products at climatologically distinctive places in the three case study areas. Here, it is

worthwhile to mention that the implementation of the blending technique does not always increase the accuracy of TRMM rainfall products. One reason could be the TRMM pixel size (0.25° x 0.25°). Since, this technique was applied for ground-based radar-rain gauge blending where the pixel size is 1 km x 1 km whereas the TRMM pixel size is about 28 km x 28 km. Another reason could be the inaccurate and / or interrupted rain gauge records with sparse rain gauge network. Accuracy of the blending technique may also be affected by the orography of the area (e.g. local convective events).

5.2. Results and contribution of the thesis

In each chapter of the thesis, the corresponding results have been shown. Here, a general review of the results with the contribution are emphasized:

We have presented the estimation difference of two satellite rainfall products with different temporal resolutions at global scale, which depicts the quantitative variation of the two products.

Precipitation pattern of the case study areas with different latitude and longitude have been showed using satellite rainfall products that represents the accuracy of the satellite rainfall products to identify the climatological form of rainfall of the corresponding areas.

We have shown the performance of satellite rainfall products for few extraordinary rainfall events in daily and monthly temporal resolutions at distinct locations of the globe. The variation of performance has also been revealed with respect to space and time. Moreover, the temporal accuracy of the products has also been illustrated.

Finally, we have presented the results of blending rainfall products, which demonstrates the constraints of using satellite rainfall products and also enlightens how we can get rid of these limitations.

5.3. Future works

During the development of the thesis, we have found few aspects or issues that could be improved in future. The present work could also be extended in some directions that will definitely strengthen the findings of the current work. These are listed below:

The blending technique implemented here can be compared with other blending techniques to find the most efficient or effective one at each case study area. The inclusion of pixel size in the blending method (block kriging) may also improve the performance of the blending technique.

The impact of the density of the rain gauge network can also be evaluated in future, which will certainly reveal the dissimilarities of performance of the blending method.

References

©FAO, 2005: South Africa. Country Pasture/Forage Resource Profiles, 15 July 2013.

Adler, R. F., C. Kidd, G. Petty, M. Morissey, and H. M. Goodman, 2001: Intercomparison of Global Precipitation Products: The Third Precipitation Intercomparison Project (PIP-3). Bulletin of the American Meteorological Society, 82, 1377-1396.

AghaKouchak, A., A. Behrangi, S. Sorooshian, K. Hsu, and E. Amitai, 2011: Evaluation of satellite-retrieved extreme precipitation rates across the central United States. Journal of Geophysical Research, 116.

Ahasan, M. N., D. M. A. M. Chowdhury, and D. A. Quadir, 2011: Simulation of a Heavy Rainfall Event on 14 September 2004 over Dhaka, Bangladesh Using MM5 Model. Journal of Scientific Research, 3, 261-270.

Artan, G., H. Gadain, J. Smith, K. Asante, C. Bandaragoda, and J. Verdin, 2007: Adequacy of satellite derived rainfall data for stream flow modeling. Nat Hazards, 43, 167-185.

Bell, T. L., A. Abdullah, R. L. Martin, and G. R. North, 1990: Sampling errors for satellite-derived tropical rainfall: Monte Carlo study using a space-time stochastic model. J. Geophys. Res., 95(D3), 2195–2205.

Bitew, M. M., and M. Gebremichael, 2011: Evaluation of satellite rainfall products through hydrologic simulation in a fully distributed hydrologic model. Water Resources Research, 47.

Bitew, M. M., and M. Gebremichael, 2011: Assessment of satellite rainfall products for streamflow simulation in medium watersheds of the Ethiopian highlands. Hydrology and Earth System Sciences, 15, 1147-1155.

Brown, J. E. M., 2006: An analysis of the performance of hybrid infrared and microwave satellite precipitation algorithms over India and adjacent regions. Remote Sensing of Environment, 101, 63-81.

Calheiros, R. V., and I. Zawadzki, 1987: Reflectivity-rain rate relationship for radar hydrology in Brazil. Journal of Climate and Applied Meteorology, 26, 118-132.

Cassiraga, E. F., C. Guardiola-Albert, and J. J. Gomez-Hernandez, 2002: Automatic Modeling of Cross-Covariances for Rainfal Estimation Using Raingage and Radar Data in geoENV II., Barcelona, Spain: Kluwer Academic Publishers.

Chumchean, S., A. Seed, and A. Sharma, 2006: Correcting of real-time radar rainfall bias using a Kalman filtering approach. Journal of Hydrology, 317, 123-137.

Crétat, J., Y. Richard, B. Pohl, M. Rouault, C. Reason, and N. Fauchereau, 2012: Recurrent daily rainfall patterns over South Africa and associated dynamics during the core of the austral summer. International Journal of Climatology, 32, 261-273.

Creutin, J. D., G. Delrieu, and T. Lebel, 1988: Rain Measurement by Raingage-Radar Combination: A Geostatistical Approach. Journal of Atmospheric and Oceanic Technology, 5, 102-115.

Duncan, J. M. A., and E. M. Biggs, 2012: Assessing the accuracy and applied use of satellite-derived precipitation estimates over Nepal. Applied Geography, 34, 626-638.

Ebert, E. E., J. E. Janowiak, and C. Kidd, 2007: Comparison of Near-Real-Time Precipitation Estimates from Satellite Observations and Numerical Models. Bulletin of the American Meteorological Society, 88, 47-64.

Framji, K. K., B. C. Garg, and S. D. L. Luthra, 1982: Irrigation and Draianage in the World: A Global Review. ICD, Delhi.

GCIS, 2013: Geography and climate. About South Africa, 15 July 2015.

Goovaerts, P., 1997: Geostatistics for natural resources evaluation. Oxford University Press, 483 pp.

Gottschalck, J., J. Meng, M. Rodell, and P. Houser, 2005: Analysis of Multiple Precipitation Products and Preliminary Assessment of Their Impact on Global Land Data Assimilation System Land Surface States. Journal of Hydrometeorology, 6, 573-598.

Grimes, D. I. F., and M. Diop, 2003: Satellite-based rainfall estimation for river flow forecasting in Africa. I: Rainfall estimates and hydrological forecasts. Hydrological Sciences Journal, 48, 567-584.

Grimes, D. I. F., E. Pardo-Iguzquiza, and R. Bonifacio, 1999: Optimal areal rainfall estimation using raingauges and satellite data. Journal of Hydrology, 222, 93-108.

Groisman, P. Y., and D. R. Legates, 1994: The Accuracy of United States Precipitation Data. Bulletin of the American Meteorological Society, 75, 215-227.

Gupta, H. V., K. J. Beven, and T. Wagener, 2005: Model Calibration and Uncertainty Estimation. Encyclopedia of Hydrological Sciences.

Haile, A. T., E. Habib, M. Elsaadani, and T. Rientjes, 2013: Inter-comparison of satellite rainfall products for representing rainfall diurnal cycle over the Nile basin. International Journal of Applied Earth Observation and Geoinformation, 21, 230-240.

Harrold, T. W., and P. M. Austin, 1974: The structure of Precipitation systems. Journal of Atmospheric Research, 8, 41-57.

Hengl, T., G. B. M. Geuvelink, and A. Stein, 2003: Comparison of kriging with external drift and regression-Kriging. Technical Note, ITC.

Hevesi, J. A., J. D. Istok, and A. L. Flint, 1992: Precipitation Estimation in Mountainous Terrain Using Multivariate Geostatistics. Part I: Structural Analysis. Journal of Applied Meteorology, 31, 661-676.

Hevesi, J. A., A. L. Flint, and J. D. Istok, 1992: Precipitation Estimation in Mountainous Terrain Using Multivariate Geostatistics. Part II: Isohyetal Maps. Journal of Applied Meteorology, 31, 677-688.

Homar, V., R. Romero, C. Ramis, and S. Alonso, 2002: Numerical study of the October 2000 torrential precipitation event over eastern Spain: analysis of the synoptic-scale stationarity. Annales Geophysicae, 20, 2047-2066.

Hossain, F., and E. N. Anagnostou, 2004: Assessment of current passive-microwave- and infrared-based satellite rainfall remote sensing for flood prediction. Journal of Geophysical Research: Atmospheres, 109, D07102.

Huffman, G. J., and D. T. Bolvin, 2013: TRMM and Other Data Precipitation Data Set Documentation (Recent News). Mesoscale Atmospheric Processes Laboratory, NASA Goddard Space Flight Center and Science Systems and Applications, Inc.

Huffman, G. J., D. T. Bolvin, E. J. Nelkin, D. B. Wolff, R. F. Adler, G. Gu, Y. Hong, K. P. Bowman, and E. F. Stocker, 2007: The TRMM Multisatellite Precipitation Analysis (TMPA): Quasi-Global, Multiyear, Combined-Sensor Precipitation Estimates at Fine Scales. Journal of Hydrometeorology, 8, 38-55.

Isaaks, E. H., and R. M. Srivastava, 1989: An introduction to applied geostatistics. Oxford University Press.

Islam, A. S., and M. A. Hasan, 2012: Climate induced changes of precipitation extremes over Bangladesh. Proceedings of 3rd International Conference on Environmental Aspects of Bangladesh [ICEAB 2012]; October 13~14, 2012.

Krajewski, W. F., G. J. Ciach, J. R. McCollum, and C. Bacotiu, 2000: Initial Validation of the Global Precipitation Climatology Project Monthly Rainfall over the United States. Journal of Applied Meteorology, 39, 1071-1086.

Kummerow, C., J. Simpson, O. Thiele, W. Barnes, A. T. C. Chang, E. Stocker, R. F. Adler, A. Hou, R. Kakar, F. Wentz, P. Ashcroft, T. Kozu, Y. Hong, K. Okamoto, T. Iguchi, H. Kuroiwa, E. Im, Z. Haddad, G. Huffman, B. Ferrier, W. S. Olson, E. Zipser, E. A. Smith, T. T. Wilheit, G. North, T. Krishnamurti, and K. Nakamura, 2000: The Status of the Tropical Rainfall Measuring Mission (TRMM) after Two Years in Orbit. Journal of Applied Meteorology, 39, 1965-1982.

Lana, X., A. Burgueno, M. D. Martinez, and C. Serra, 2009: A review of statistical analyses on monthly and daily rainfall in Catalonia. Journal of Weather & Climate of the Western Mediterranean, 6, 15 - 30.

Legates, D. R., and T. L. DeLiberty, 1993: Precipitation measurement biases in the United States. Water Resour. Bull., 29.

Li, M., and Q. Shao, 2010: An improved statistical approach to merge satellite rainfall estimates and raingauge data. Journal of Hydrology, 385, 51-64.

Lindesay, J. A., and M. R. Jury, 1991: Atmospheric circulation controls and characteristics of a flood event in central South Africa. International Journal of Climatology, 11, 609-627.

Liu, X., Y. Fu, and Q. Liu, 2012: Significant impacts of the TRMM satellite orbit boost on climatological records of tropical precipitation. Chinese Science Bulletin, 57, 4627-4634.

Llasat, M. C., M. Llasat-Botija, A. Rodriguez, and S. Lindbergh, 2010: Flash floods in Catalonia: a recurrent situation. Adv. Geosci., 26, 105-111.

Llasat, M. d. C., M. Barnolas, M. Ceperuelo, M. Llasat, and M. A. Prat, 2004: Algunos aspectos del impacto social de las inundaciones en Cataluña. Revista del Aficionado a la Meteorología (RAM-20).

Llebot, J. E., 2012: Second Report on Climate Change in Catalonia. Interdepartmental Commission on Climate Change (CICC) of the Catalan Government (Generalitat of Catalonia).

Llort, X., 2010: A study of the structure of radar rainfall and its errors, Ph.D. Thesis: Universitat Politecnica de Catalunya.

Mason, S. J., and M. R. Jury, 1997: Climatic variability and change over southern Africa: a reflection on underlying processes. Progress in Physical Geography, 21, 23-50.

McCollum, J. R., W. F. Krajewski, R. R. Ferraro, and M. B. Ba, 2002: Evaluation of Biases of Satellite Rainfall Estimation Algorithms over the Continental United States. Journal of Applied Meteorology, 41, 1065-1080.

Morin, E., W. F. Krajewski, D. C. Goodrich, X. Gao, and S. Sorooshian, 2003: Estimating Rainfall Intensities from Weather Radar Data: The Scale-Dependency Problem. Journal of Hydrometeorology, 4, 782-797.

Pebesma, E. J., 2004: Multivariable geostatistics in S: the gstat package. Computers & Geosciences, 30, 683-691.

Petty, G. W., and W. F. Krajewski, 1996: Satellite estimation of precipitation over land. Hydrological Sciences Journal, 41, 433-451.

Philippon, N., M. Rouault, Y. Richard, and A. Favre, 2012: The influence of ENSO on winter rainfall in South Africa. International Journal of Climatology, 32, 2333-2347.

Raspa, G., M. Tucci, and R. Bruno, 1997: Reconstruction of rainfall fields by combining ground rain gauges data with radar maps using external drift method. In: Baafi EY, Schofield NA editors. Geostatistics wollongong'96. Kluwer Academic Publishers, 1306-1315 pp.

Rosenfeld, D., D. B. Wolff, and E. Amitai, 1994: The Window Probability Matching Method for Rainfall Measurements with Radar. Journal of Applied Meteorology, 33, 682-693.

Rouault, M., and Y. Richard, 2003: Spatial extension and intensity of droughts since 1922 in South Africa. Water SA, 19, 489-500.

Scheel, M. L. M., M. Rohrer, C. Huggel, D. Santos Villar, E. Silvestre, and G. J. Huffman, 2011: Evaluation of TRMM Multi-satellite Precipitation Analysis (TMPA) performance in the Central Andes region and its dependency on spatial and temporal resolution. Hydrol. Earth Syst. Sci., 15, 2649-2663.

Schiemann, R., R. Erdin, M. Willi, C. Frei, M. Berenguer, and D. Sempere-Torres, 2011: Geostatistical radar-raingauge combination with nonparametric correlograms: methodological considerations and application in Switzerland. Hydrology and Earth System Sciences, 15, 1515-1536.

Schuurmans, J. M., M. F. P. Bierkens, E. J. Pebesma, and R. Uijlenhoet, 2007: Automatic Prediction of High-Resolution Daily Rainfall Fields for Multiple Extents: The Potential of Operational Radar. Journal of Hydrometeorology, 8, 1204-1224.

Sempere-Torres, D., M. Berenguer, and C. A. Velasco-Forero, 2012: (IAHS red book).

Sempere-Torres, D., C. Corral, J. Raso, and P. Malgrat, 1999: Use of Weather Radar for Combined Sewer Overflows Monitoring and Control. Journal of Environmental Engineering, 125, 372-380.

Seo, D.-J., W. F. Krajewski, and D. S. Bowles, 1990: Stochastic interpolation of rainfall data from rain gages and radar using cokriging: 1. Design of experiments. Water Resources Research, 26, 469-477.

Seo, D. J., 1998: Real-time estimation of rainfall fields using rain gage data under fractional coverage conditions. Journal of Hydrology, 208, 25-36.

——, 1998: Real-time estimation of rainfall fields using radar rainfall and rain gage data. Journal of Hydrology, 208, 37-52.

Shimizu, S., T. Iguchi, R. Oki, M. Hirose, and T. Tagawa, 2008: Evaluation of the Effect of the Orbit Boost of the TRMM Satellite on the PR Rain Estimates. Geoscience and Remote Sensing Symposium, 2008. IGARSS 2008. IEEE International, IV - 133-IV - 136.

Shimizu, S., R. Oki, T. Tagawa, T. Iguchi, and M. Hirose, 2009: Evaluation of the Effects of the Orbit Boost of the TRMM Satellite on PR Rain Estimates. Journal of the Meteorological Society of Japan, 87A, 83-92.

Sinclair, S., and G. Pegram, 2005: Combining radar and rain gauge rainfall estimates using conditional merging. Atmospheric Science Letters, 6, 19-22.

Sivapalan, M., K. Takeuchi, S. W. Franks, V. K. Gupta, H. Karambiri, V. Lakshmi, X. Liang, J. J. McDonnell, E. M. Mendiondo, P. E. O'Connell, T. Oki, J. W. Pomeroy, D. Schertzer, S. Uhlenbrook, and E. Zehe, 2003: IAHS Decade on Predictions in Ungauged Basins (PUB), 2003‚Äì2012: Shaping an exciting future for the hydrological sciences. Hydrological Sciences Journal, 48, 857-880.

Smith, J. A., D. J. Seo, M. L. Baeck, and M. D. Hudlow, 1996: An Intercomparison Study of NEXRAD Precipitation Estimates. Water Resources Research, 32, 2035-2045.

Sorooshian, S., K.-L. Hsu, X. Gao, H. V. Gupta, B. Imam, and D. Braithwaite, 2000: Evaluation of PERSIANN System Satellite Based Estimates of Tropical Rainfall. Bulletin of the American Meteorological Society, 81, 2035-2046.

Su, F., Y. Hong, and D. P. Lettenmaier, 2008: Evaluation of TRMM Multisatellite Precipitation Analysis (TMPA) and Its Utility in Hydrologic Prediction in the La Plata Basin. Journal of Hydrometeorology, 9, 622-640.

Todini, E., 1999: A Bayesian technique for conditioning radar precipitation estimates to rain-gauge measurements. Hydrol. Earth Syst. Sci., 5, 187-199.

Tsintikidis, D., K. P. Georgakakos, G. A. Artan, and A. A. Tsonis, 1999: A feasibility study on mean areal rainfall estimation and hydrologic response in the Blue Nile region using METEOSAT images. Journal of Hydrology, 221, 97-116.

Velasco-Forero, C. A., D. Sempere-Torres, E. F. Cassiraga, and J. Jaime Gomez-Hernandez, 2009: A non-parametric automatic blending methodology to estimate rainfall fields from rain gauge and radar data. Advances in Water Resources, 32, 986-1002.

Wackernagel, H., 1995: Multivariate Geostatistics an introduction with applications. Berlin: Springer-Verlag, 256 pp.

Wilk, J., D. Kniveton, L. Andersson, R. Layberry, M. C. Todd, D. Hughes, S. Ringrose, and C. Vanderpost, 2006: Estimating rainfall and water balance over the Okavango River Basin for hydrological applications. Journal of Hydrology, 331, 18-29.

Wilson, J. W., and E. A. Brandes, 1979: Radar Measurement of Rainfall - a Summary. Bulletin of the American Meteorological Society, 60, 1048-1058.

Winchell, M., H. V. Gupta, and S. Sorooshian, 1998: On the simulation of infiltration- and saturation-excess runoff using radar-based rainfall estimates: Effects of algorithm uncertainty and pixel aggregation. Water Resources Research, 34, 2655-2670.

Yao, T., and A. Journel, 1998: Automatic Modeling of (Cross) Covariance Tables Using Fast Fourier Transform. Mathematical Geology, 30, 589-615.

Yilmaz, K. K., T. S. Hogue, K.-l. Hsu, S. Sorooshian, H. V. Gupta, and T. Wagener, 2005: Intercomparison of Rain Gauge, Radar, and Satellite-Based Precipitation Estimates with Emphasis on Hydrologic Forecasting. Journal of Hydrometeorology, 6, 497-517.